DEVELOPMENT AND APPLICATIONS OF A MICROCHIP CAPILLARY
ELECTROPHORESIS-HIGH PRESSURE MASS SPECTROMETRY PLATFORM

William M. Gilliland, Jr.

A dissertation submitted to the faculty at the University of North Carolina at Chapel Hill in partial fulfillment of the requirements for the degree of Doctor of Philosophy in the Department of Chemistry.

Chapel Hill
2017

Approved by:

J. Michael Ramsey

James W. Jorgenson

Joanna M. Atkin

Leslie M. Hicks

Elias P. Rosen

ABSTRACT

William M. Gilliland, Jr.: Development and Applications of a Microchip Capillary
Electrophoresis-High Pressure Mass Spectrometry Platform
(Under the direction of J. Michael Ramsey)

This work describes the pairing of electrospray ionization (ESI) with high pressure mass

spectrometry (HPMS) with the goal of developing a miniature analytical platform as an

alternative to traditional liquid chromatography-MS (LC-MS) systems. LC-MS systems are the

standard for many chemical analyses and are used for a wide range of applications, but their size

and complexity limits them to centralized labs. Microchip capillary electrophoresis (CE) coupled

with HPMS presents an opportunity to provide an inexpensive, simple, and targeted separations-

MS system. The work here demonstrates the initial steps for coupling ESI and HPMS,

improvements for the analysis of small molecules, and strategies and applications for ESI-HPMS

of intact proteins.

The first step for ESI-HPMS was designing an interface to conduct ions from

atmospheric pressure into the ion trap at ~1 Torr. The initial interface consisted of a capillary

inlet and a simple DC "gate" lens. With this interface, the twenty common amino acids were

detected when infused. Small peptides were detected with much greater sensitivity than amino

acids for this interface, and microchip CE-HPMS of peptide standards was demonstrated. In

addition, tandem mass spectrometry under HPMS conditions was performed with clusters of

small molecules as well as with a small peptide (RGES).

After initial development and proof-of-concept demonstration, several improvements

were made with ESI-HPMS. An aperture was used in place of a capillary, and a tube lens was

found to be more effective for small molecules than the "gate" lens. The RF drive frequency was

increased to 30 MHz to improve resolution, and the trap size was decreased to critical

dimensions of about 100 μm to maintain mass range. A SLIT trap was used to increase ion

storage capacity. With these improvements, the twenty common amino acids were infused and

detected with a 28-fold improvement in S/N and a 2.6-fold improvement in peak width over the

previous HPMS analysis. Microchip CE-HPMS was then used for two applications: the analysis

of amino acids in cell growth medium and the detection of opiates in urine.

Finally, CE-HPMS was used for the analysis of intact proteins. A printed circuit board

ion funnel was designed and implemented. The small proteins cytochrome c (12.3 kDa) and

myoglobin (17 kDa) were detected. The mass range was adjusted to detect large proteins BSA

(66 kDa) and an IgG2 (~150 kDa). CE-HPMS was then used for the detection of glycated

hemoglobin in whole blood lysate. HPMS calculations of hemoglobin glycation in clinical

samples were then correlated ($R^2 = 0.75$) with HbA1c detection by immunoassay.

"Piglet noticed that even though he had a very small heart, it could hold a rather large amount of gratitude" – A.A. Milne

To my family

ACKNOWLEDGEMENTS

I would first like to thank Professor Mike Ramsey for his advisement and the opportunity to do research in his laboratory. There are many current and former members of the lab who I would to thank as well. Derek Wolfe, Kenion Blakeman, Kevin Schultze, Andrew Hampton, and Craig Cavanaugh were all helpful in training me when I first joined the lab. A special thank you to Craig for many early morning and weekend conversations about both science and life. Nick Batz, Erin Redman, and Scott Mellors were all gracious with their time when I was learning the ins and outs of microchip CE (especially in microchip fabrication). Thank you to Oscar McCrate for his help with bacterial cell culture and overall biological knowledge. I'd like to thank our collaborators at 908 Devices, specifically Glenn Harris and Mike Goodwin, who provided many phone conversations and several visits that helped me along the way. I'd like to thank J.P. Alarie and Tina Stacy both for their guidance and for revisions of many, many documents, including this dissertation. The last members of the lab I would like thank are Davey West, Kristina Herrera, and Esme Candish who were great friends and support throughout my time at UNC.

The community at UPC has made my time at UNC better than I could have ever hoped. Thanks to John Rogers for his friendship and pastoral counsel, and to the PCM community for allowing me to be a small part of their lives. Special thanks to best friends Chelsey McElwee (and her cats), Patty Baum, Claire Chipman, Jessime Kirk, Laura Zolman Kirk, Kathleen Jasinskas, Charlie Hyland, Kate Fiedler, Catherine McKenas, Julia Ward, Greg Pitcher, Alan Haydon, and Chris Shore. I cannot begin to explain how much I appreciate their friendship, love, and support.

TABLE OF CONTENTS

LIST OF TABLES

LIST OF FIGURES

LIST OF ABBREVIATIONS AND SYMBOLS

2D	Two dimensional
3D	Three dimensional
η	Viscosity
μ_{app}	Apparent electrophoretic mobility
μ_{EO}	Electroosmotic mobility
μ_{EP}	Electrophoretic mobility
μg	Microgram
μm	Micrometer
μM	Micromolar
Ω	Angular drive frequency
AC	Alternating current
APDIPES	(3-Aminopropyl)di-isopropylethoxysilane
APS	Aminopropyl silane
a_u	Mathieu stability parameter in u dimension
BGE	Background electrolyte
BOE	Buffered oxide etchant
BPI	Base peak intensity
BSA	Bovine serum albumin
CAD	Computer assisted design
CE	Capillary electrophoresis
CEES	2-chloroethyl ethyl sulfide

CID	Collision induced dissociation
CIT	Cylindrical ion trap
cm	Centimeter
CVD	Chemical vapor deposition
CZE	Capillary zone electrophoresis
Da	Dalton
DC	Direct current
DRIE	Deep reactive ion etching
D_z	Pseudopotential well depth
e	Ion charge in Coulombs
EI	Electron ionization
EO	Electroosmotic
EOF	Electroosmotic flow
ESI	Electrospray ionization
FWHM	Full width at half maximum
GC	Gas chromatography
GDEI	Glow discharge electron ionization
GND	Ground
HbA1c	Glycated hemoglobin
HPMS	High pressure mass spectrometry
Hz	Hertz
ID	Inner diameter
in	Inch

K	Kelvin
kΩ	Kiloohm
kDa	Kilodalton
kV	Kilovolt
LB	Luria-Bertani
LC	Liquid chromatography
LOD	Limit of detection
LOQ	Limit of quantitation
m	Ion mass
$(M+H)^+$	Protonated molecule
mAb	Monoclonal antibody
MALDI	Matrix assisted laser desorption/ionization
MHz	Megahertz
min	Minute
mm	Millimeter
MS	Mass spectrometry
MS/MS	Tandem mass spectrometry
ms	Millisecond
m/z	Mass-to-charge ratio
nESI	Nano-electrospray ionization
nF	Nanofarad
nL	Nanoliter
nm	nanometer

OD	Outer diameter
OD_{600}	Optical density at 600 nm
P	Pressure
PCB	Printed circuit board
PE	Potential energy
PEG	Polyethylene glycol
PTFE	Teflon
q	Ion charge in solution
QA/QC	Quality assurance/quality control
QIT	Quadrupolar ion trap
q_u	Mathieu stability parameter in u dimension
r_0	Ion trap radius
r_h	Hydrodynamic radius
RIT	Rectilinear ion trap
RF	Radio frequency
s	Second
SDS	Statistical diffusion simulation
SLIT	Stretched length ion trap
S/N	Signal-to-noise
SPE	Solid phase extraction
SWaP	Size, weight, and power
SWIFT	Stored waveform inverse Fourier transform
TOF	Time-of-flight

UV	Ultraviolet
V	Volt
V_{0-p}	Zero-to-peak AC voltage
V_{p-p}	Peak-to-peak AC voltage
z_0	Axial trap dimension

Chapter 1: Introduction

1.1   Background and Motivation

Mass spectrometry (MS) is a powerful analytical technique due to its sensitivity, versatility, and ability to provide chemical and structural information of molecules and has long been the 'gold standard' for many types of chemical analyses. However, most MS systems are limited to centralized or academic laboratories because of their complexity and their size, weight, and power (SWaP) requirements. Because of the ability of MS to rapidly and reliably detect and identify molecules, there are many applications that would benefit from having an MS on-site. To that end, many research groups have developed miniature mass spectrometers for environmental monitoring,[1–3] explosives[4] and chemical warfare agent detection,[5,6] forensics,[7,8] and clinical analyses.[9] The primary limitation to the miniaturization/portability of these systems is the strenuous vacuum requirements to operate the mass analyzer at pressures much below atmosphere (<1 mTorr).

Since before the 2000's, the Ramsey group has been working to develop miniature mass spectrometers based on a technique called high pressure mass spectrometry (HPMS). Operation of the components of the mass spectrometer at high pressures (>1 Torr) greatly reduces the vacuum requirements such that turbomolecular pumps are no longer required, and the mass spectrometer can be operated using only mechanical pumps. While turbo pumps can produce low pressures necessary for most MS analysis, they are bulky, high-power, and expensive, which are

all undesirable qualities for a miniature mass spectrometer. Thus, moving to higher operational pressures and using mechanical pumps facilitates miniaturization.

The centerpiece of HPMS is the miniature ion trap mass analyzer. The use of miniature ion traps maintains practical voltage and power requirements for the high radio frequency (RF) drive signal required for HPMS. The development of mini-CITs and HPMS has led to a commercially available hand-held mass spectrometer from 908 Devices, Inc., primarily developed for threat detection of various gaseous and volatile analytes.

While previous HPMS work has used an electron ionization (EI) source, the use of electrospray ionization (ESI) expands the range of analytes to include biomolecules and other liquid-borne analytes.[10] In addition to broadening the number and type of analytes available for characterization by MS, ESI provides a method for coupling liquid-phase separations to MS systems. These separation steps prior to mass analysis can greatly aid in the identification and characterization of compounds and are necessary for the analysis of complex mixtures. As there is some loss in mass spectral resolution under HPMS conditions, a separation step prior to the MS is a method for recapturing some of the selectivity incurred by this loss. Currently, liquid chromatography separations coupled to MS (LC-MS) are the standard for many chemical analyses, but LC systems require large pumps and complex sets of valves and tubing, neither of which are amenable to a miniature analytical platform.

A smaller and simpler alternative to LC is microchip capillary electrophoresis. Microchip capillary electrophoresis (CE) was pioneered in the Ramsey lab separately but simultaneously to the development of miniature mass spectrometry. Initial research focused on fluorescence detection but these CE devices were eventually interfaced to commercial mass spectrometers via ESI. Since then, CE-MS research in the Ramsey lab has focused primarily on strategies for the

separation and detection of biomolecules, including surface chemistries for the microfluidic devices. Microfluidic CE-MS has been demonstrated for many biological and biochemical applications from the analysis of small molecules to intact antibodies. While the usefulness of microfluidic CE-ESI devices coupled with commercial mass spectrometers is proven, the small footprint, simplicity, and wide range of applications for these devices also make them excellent candidates for pairing with a miniature mass spectrometer.

The marriage of microfluidic CE and HPMS presents an opportunity for a fully miniature analysis platform for biomolecule analysis, which could provide a simple and inexpensive alternative to conventional LC-MS systems. The following sections detail the principles and strategies underlying HPMS and microfluidic CE, as well as considerations for an ESI interface to HPMS and its combination with microfluidic CE into a single analytical platform.

1.2   High Pressure Mass Spectrometry

1.2.1   Miniature Mass Analyzers

The miniaturization of the mass analyzer is central to the reduction in the overall size of the mass spectrometer. Nearly all types of common mass analyzers have been reduced in size to varying extents, including time-of-flight (TOF),[11,12] sector-type analyzers,[13,14] linear quadrupoles,[15,16] and many variations on quadrupolar ion traps.[17–20] Ion traps have been at the center of most miniaturization efforts for several reasons. First, their performance scales favorably with decreasing size as the dimensions of an ion trap do not fundamentally affect the mass resolution. Second, ion traps can be produced with simplified geometries, easing fabrication at reduced scales. CITs[18,21–23] and rectilinear ion traps (RITs)[19] consist of exclusively planar electrodes, giving them simple geometries compared with their hyperbolic counterparts,

but still produce useful MS data.[24,25] Third, ion traps have the ability to perform tandem mass spectrometry (MS/MS) with a single analyzer, which reduces the overall footprint of the instrument, reduces chemical noise, and increases the selectivity of the instrument. Finally, ion traps have significantly higher operating pressures than other mass analyzers (~1 mTorr compared to 10^{-4} Torr or lower). Operation at higher pressures is important for reducing the vacuum requirements in a miniature instrument. Because of their favorable scaling, simple geometry, and ability to perform MS/MS, ion traps were chosen as the mass analyzer for our miniaturization efforts.

1.2.2 Quadrupole Ion Traps (QITs)

The quadrupole ion trap was first introduced by Paul and Steinwedel in the 1950s[26] and became commercially available as a mass analyzer and detector for gas chromatography in 1983 from Finnigan, Corp.[27] A picture and a schematic of a QIT are shown in Figure 1.1 with the trap's size defined by the r_0 and z_0 dimensions labeled in Figure 1.1b. The r_0 parameter is the radius of the ring electrode, and z_0 is half the distance of the space between endcaps. The field in the trap is produced by voltages applied to the three electrodes, a ring and two endcaps. Ions enter and exit the trap via holes in each of the endcap electrodes. The hyperbolic shape of the electrodes produces a field that is largely quadrupolar.

In the QIT's normal mode of operation, an RF potential is applied to the ring electrode, and the endcaps are grounded. Ion motion in the quadrupolar field created by the voltages applied can be described by the second order differential Mathieu equation. A solution to the Mathieu equation in the axial (z) and radial (r) dimensions gives $a_z, q_z, a_r,$ and q_r, known as trapping parameters:[28]

$$a_z = -\frac{16eU}{m(r_0^2 + 2z_0^2)\Omega^2}$$

<div align="right">1.1</div>

$$q_z = \frac{8eV}{m(r_0^2 + 2z_0^2)\Omega^2}$$

<div align="right">1.2</div>

$$a_r = \frac{8eU}{m(r_0^2 + 2z_0^2)\Omega^2}$$

<div align="right">1.3</div>

$$q_r = -\frac{4eV}{m(r_0^2 + 2z_0^2)\Omega^2}$$

<div align="right">1.4</div>

where U is a DC potential applied to the ring electrode, e is the elementary charge of the ion, m is the mass of the ion, r_0 is the radius of the ring electrode, $2z_0$ is the endcap spacing, V is the drive RF voltage (0-p) amplitude applied to the ring electrode, and Ω is the angular RF frequency applied to the ring ($2\pi f$). Because the trapping parameters in each dimension are related to each other by a factor of two and opposite in sign, regions of radial (upward pointing) and axial stability (downward pointing) can be plotted in q_z and a_z space (Figure 1.2). Areas where the regions overlap are points at which ions can be stably trapped and are known as stability regions. Region A is of particular interest for use of the QIT as a mass analyzer, and a close-up of Region A from Figure 1.2 is shown in Figure 1.3.

When operated as a mass analyzer, ion traps are often operated without a DC potential on the ring, and therefore $a_z = 0$. Under these conditions, trapped ions lie along the q_z axis, with lower m/z ions having higher values of q for a given RF voltage and frequency, as shown in Equation 1.2. Ions can be ejected from the trap in order of increasing mass by ramping the

amplitude of the RF voltage, scanning the ions along the q_z axis until they reach the boundary of the stability region at $q_z = 0.908$ (shown in Figure 1.3). At $q_z > 0.908$, ions no longer have a stable trajectory in the axial dimension and are ejected through holes in the endcap electrodes. This type of scan is known as a mass-selective instability scan. The time and voltage at the point of ejection can be used to determine an ion's *m/z*.

1.2.3   Considerations for High Pressure Operation

As the pressure of the mass analyzer is increased to facilitate miniaturization, it is important to take into account the effects of pressure on MS performance. Two important measures for a mass spectrometer's analytical performance are its resolving power and its mass range. Resolving power for QIT, assuming slow scan conditions, can be expressed as:[29]

$$\frac{m}{\Delta m} \propto \frac{\Omega \tau}{4\sqrt{3}} \qquad\qquad 1.5$$

where *m* is the ion mass, *Δm* is the width of the mass spectral peak, *Ω* is the applied angular RF frequency, and *τ* is the collisional relaxation time, which is inversely proportional to the pressure (*P*) of the buffer gas. As a result, the resolving power can be expressed proportionally:

$$\frac{m}{\Delta m} \propto \frac{\Omega}{P} \qquad\qquad 1.6$$

Thus, in order to maintain resolving power, the operational frequency must be increased proportionally with the increased pressure. Increases in frequency improve the resolving power but result in a decreased mass range if all other parameters remain constant. The mass range can

be considered using the maximum mass that can be ejected from a trap (rearranged from

Equation 1.2):

$$\left(\frac{m}{z}\right)_{max} = \frac{8V_{max}}{q_{max}\Omega^2\left(r_0^2+2z_0^2\right)}$$

1.7

where z is the charge, m is the ion mass, V_{max} is the maximum amplitude of the RF voltage, q_{max}

is the trapping parameter and constant (usually 0.908), and r_0 and z_0 are the dimensional

parameters of the trap. To make up for the loss of mass range at increased frequencies, the drive

RF voltage can be increased or the dimensions of the trap can be decreased. There are, however,

practical limits to increasing the voltage, both due to the overall power constraints of a miniature

mass spectrometer and the possibility of electrical breakdown (arcing). Thus, decreasing the trap

size is necessary in order to increase the frequency and maintain practical voltages. For

comparison, typical QITs have r_0 of 1 cm and operate with a frequency around 1 MHz.

Therefore, an increase in frequency to 10 MHz would require a decrease in the size of the trap to

an r_0 of about 1 mm to maintain similar operating voltage.

1.2.4   Miniature Cylindrical Ion Traps (CITs)

Cylindrical ion traps produce similar trapping fields to QITs but with a simplified

geometry. CITs consist of two planar endcaps and a cylindrical ring electrode, and this simple

geometry makes them much more amenable to miniaturization than QITs. While ion trap

operation remains the same for CITs (RF applied to the ring electrode), the electric field

produced is slightly different than that of QITs. For QITs, the electrodes are hyperbolic and the

trapping field is largely quadrupolar, but some deviations from a purely quadrupolar field exist

due to truncation of electrodes to a finite size, endcap apertures, machining imperfections, and

often an intentional axial stretch to a non-ideal geometry. The trapping field in CITs is largely

similar to QITs but has more significant components of higher than quadrupolar order (due to

geometry simplifications), especially near the edges of the trap. To illustrate this point, simulated

equipotential lines for a QIT and CIT are shown in Figure 1.4.[30] Near the center of the trap, the

field in a CIT closely resembles that of a QIT, where higher order fields are weakest, and where

ions are typically found when trapped. At the edges of the CIT, deviation from quadrupolar

character are expected and higher order fields are strongest. These higher order fields can

contribute to a reduction in stability at higher q_z values.

Although they result in instability at higher q_z, higher order multipole fields can be used for

what is known as double resonance ejection.[31] A small axial RF voltage (with frequency ω) may

be applied to one or both endcaps to take advantage of these multipole fields. When the secular

frequency (or a harmonic) of the ions is doubly resonant with the frequency of the axial RF

signal and the frequency of nonlinear resonances in the trap, ions can be ejected from the trap.

The resonances occur at specific fractions of the drive RF frequency, most notably at ω = Ω/3

and 2Ω/3 (hexapolar), and Ω/4 (octopolar). The application of an axial RF voltage for resonant

ejection expands the mass range by reducing the ejection q_z and voltage necessary for ejection

and has been shown to improve both the resolution and signal intensity of the mass analyzer.

CITs at traditional QIT dimensions ($r_0 \approx 1$ cm) have been researched since the

1970s,[22,32,33] and miniaturization efforts began at least as early as 1991, with a CIT of

$r_0 = 2.5$ mm used as a mass analyzer.[24] Since then, the use of miniature CITs for mass

spectrometry applications was pioneered primarily by groups at Purdue[17] and Oak Ridge

National Laboratory.[18,34] MS miniaturization efforts at Purdue moved primarily to rectilinear ion

traps in the early 2000s.[19,35] At Oak Ridge, miniature ion traps were developed with sub-mm

dimensions,[18,34,36] with ion traps as small as $r_0 = 20$ μm fabricated and operated.[37]

1.2.5 Previous Work in High Pressure Mass Spectrometry

Operation of an ion trap mass spectrometer at higher than traditional pressures

(>1 mTorr) would facilitate miniaturization by reducing the pumping requirements to reach the

desired pressure. Cooks and Ouyang demonstrated that a rectilinear ion trap could be operated at

pressures up to 50 mTorr with helium as the buffer gas[38] and theoretically characterized mass

spectral performance at pressures up to 250 mTorr.[39] Other work from Cooks and Ouyang has

shown that ions can be trapped at high pressure (~1 Torr), but mass analysis was still performed

at low pressures (<10 mTorr) using a discontinuous atmospheric pressure interface (DAPI).[40]

The work described here aims to operate CITs at pressures near 1 Torr, where

turbomolecular pumps are no longer needed. As discussed in Section 1.2.3 and described

theoretically,[41] the frequency applied to the ion trap must be increased at higher pressures in

order to maintain reasonable mass resolution, with a corresponding decrease in trap size to

maintain practical voltages. Before operation at high pressure, the first steps in high frequency

operation of miniature ion traps were initially demonstrated at traditional buffer gas pressures

(~1 mTorr), to ensure that CITs could function as mass analyzers with higher frequencies.

Miniature cylindrical ion traps with radii between 0.5 and 2.5 mm were tested at low pressures

(~1 mTorr) by several research groups at frequencies from 1.6 to about 8 MHz.[17,31,34,36,42,43]

While miniaturization efforts have continued, mass analysis at pressures greater than 50 mTorr

remains relatively unexplored.

The first mass analysis with both high pressure and high frequency using a microscale

CIT has recently been demonstrated by Blakeman, *et al.*[44] The pressure was 1 Torr with helium

as the buffer gas, and the CIT had r_0 of 500 μm and was operated at up to 9.5 MHz. A filament

or yttria coated disc was used as an electron ionization (EI) source. Spectra of 2-chloroethyl ethyl

sulfide, a common chemical warfare agent simulant for mustard gas, at three pressures are shown

in Figure 1.5. As the helium buffer gas pressure was increased from 0.062 to 1.21 Torr, the peaks

broaden slightly, but the primary peaks in the spectrum remain visible at m/z 124 (molecular

ion), 89 (loss of chlorine), and 75 (loss of methyl chloride).

While the demonstration of HPMS in helium is a good step toward miniaturization,

operation of HPMS with ambient air as the buffer gas would eliminate the need for an external

gas source and further reduce the final size of the instrument. HPMS was demonstrated with

another $r_0 = 500$ μm CIT with a glow discharge ionization source in nitrogen and air buffer

gases.[45] Figure 1.6 shows mass spectra of p-xylene in helium, nitrogen and air buffer gases. The

peaks in nitrogen and air were significantly broader than those in helium. Isotopic features were

not visible in nitrogen and air, but three major features of p-xylene were observable around

m/z 106, 91, and 77, demonstrating that useful molecular information could still be obtained

using HPMS with air as a buffer gas.

The next steps for HPMS development, as suggested in Equations 1.6 and 1.7, is to

increase the drive frequency to improve mass resolution and decrease the size of the ion trap to

minimize RF voltage requirements. At 1 Torr of ambient air buffer gas, Blakeman showed that

peak widths of p-xylene could be improved from 5.5 to 0.8 m/z with increased drive frequency

and appropriate scaling of the trap.[46] The frequency was operated from 6.14 up to 59.44 MHz,

and traps were scaled down from $r_0 = 500$ μm to $r_0 = 100$ μm. While ion traps as small as

$r_0 = 20$ μm have been fabricated[37] and traps as small as $r_0 = 1$ μm theoretically studied,[47,48] the

CIT with r_0 of 100 μm is, at this point, the smallest used to perform mass spectrometry.

A major concern with the miniaturization of CITs is the loss of ion trapping capacity incurred at smaller dimensions, which in turn decreases the dynamic range of the mass analyzer. Dehmelt introduced an approximation for ion storage in a QIT:[49]

$$N_{max} = (2.8 \times 10^7) D_z z_0 \qquad\qquad 1.8$$

where N_{max} is the maximum number of ions that can be stored in the trap, z_0 is the axial dimension of the trap, and D_z is the pseudopotential well depth in the z direction, at low values of q_z given by:

$$D_z = \frac{q_z V}{8} \qquad\qquad 1.9$$

where q_z is the Mathieu parameter introduced in Equation 1.2 and V is the 0-to-peak trapping voltage applied to the ring electrode. From Equation 1.8, the capacity of the trap decreases linearly with trap size. One way to make up for lost ion trapping capacity and increase dynamic range of miniature CITs is to operate an array of CITs in parallel.[37,50,51] While arrays of CITs can increase the sensitivity, the primary drawback is the possibility of heterogeneity between each of the individual trapping elements, which could result in significant loss of mass resolution.

A recently developed alternative to arrays of CITs for improving the sensitivity of miniature ion traps is the stretched length ion trap, or SLIT, which stretches the CIT in the plane of the electrode.[52,53] A schematic showing the differences in geometry between the CIT and SLIT is shown in Figure 1.7. The operation of the SLIT is fundamentally the same as a CIT, with RF applied to the ring electrode and two grounded endcaps, just with a larger ion storage

volume. SLITs have been successfully operated as mass analyzers, and, at low pressure, SLITs have been demonstrated to have an order of magnitude better sensitivity than CITs without loss of resolution. In the same work, SLITs were shown to operate at 1 Torr with nitrogen as the buffer gas. To further improve the sensitivity of the mass analyzer, arrays of SLITs or a serpentine geometry could be implemented.

In addition to improving the sensitivity of miniature ion traps, improving the selectivity, or the ability to distinguish similar chemical components, is also of interest, especially at high buffer gas pressures, where mass resolution degrades. Ion traps have the ability to perform tandem mass spectrometry, and it has recently been demonstrated that MS/MS can be performed with both microscale CITs and SLITs at pressures up to 1 Torr with air as the buffer gas.[54] Hampton's work focused primarily on small organic analytes such as bromobenzene, trichlorbenzene, and N,N-dimethylaniline.

Thus far, all HPMS research with miniature ion traps has used an EI or glow discharge (GDEI) ion source. These sources produce ions using a high energy electron beam (EI) or plasma (GDEI), so the analytes must be in the gas phase prior to ionization and mass analysis. Thus, small volatile and gas phase analytes were the initial primary targets for HPMS analysis. However, HPMS could be applied to many more applications for the analysis of larger and/or nonvolatile molecules with changes in optimal operational parameters and a different ion source, such as ESI. In addition, coupling HPMS with ESI opens the possibility of including a liquid-phase separation step such as CE to further expand the utility of the technique.

1.3 Microchip Capillary Electrophoresis and Electrospray Ionization

The primary goal of this work is to optimize HPMS operation with ESI as the ion source, specifically microchip ESI devices. Because many of the applications for ESI-HPMS involve coupling HPMS with microchip capillary electrophoresis, a brief introduction to CE, microchip CE-ESI devices, and previous applications of microchip CE-ESI-MS is presented here.

1.3.1 Capillary Electrophoresis

Electrophoresis can be defined as the movement of electrically charged species in a conductive liquid medium under the influence of an electric field.[55] Initial developments using electrophoresis as the separation mechanism needed a solid support such as paper or gels to prevent convectional distortion of analyte bands.[56] While gel electrophoresis has been an extremely valuable asset to biological and biochemical research, its primary disadvantage is the speed of the separation, which is limited by Joule heating. In the early 1980s, Jorgenson and Lukacs showed that electrophoresis could be performed in free solution using narrow-bore, open tubular capillaries, termed capillary zone electrophoresis (CZE).[57–59] The high surface area-to-volume ratio gave these capillaries the ability to efficiently dissipate heat, and CZE separations could be performed with up to 30 kV applied at ambient temperature.

The typical instrumental setup for CZE has remained relatively unchanged since its introduction. A basic instrumental schematic for CZE is shown in Figure 1.8.[60] Two buffer reservoirs are in fluidic connection via a capillary, across which a potential is applied. The applied potential generates an electric field that drives the separation. After sample injection, analytes are separated based on their apparent mobility (μ_{app}), which is the sum of both their electrophoretic mobility (μ_{EP}) and the electroosmotic mobility of the system (μ_{EO}):

13

$$\mu_{app} = \mu_{EP} + \mu_{EO} \qquad\qquad 1.10$$

The electrophoretic mobility of an analyte ion is dependent on the charge of the ion (q), the viscosity of the solution (η), and the hydrodynamic radius of the ion (r_h):

$$\mu_{EP} = \frac{q}{6\pi\eta r_h} \qquad\qquad 1.11$$

Thus, CZE separates analytes based on their charge to size ratio and conformation in solution. A smaller, more highly charged particle will migrate faster than a larger, less charged particle.

The electroosmotic mobility of an analyte depends on the electroosmotic flow (EOF) produced in the capillary. EOF arises from the formation of an electrical double layer at the wall of the capillary. Briefly, the double layer consists of an immobile layer of counter ions of opposite charge to those fixed to the wall and a diffuse layer, containing a high concentration of mobile counter ions. When an electric field is generated across the capillary, the mobile counter ions will migrate, generating bulk fluid flow in the capillary via viscous drag. In an uncoated silica capillary, the surface silanol groups are usually negatively charged, so the double layer consists of an immobile layer of cations and a diffuse layer of cations. When a voltage is applied, the mobile cations in the diffuse layer will migrate toward the cathode. Thus, if the magnitude of the EOF is great enough, all species (anions, cations, and neutrals) will migrate in the same direction.

1.3.2   Microchip Capillary Electrophoresis

About a decade after the development of CZE, capillary electrophoresis was performed on glass or silicon microchips fabricated with micromachining techniques pioneered by the

semiconductor industry.[61–67] Performing CE in planar microchannels (10-100 μm) with high aspect ratios (width to height) provided the same Joule heat dissipation advantages of small-bore capillaries.[68,69] One of the primary advantages of microchip CE over traditional CZE is the ability to incorporate many steps of analysis on a single device, and for this reason, initial devices were termed μ-total analysis systems.[69,70]

The devices used for this work are adapted from this initial work on microchips, with the primary difference being the monolithic integration of an ESI emitter onto the device. A typical device is shown in Figure 1.9.[60] The channels are created in glass using photolithography and wet etching, and the fabrication process is described in detail in Appendix I. The device incorporates four important elements onto a single platform: an injection cross, the separation channel, the pumping channel, and the integrated ESI emitter.

The injection cross provides a simple method for sample handling and injection prior to CE separation. This strategy has been used previously and is common for microfluidic architectures.[62,65,68] Compared to conventional CZE, this method of sample introduction is simpler and faster, resulting in less band broadening. Normal methods of injection for CZE usually involve moving the sample or buffer reservoirs, which can be mechanically complicated and can result in diffusional broadening before voltage is applied for the separation. By contrast, sample handling on the microfluidic platform is performed without complex moving parts. Injections on the microchip are performed either electrokinetically or hydrodynamically, described in detail in Appendix II. For electrokinetically gated injections, appropriate voltages are applied to all reservoirs to gate the sample in reservoir 1 towards the waste reservoir (3) and then switched to balance reservoirs 2 and 3, injecting sample into the separation channel. After an appropriate plug has been injected, the voltages are switched to the initial conditions to

15

perform the separation. Electrokinetic injections are simple and very fast but can result in sample

injection bias if analytes have significantly different electrophoretic mobilities. In contrast,

hydrodynamic injections are slower but do not produce any sample introduction bias. For

hydrodynamic injections, all voltages are turned off and pressure is applied to reservoirs 2

(sample) and 1 (buffer) resulting in sample being directed into the separation channel. After a

short time, pressure is only applied to reservoir 1 to load the sample band completely into the

separation channel. Voltages are then applied to reservoirs 1 and 4 and pressure removed from

reservoir 2 and normal zone electrophoresis occurs.

The separation channel pictured in Figure 1.9 is typically 23 cm in length with six turns

to minimize the footprint of the device. The turns are asymmetrically tapered (see inset) in order

to minimize geometric dispersion known as the "racetrack effect."[71–73] The racetrack effect refers

to turns with uniform channel dimensions where analytes on the inside of the turn migrate

significantly faster than analytes on the outside of the turn, resulting in a wider overall band. The

effect can be reduced by increasing the turn radius or as done here reducing the width of the

channel. The separation channel and pumping channel join just before terminating at the corner

of the device, which acts as the integrated ESI emitter.

Many research groups have worked to interface microchip platforms with ESI. Strategies

for developing this interface include spraying from the flat surface of a microchip,[74,75] inserting

an electrospray emitter,[68,76,77] or monolithic integration of an emitter.[78–80] Of these, monolithic

integration of the emitter would be best to minimize band broadening and preserving ESI

integrity, but many strategies for monolithic integration involve complex fabrication. A simple

solution to this complex fabrication problem was a variation on spraying from a surface of the

microchip introduced by Mellors, *et al.*, where electrospray was performed from the corner of

the glass substrate.[81] The sensitivity and stability of the ESI source using this strategy was found to be comparable to typical pulled capillary emitters with no detectable band broadening. Thus, the portion of the device involving the ESI emitter has remained relatively unchanged since its introduction in 2008.

The final element of the microfluidic ESI device is the pumping channel, labeled in Figure 1.9. To perform ESI, bulk fluid flow and an emitter with an applied voltage are necessary. For these microchips, the pumping channel intersects the separation channel near the electrospray emitter and serves both of these purposes. The voltage applied at reservoir 4 completes the circuit for performing CE and simultaneously provides the voltage necessary for ESI to occur. The pumping channel also provides the bulk fluid flow necessary for ESI, either via an applied head pressure or using an electroosmotic pumping strategy involving different surface coatings in the separation and pumping channels.[74,81]

The architecture shown in Figure 1.9 has remained relatively unchanged since its initial development and has been used for many applications, providing high efficiency separations with the added benefit of MS detection. Efficient surface coatings[82] have enabled the use of these microfluidic devices for many biological applications including 2D separations (LC-CE) of peptides and proteins,[83] characterization of monoclonal antibodies and antibody drug conjugates,[84,85] study of hemoglobin glycation for diabetes diagnostics,[86] and hydrogen-deuterium exchange to study protein structure.[87] Because of their small platform, simple operation, and ability to perform high efficiency separations, these microfluidic CE-ESI devices are ideal candidates to pair with a miniature HPMS-based mass spectrometer.

1.4 Design Considerations for CE-ESI-HPMS

Because all previous HPMS analysis has involved an EI or GDEI ion/ionization source, there are additional design considerations for ESI-HPMS analysis. First, ions must be efficiently transported from atmospheric pressure into the vacuum chamber containing the mass analyzer. Previously, ions were generated in the same chamber as the mass analyzer or already in the trapping volume. After transport into the chamber containing the mass analyzer, externally generated ions must be trapped, so the reduced pseudopotential well depth of miniature ion traps may be of concern. Finally, parameters for operation of the mass analyzer must be adjusted to accommodate significantly higher mass and higher m/z ions. Thus far, mass analysis has focused on small organic ions of less than about 150 m/z, and those ions are usually singly charged, meaning the masses are also usually less than 150 Da. One of the advantages of ESI is the ability to volatilize and ionize large species that are often multiply charged, so HPMS conditions will have to be optimized to accommodate analysis of these species.

1.4.1 Ion Source and Ion Transport to the Mass Analyzer

The sensitivity of an ESI-MS system is dependent upon the ionization efficiency of the source as well as the efficiency of ion transport to the mass analyzer, often through multiple vacuum stages. A typical ESI-MS system has an emitter and an inlet capillary or orifice to conduct ions into the first vacuum stage. Improvements to the ESI source itself have largely focused on reducing the flow rate of the electrospray to improve sensitivity. Termed nano-ESI (nESI), the reduction in flow rate subsequently reduces the size of the droplets produced, and therefore fewer collisions and less evaporation is required for the desolvation of analyte ions.[88–90] Ionization efficiency for nESI approaches 100% in the low nL/min flow regime, but on-line separations typically operate at higher flow rates.[91,92]

18

Despite improvements in the ion source and ionization efficiency, the primary limitation of the sensitivity of ESI-MS systems is in the transport of ions to the mass analyzer. A significant portion of analyte ions are lost due to limited flow or collisions with surfaces at the inlet or other conductance limits in the instrument.[93–95] Ion transmission efficiencies from ESI source to detector are reported in the $0.01 - 0.1\%$ range.[96–100] Strategies to improve sensitivity include using larger bore capillaries or apertures,[101] multiple inlet capillaries and/or nESI sources,[102,103] different capillary or aperture geometries,[104,105] performing nESI in the first vacuum stage of the mass spectrometer (sub-ambient ESI),[95,106–108] and improved ion optics in each vacuum region of the mass spectrometer. Large ID capillaries and multiple ESI emitters improve sensitivity but significantly increase the pumping requirements of the mass spectrometer. Special capillary geometries can be difficult to fabricate, and performing ESI below atmospheric pressure becomes complex with a microchip as the ionization source. For these reasons, ESI-HPMS development has focused on the ion optics that transport ions throughout the mass spectrometer.

Ion funnels are of particular interest as an ion transport strategy for HPMS. The ion funnel was first developed at Pacific Northwest National Laboratory in the late 1990's by Dick Smith's group as a way of transporting ions with near 100% efficiency through the first pumping stage (typically 0.1 to 30 Torr) of a mass spectrometer.[109] Many improvements have been made to ion funnels since their development, but most of the overall features remain the same. Ion funnels consist of a stack of concentric, closely spaced ring electrodes decreasing in diameter to a conductance-limiting electrode, radially confining the ions' trajectories. A pair of RF voltages 180 degrees out of phase are applied to each adjacent electrode, and a DC gradient is usually applied along the axis of the funnel to propel ions towards the conductance limiting electrode. Because of their excellent ion transfer efficiency and high pressure operation range, ion funnels

are ideal candidates to use with ESI-HPMS. It is important to note that ion funnels, while extremely efficient for many large species, suffer from poor ion transmission of low m/z (<200) species. For small molecule applications of HPMS, other ion transport strategies, such as DC-only optics, will be investigated.

1.4.2   External Ion Trapping

All HPMS work to date has used an EI or GDEI source, targeting gaseous and volatile analytes. Analytes are introduced into the mass spectrometer and ionized after entering the vacuum chamber. Because the analytes are already in the vacuum chamber (and often already in the trapping volume) when ionized, they have only a small amount of kinetic energy and can be easily trapped by the oscillating field of the CIT. For ESI, ions are generated at atmospheric pressure and must be transported into the vacuum chamber and the mass analyzer. Because the ions must be transported to the mass analyzer, they will likely have significantly more kinetic energy than ions generated inside the vacuum chamber. Recalling Equation 1.9, the pseudopotential well depth is a function of the dimension of the trap (via q_z), and miniature CITs used for HPMS have reduced dimensions, and therefore reduced well depths, compared to conventional ion traps. The well depth affects not only the trapping capacity, but also limits the maximum possible kinetic energy of an ion that can be trapped. The increased kinetic energy of externally generated ions may make them more difficult to trap in the pseudopotential well of the CIT and must be considered carefully for ESI-HPMS.

The trapping of externally generated ions in QITs has been considered extensively. Methods to trap external ions include "static trapping," where the RF amplitude is constant throughout the injection period (traditional operation), and "dynamic trapping," a strategy to improve trapping where the amplitude of the drive RF is adjusted during ejection to most

20

efficiently trap ions.[110–113] Other methods to increase the number of trapped ions include simply increasing the flux of ions entering the trap with better optics (ion transfer efficiency, as in Section 1.4.1) and increasing the mass or pressure of the buffer gas to reduce the kinetic energy of the ions.[112,114] The strategy of increasing the pressure of the buffer gas is of particular interest for HPMS. In this case, if ions can be efficiently transported to the mass analyzer, the increased pressure of HPMS may aid in the trapping of externally generated ions by reducing their kinetic energy.

Externally generated ions have been trapped and analyzed under HPMS conditions both with glow discharge and EI. Cavanaugh demonstrated that ions could be produced and trapped with a filament 90 degrees off-axis from the axial dimension of the trap. Cavanaugh and Blakeman have both shown that the polarity of the glow discharge source can be reversed from EI operation to produce and accelerate ions toward the trap for mass analysis.[46,115] While trapping externally generated ions in these cases shows promise, ions were still always produced in the same chamber as the mass analyzer. In contrast, ions produced by ESI outside of the vacuum chamber must undergo an additional transport step.

1.4.3   Trapping and Analyzing Ions of High Mass and *m/z*

An important feature of ESI is the ability to ionize molecules of high mass, especially peptides and proteins. Previous work with HPMS focused on the analysis of small molecules. Given the limited mass range of ion traps, parameters have to be adjusted to accommodate ions of higher *m/z*. Recalling Equation 1.7, the mass range depends on the applied voltage, the RF frequency, and the size of the trap. In order to trap ions with *m/z* values higher than previously analyzed (>150), appropriate scaling of these parameters is necessary. The voltage could be increased, but this is impractical for a miniature system for the same reasons discussed above.

21

The frequency can be decreased but must be sufficiently high (enough RF cycles per collision) to trap ions at HPMS pressures. Finally, the size of the trap can be decreased further. Blakeman used traps as small as $r_0 = 100$ μm but increased the frequency to have roughly the same mass range and improve resolution.[46] Traps of that size could be used for ESI-HPMS of larger molecules if the frequency were decreased, with the likely tradeoff of decreased mass resolution. For example, an order of magnitude decrease in frequency (i.e. 60 to 6 MHz) would result in a 100-fold increase in the largest mass possible to be ejected, all else being equal. Thus, ESI-HPMS analysis will consist of appropriately scaling the size of the trap, frequency, and voltage depending on the mass and m/z of the analyte.

In addition to higher m/z, ions from ESI are typically larger in mass and are multiply charged. As a result, space charge effects in ESI related to mass resolution and ion storage capacity will have to be considered. SLIT geometries will likely need to be employed in order to accommodate the larger, more highly charged ions. A possible benefit of the analysis of larger ions compared to smaller analytes is the relative size of the buffer gas, especially when air is used. The primary components of air (nitrogen, oxygen) have relatively high masses compared to many volatile and gaseous analytes, and scattering of ions in the trap and in ion transport can be problematic. Larger species like proteins will have a large mass relative to the buffer gas, so it is possible that they will be less scattered and more efficiently trapped than ions of lower mass.

1.5   Current ESI-Miniature MS Interfaces

Many miniature MS platforms have been developed for ESI and other atmospheric pressure ionization techniques. Many of these systems are covered in a recent review,[116] so only a few ESI-MS systems will be discussed here. Most of the miniature MS systems are designed

for direct infusion of analytes, without a separation step beforehand. Many of the miniature systems use ambient ionization techniques such as desorption electrospray ionization (DESI) or paper spray ionization, which can provide useful information but would be difficult to use for complex mixtures.[9,117] In addition, these systems still operate the mass analyzer at <10 mTorr pressures so the strenuous pumping requirements for an atmospheric inlet necessitates the use of a turbo pump for all of these platforms. One proposed solution to breaking the pumping barrier is to introduce ions discontinuously with a technique called discontinuous atmospheric pressure ionization, or DAPI.[9,118] DAPI instruments use a pinch valve in the center of a capillary so that ions are collected and trapped in a linear ion trap at high pressure when the valve is opened. The valve is then closed, the mass analysis chamber is pumped down to a low pressure (<10 mTorr), then mass analysis is performed. Instruments developed using DAPI show promise, but they suffer from poor sampling rates (~1 Hz) and a power-hungry turbo pump is still required for mass analysis.

A miniature CE separation has been coupled to a miniature mass spectrometer using a DAPI inlet, using a short capillary and nESI source.[119] This system uses conventional silica capillaries for CE, and migration times were slow, so the low sampling rate of the DAPI configuration was adequate for their analysis. In addition, the system suffers from the conventional complexities of CE-ESI including injection and a sheath-flow interface. Finally, the system still requires a turbo pump and low pressures for mass analysis.

A microchip CE-HPMS platform should provide several advantages over other similar miniature analytical platforms. HPMS reduces the pumping requirements and aids in reducing the size and cost of the instrument. Operation at high pressure should also facilitate continuous

sampling, increasing the duty cycle of the instrument. The microchip CE platform is simple to operate, has a small footprint, and produces high efficiency and rapid separations.

1.6   Objectives

The primary objective of this work is to develop a miniature CE-MS platform integrating the microchip CE-ESI and HPMS technologies. Chapter 2 focuses on the initial efforts and development involved in integrating microchip CE-ESI with HPMS, including ion transport and tandem mass spectrometry of electrosprayed species. Chapter 3 discusses improvements and modifications made for the analysis of small molecules, specifically focusing on amino acids. Chapter 4 presents further modifications and optimization of optics and operational conditions for the analysis of large biomolecules, including intact proteins. The final chapter consists of conclusions and future directions.

1.7　Figures

A

B

Ring

Endcaps

z_0

r_0
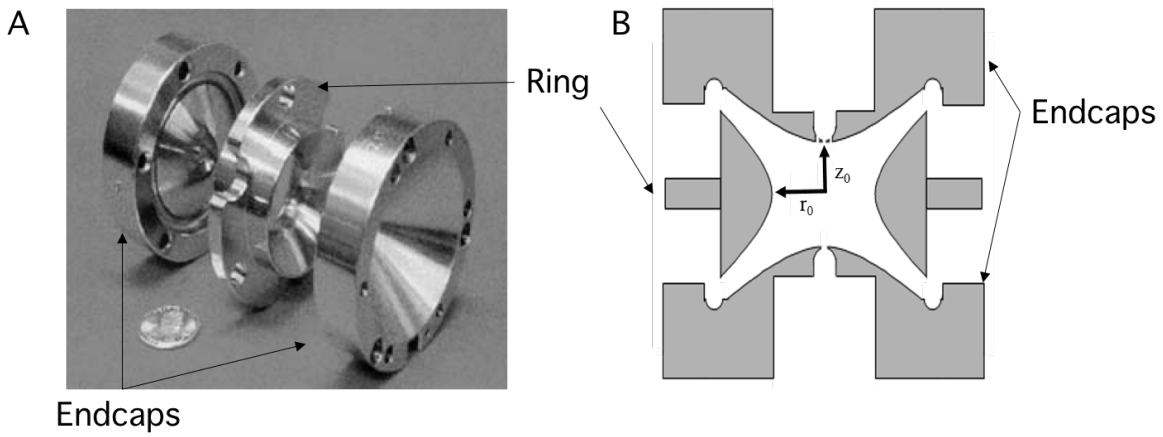
Endcaps

Figure 1.1: A) Picture of quadrupolar ion trap electrodes and B) Cross-sectional schematic of quadrupolar ion trap. The trap consists of a ring electrode and two endcaps. The dimensions of the trap are defined by the radial (r_0) and axial (z_0) dimensions shown in the schematic.
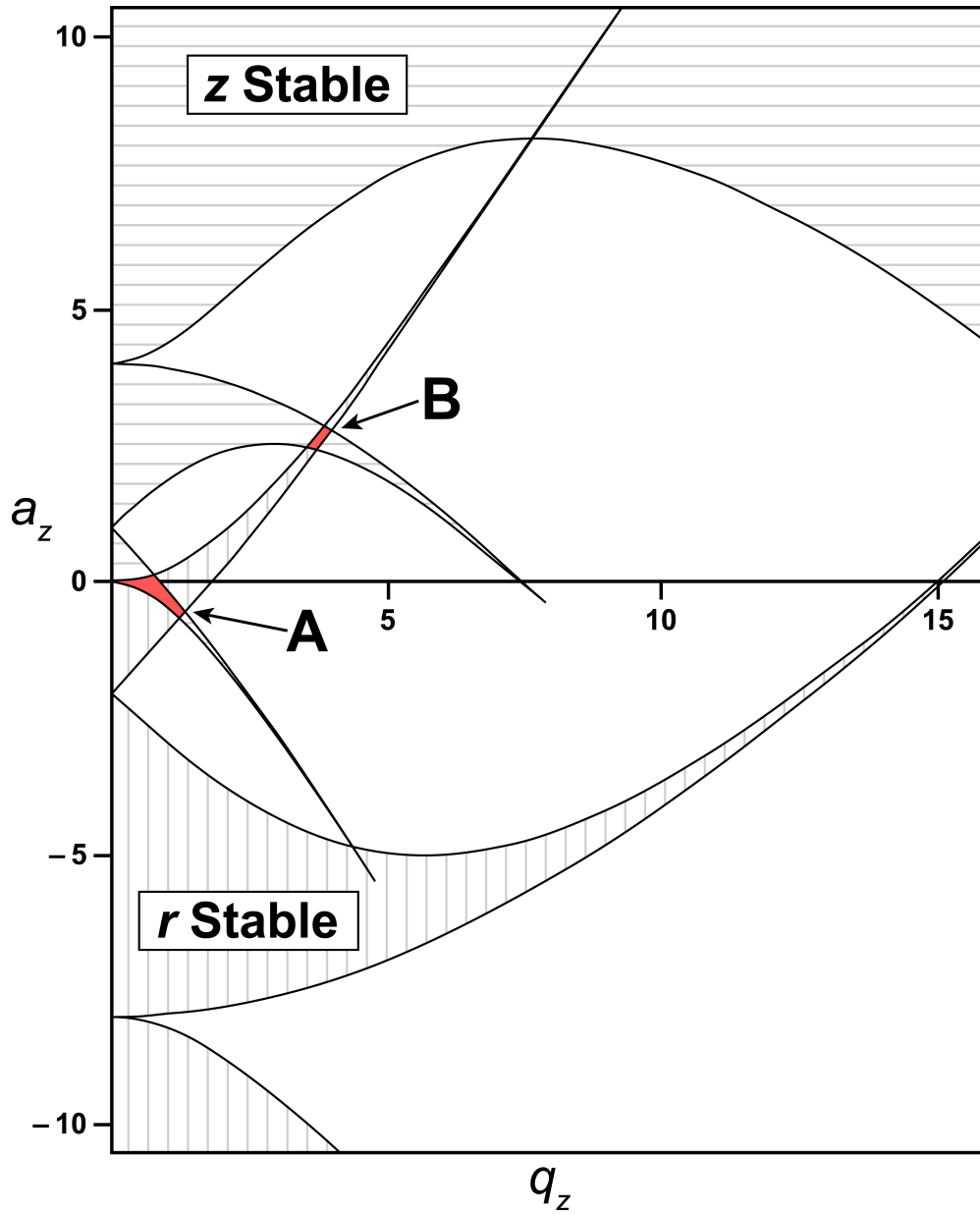
Figure 1.2: Theoretical regions of radial (*r*) and axial (*z*) stability for a quadrupolar ion trap, ploted in a_z, q_z space. The areas labeled A and B correspond to important overlapping regions of *r* and *z* stability, where ions are stably trapped (reprinted from reference 120).
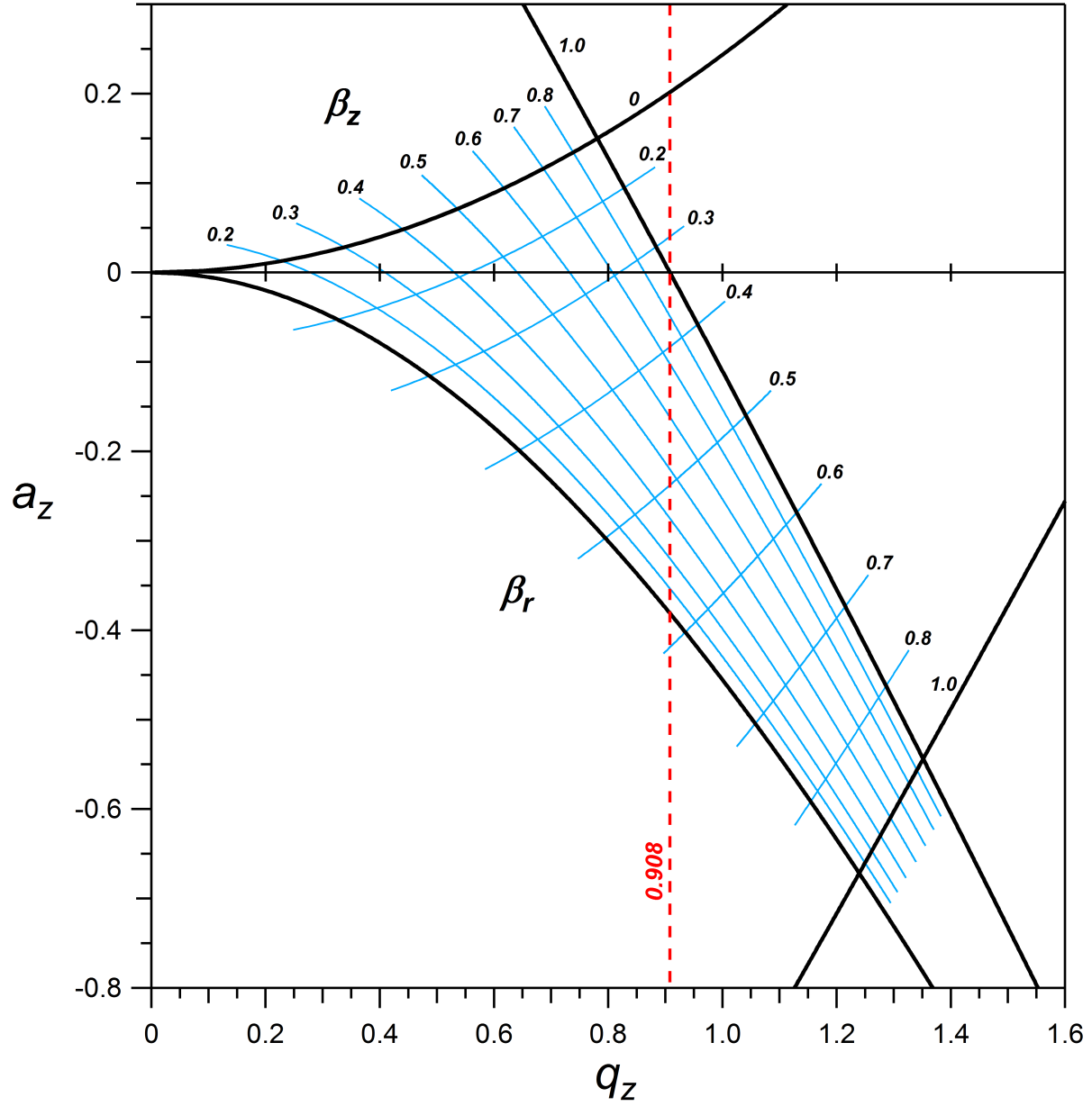
Figure 1.3: Zoom of region A from Figure 1.2, shown with iso-β lines, a parameter corresponding to the motion of the ion in the trap. Ions are stably trapped in the region bounded by the solid black lines. Under normal ion trap operational conditions with no DC voltage, ions lie along the q_z axis. The voltage can be ramped and ions become unstable in order of increasing m/z at the point where q_z is 0.908, labeled in the figure (reprinted from reference 120).
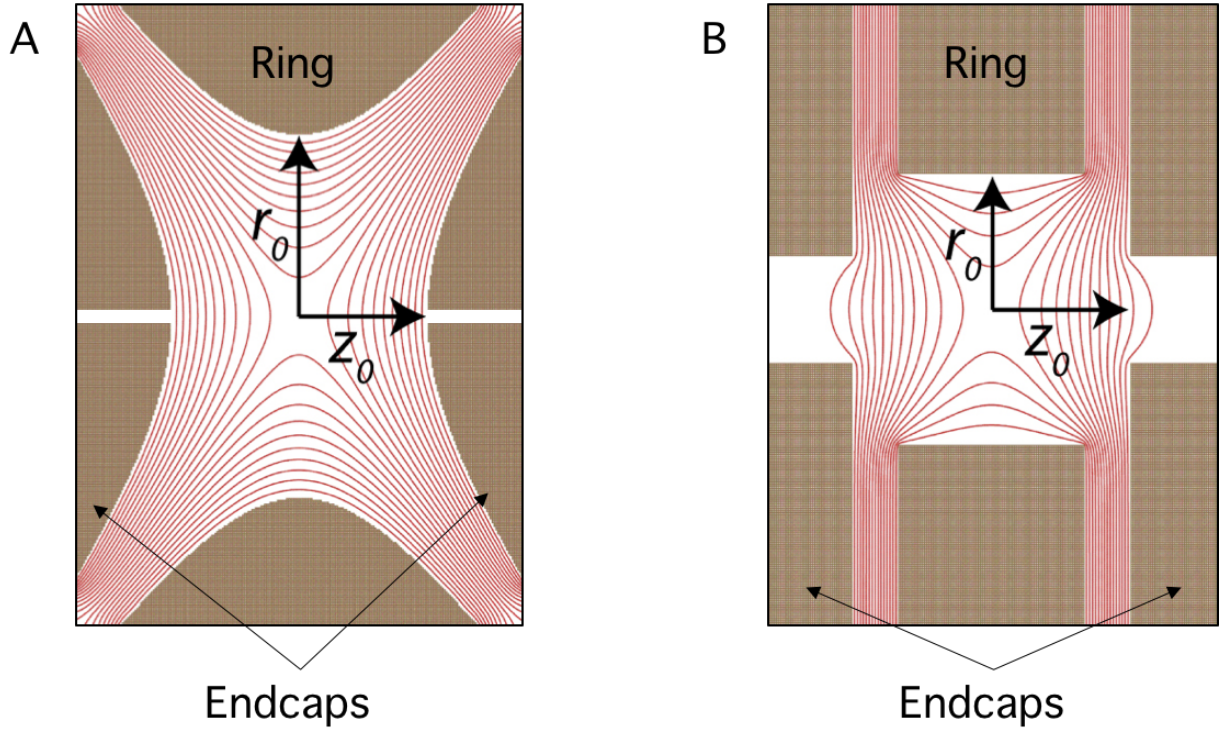
Figure 1.4: Equipotential lines for A) Quadrupole ion trp with hyperbolic electrodes where $r_0 = 10$ mm, $z_0 = 7.07$ mm and B) Cylindrical ion trap with planar electrodes and $r_0 = z_0 = 5.0$ mm. Near the center of the CIT, the field is largely quadrupolar (reprinted from reference 19).
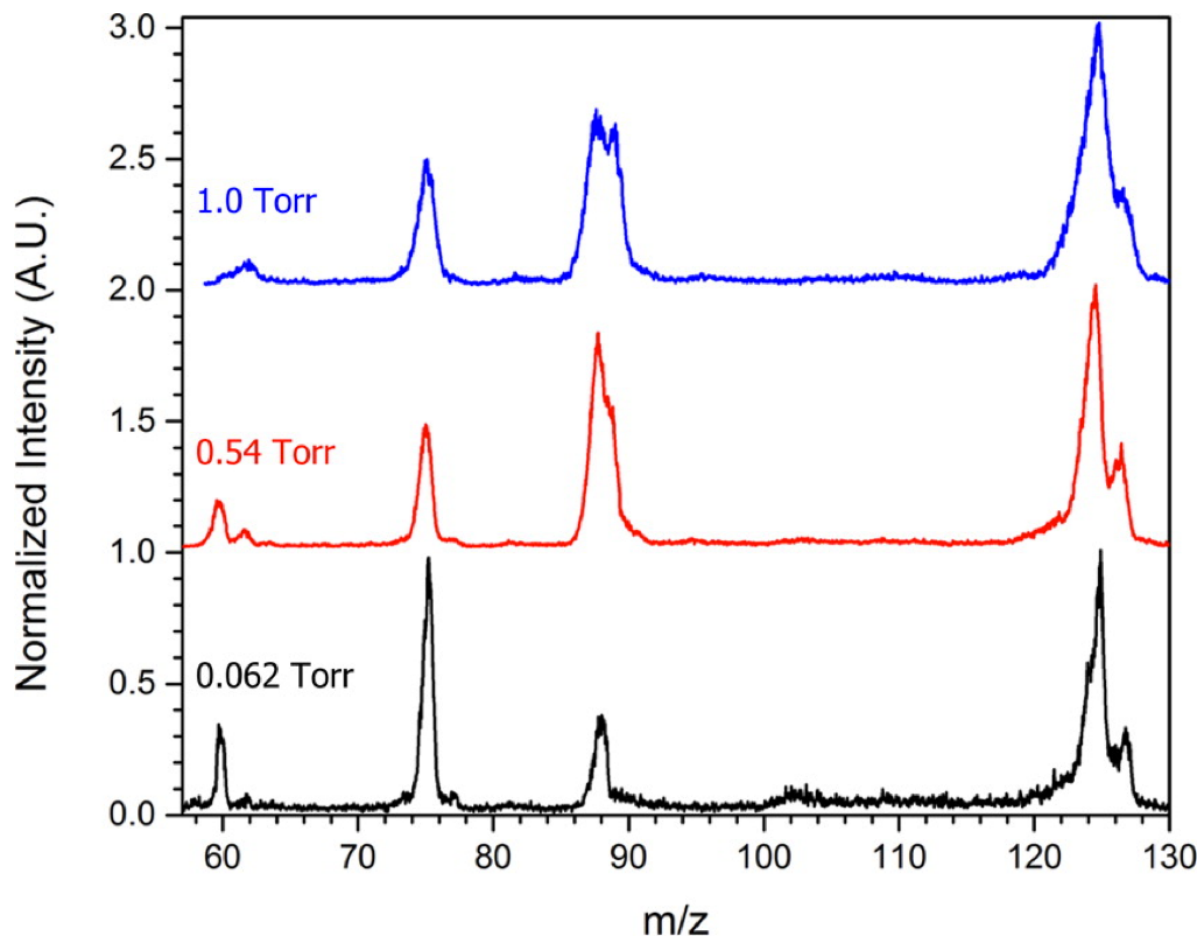
Figure 1.5: Effects of pressure on mass spectra of 2-chloroethyl ethyl sulfide (CEES) in helium buffer gas with CIT r_0 = 500 μm and RF at 6.73 MHz (reprinted from reference 46).
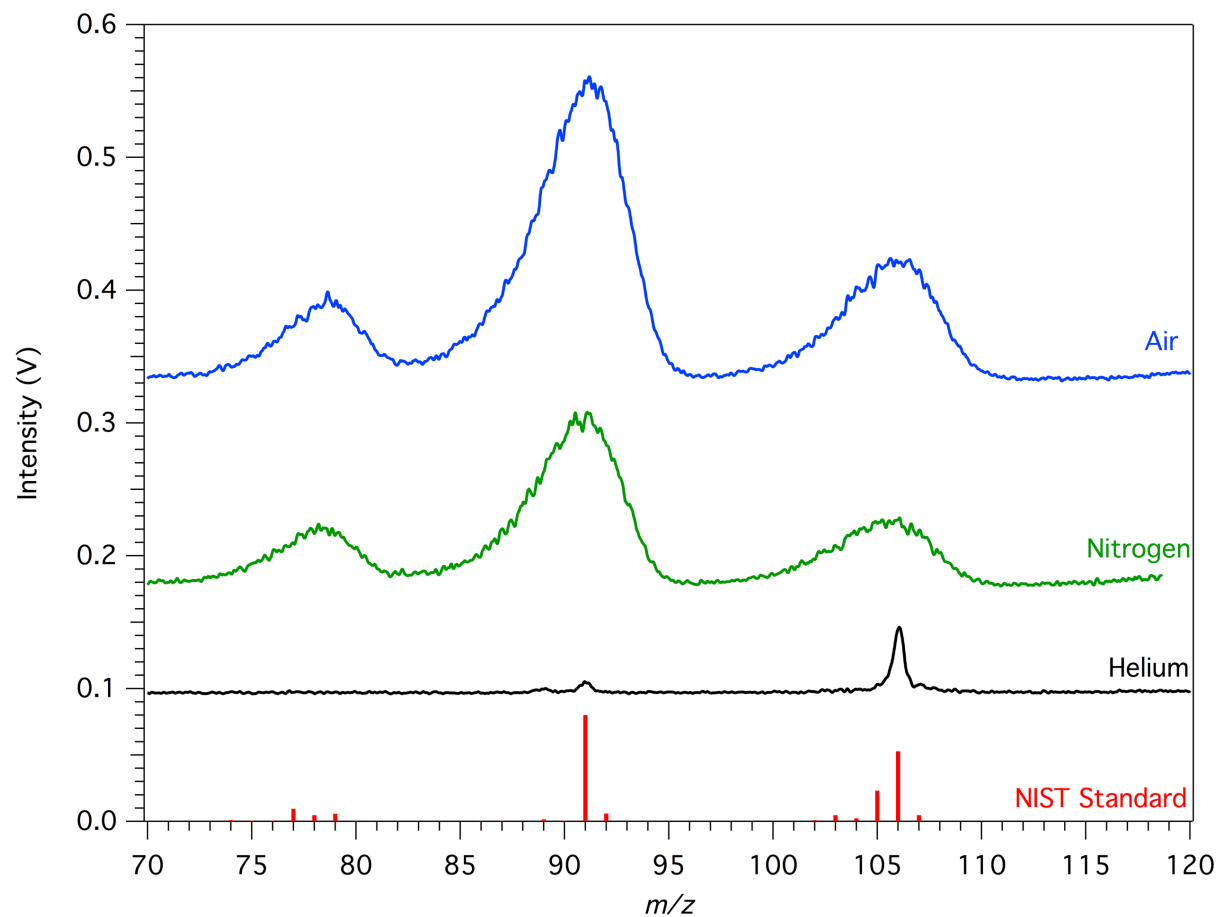
Figure 1.6: Effects of buffer gas composition on mass spectra of *p*-xylene at 1 Torr with a CIT of $r_0 = 500$ μm and RF at 10.0 MHz (reprinted from reference 46).
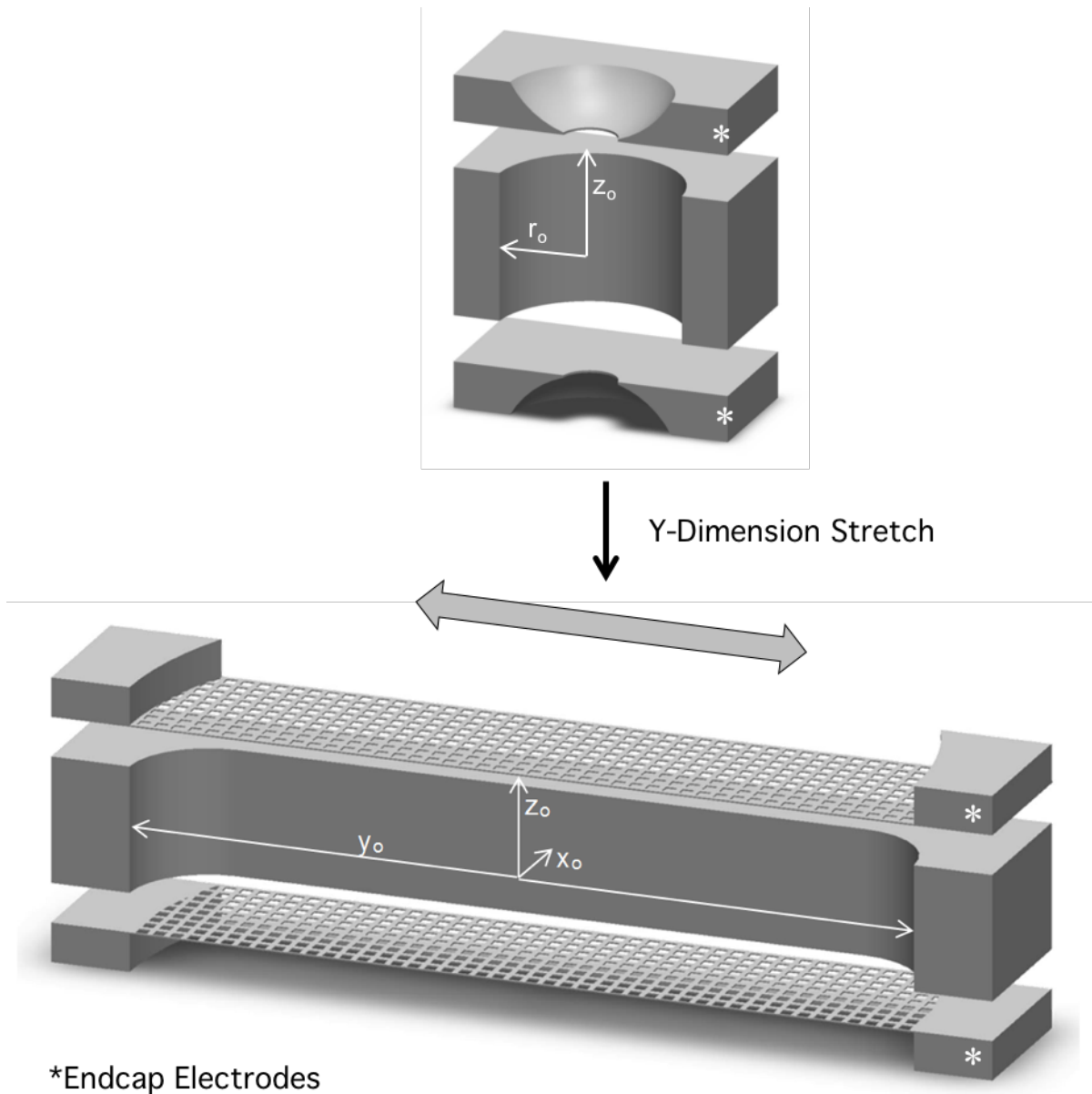
Figure 1.7: 3D cross-section of CIT (top) and SLIT (bottom). Both traps consist of a ring electrode and two endcap electrodes. The SLIT operates the same as the CIT but is stretched in the y-dimension labeled in the figure (reprinted from reference 52).
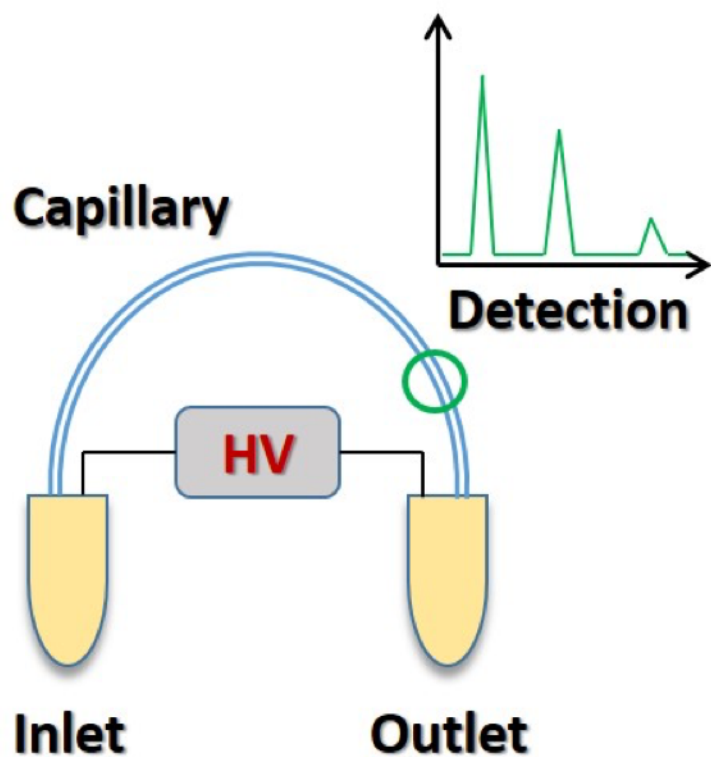
Figure 1.8: Traditional setup for capillary electrophoresis. Two buffer reservoirs are connected by a capillary, and high voltage is applied between the inlet and the outlet. Species migrate and optical detection (green circle) is performed near the outlet of the capillary (reprinted from reference 60).
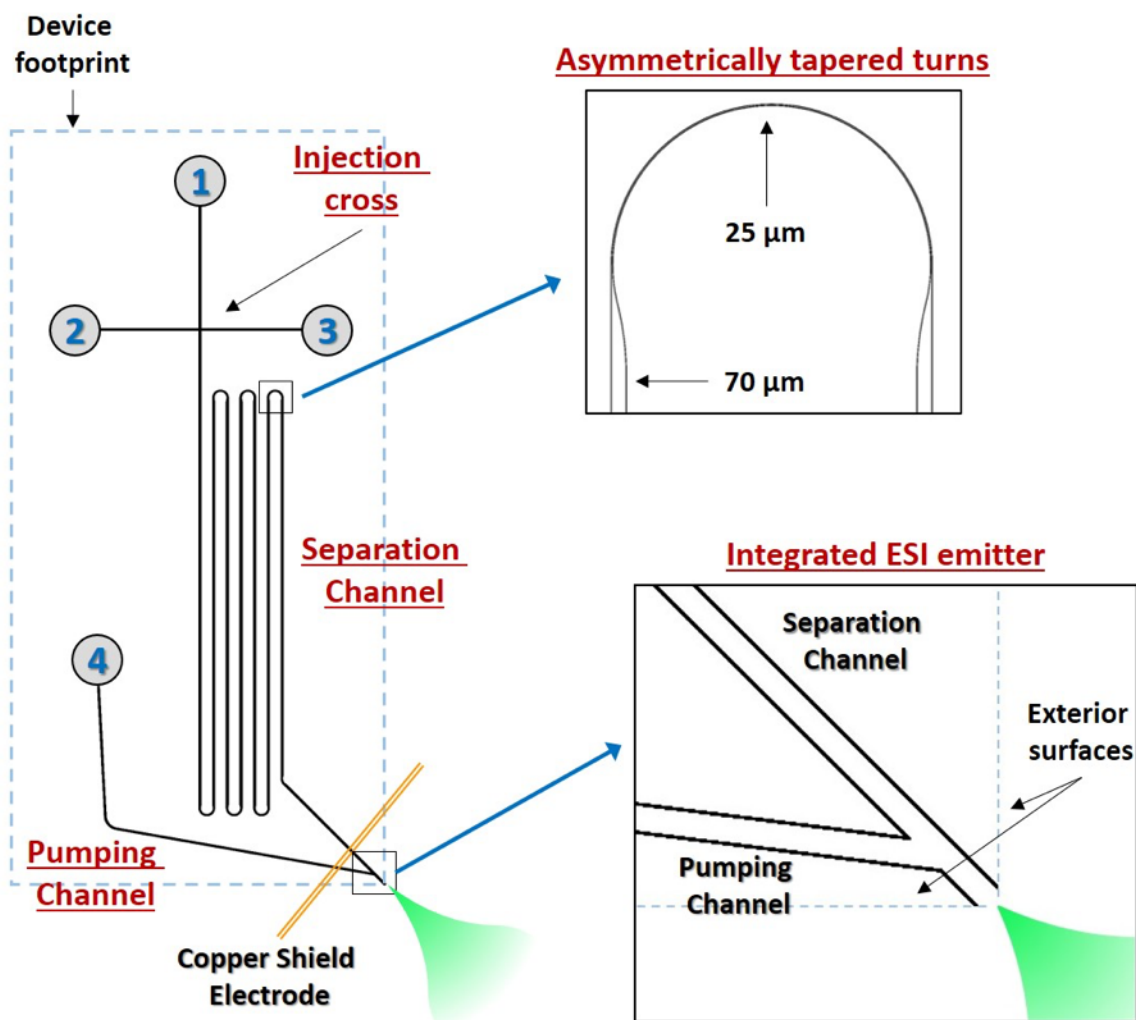
Figure 1.9: Schematic of a typical CE-ESI microchip device. The device consists of buffer reservoirs (labeled with numbers), an injection cross, a serpentine separation channel with asymmetically tapered turns (see inset), a pumping channel that intersects the separation channel near the corner of the device, and an integrated ESI emitter (see inset). A copper electrode is used to isolate the voltage at the ESI emitter and the voltages applied to the reservoirs (reprinted from reference 60).

1.8   REFERENCES

(1)   Pulliam, C. J.; Bain, R. M.; Wiley, J. S.; Ouyang, Z.; Cooks, R. G. *J. Am. Soc. Mass Spectrom.* **2015**, *26* (2), 224–230.

(2)   Bell, R. J.; Davey, N. G.; Martinsen, M.; Collin-Hansen, C.; Krogh, E. T.; Gill, C. G. *J. Am. Soc. Mass Spectrom.* **2015**, *26* (2), 212–223.

(3)   Mach, P. M.; Wright, K. C.; Verbeck, G. F. *J. Am. Soc. Mass Spectrom.* **2015**, *26* (2), 281–285.

(4)   Dalgleish, J. K.; Hou, K.; Ouyang, Z.; Cooks, R. G. *Anal. Lett.* **2012**, *45* (11), 1440–1446.

(5)   Nagashima, H.; Kondo, T.; Nagoya, T.; Ikeda, T.; Kurimata, N.; Unoke, S.; Seto, Y. *J. Chromatogr. A* **2015**, *1406*, 279–290.

(6)   Smith, J. N.; Noll, R. J.; Cooks, R. G. *Rapid Commun. Mass Spectrom.* **2011**, *25* (10), 1437–1444.

(7)   Ifa, D. R.; Jackson, A. U.; Paglia, G.; Cooks, R. G. *Anal. Bioanal. Chem.* **2009**, *394* (8), 1995–2008.

(8)   Sanders, N. L.; Kothari, S.; Huang, G.; Salazar, G.; Cooks, R. G. *Anal. Chem.* **2010**, *82* (12), 5313–5316.

(9)   Li, L.; Chen, T.-C.; Ren, Y.; Hendricks, P. I.; Cooks, R. G.; Ouyang, Z. *Anal. Chem.* **2014**, *86* (6), 2909–2916.

(10)   Whitehouse, C. M.; Dreyer, R. N.; Yamashita, M.; Fenn, J. B. *Anal. Chem.* **1985**, *57* (3), 675–679.

(11)   Bryden, W. A.; Benson, R. C.; Ecelberger, S. A.; Phillips, T. E.; Cotter, R. J.; Fenselau, C. *Johns Hopkins Apl Tech. Dig.* **1995**, *16* (3), 296–310.

(12)   Cornish, T. J.; Bryden, W. A. *Johns Hopkins APL Tech. Dig. Appl. Phys. Lab.* **1999**, *20* (3), 335–341.

(13)   Sinha, M. P.; Wadsworth, M. *Rev. Sci. Instrum.* **2005**, *76* (2), 25103.

(14)   Diaz, J. A.; Giese, C. F.; Gentry, W. R. *J. Am. Soc. Mass Spectrom.* **2001**, *12* (6), 619–632.

(15)   Syms, R. R. A.; Tate, T. J.; Ahmad, M. M.; Taylor, S. *IEEE Trans. Electron Devices* **1998**, *45* (11), 2304–2311.

(16)   Taylor, S.; Tunstall, J. J.; Leck, J. H.; Tindall, R. F.; Jullien, J. P.; Batey, J.; Syms, R. R. A.; Tate, T.; Ahmad, M. M. *Vacuum* **1999**, *53* (1), 203–206.

(17)   Badman, E. R.; Johnson, R. C.; Plass, W. R.; Cooks, R. G. *Anal. Chem.* **1998**, *70* (23),

4896–4901.

(18)   Kornienko, O.; Reilly, P. T. A.; Whitten, W. B.; Ramsey, J. M. *Rapid Commun. Mass Spectrom.* **1999**, *13* (1), 50–53.

(19)   Ouyang, Z.; Wu, G.; Song, Y.; Li, H.; Plass, W. R.; Cooks, R. G. *Anal. Chem.* **2004**, *76* (16), 4595–4605.

(20)   Ouyang, Z.; Noll, R. J.; Cooks, R. G. *Anal. Chem.* **2009**, *81* (7), 2421–2425.

(21)   J. Mitchell Wells; Ethan R. Badman, A.; Cooks, R. G.; Wells, J. M.; Badman, E. R.; Cooks, R. G. *Anal. Chem.* **1998**, *70* (3), 438–444.

(22)   Bonner, R. F.; Fulford, J. E.; March, R. E.; Hamilton, G. F. *Int. J. Mass Spectrom. Ion Phys.* **1977**, *24* (3), 255–269.

(23)   Chaudhary, A.; van Amerom, F. H. W.; Short, R. T. *Int. J. Mass Spectrom.* **2014**, *371*, 17–27.

(24)   Kaiser, R. E.; Graham Cooks, R.; Stafford, G. C.; Syka, J. E. P.; Hemberger, P. H. *Int. J. Mass Spectrom. Ion Process.* **1991**, *106*, 79–115.

(25)   Kaiser, R. E.; Cooks, R. G.; Moss, J.; Hemberger, P. H. *Rapid Commun. Mass Spectrom.* **1989**, *3* (2), 50–53.

(26)   Paul, W.; Steinwedel, H. *Zeitschrift für Naturforsch. A* **1953**, *8* (7), 448–450.

(27)   March, R. E. *Mass Spectrom. Rev.* **2009**, *28* (6), 961–989.

(28)   March, R. E. *J. Mass Spectrom.* **1997**, *32* (4), 351–369.

(29)   Goeringer, D. E.; Whitten, W. B.; Ramsey, J. M.; McLuckey, S. A.; Glish, G. L. *Anal. Chem.* **1992**, *64* (13), 1434–1439.

(30)   Ouyang, Z.; Wu, G.; Song, Y.; Li, H.; Plass, W. R.; Cooks, R. G.; Zheng Ouyang; Wu, G.; Song, Y.; Li, H.; Wolfgang R. Plass, A.; Cooks, R. G. *Anal. Chem.* **2004**, *76* (16), 4595–4605.

(31)   Moxom, J.; Reilly, P. T. A.; Whitten, W. B.; Ramsey, J. M. *Rapid Commun. Mass Spectrom.* **2002**, *16* (8), 755–760.

(32)   Benilan, M.-N.; Audoin, C. *Int. J. Mass Spectrom. Ion Phys.* **1973**, *11* (5), 421–432.

(33)   Mather, R. E.; Waldren, R. M.; Todd, J. F. J.; March, R. E. *Int. J. Mass Spectrom. Ion Phys.* **1980**, *33* (3), 201–230.

(34)   Kornienko, O.; Reilly, P. T. A.; Whitten, W. B.; Ramsey, J. M. *Rev. Sci. Instrum.* **1999**, *70* (10), 3907.

(35)   Gao, L.; Song, Q.; Patterson, G. E.; Cooks, R. G.; Ouyang, Z. *Anal. Chem.* **2006**, *78* (17), 5994–6002.

(36)   Moxom, J.; Reilly, P. T. A.; Whitten, W. B.; Ramsey, J. M. *Anal. Chem.* **2003**, *75* (15), 3739–3743.

(37)   Pau, S.; Pai, C. S.; Low, Y. L.; Moxom, J.; Reilly, P. T. A.; Whitten, W. B.; Ramsey, J. M. *Phys. Rev. Lett.* **2006**, *96* (12), 120801.

(38)   Song, Q.; Xu, W.; Smith, S. A.; Gao, L.; Chappell, W. J.; Cooks, R. G.; Ouyang, Z. *J. Mass Spectrom.* **2010**, *45* (1), 26–34.

(39)   Xu, W.; Song, Q.; Smith, S. A.; Chappell, W. J.; Ouyang, Z. *J. Am. Soc. Mass Spectrom.* **2009**, *20* (11), 2144–2153.

(40)   Gao, L.; Cooks, R. G.; Ouyang, Z. *Anal. Chem.* **2008**, *80* (11), 4026–4032.

(41)   Whitten, W. B.; Reilly, P. T. A.; Ramsey, J. M. *Rapid Commun. Mass Spectrom.* **2004**, *18* (15), 1749–1752.

(42)   Moxom, J.; Reilly, P. T. A.; Whitten, W. B.; Ramsey, J. M. *Rapid Commun. Mass Spectrom.* **2004**, *18* (6), 721–723.

(43)   Pau, S.; Whitten, W. B.; Ramsey, J. M. *Anal. Chem.* **2007**, *79* (17), 6857–6861.

(44)   Blakeman, K. H.; Wolfe, D. W.; Cavanaugh, C. A.; Ramsey, J. M. *Anal. Chem.* **2016**, *88* (10), 5378–5384.

(45)   Blakeman, K. H.; Cavanaugh, C. A.; Gilliland, W. M.; Ramsey, J. M. *Rapid Commun. Mass Spectrom.* **2016**, *31* (1), 27–32.

(46)   Blakeman, K. Development of High Pressure Mass Spectrometry for Handheld Instruments, University of North Carolina at Chapel Hill, 2015.

(47)   Blain, M. G.; Riter, L. S.; Cruz, D.; Austin, D. E.; Wu, G.; Plass, W. R.; Cooks, R. G. *Int. J. Mass Spectrom.* **2004**, *236* (1–3), 91–104.

(48)   Tian, Y.; Higgs, J.; Li, A.; Barney, B.; Austin, D. E. *J. Mass Spectrom.* **2014**, *49* (3), 233–240.

(49)   Dehmelt, H. G. *Adv. Atom. Mol. Phys.*; Academic Press, 1967.

(50)   Badman, E. R.; Cooks, R. G. *Anal. Chem.* **2000**, *72* (14), 3291–3297.

(51)   Amy M. Tabert; Jens Griep-Raming; Andrew J. Guymon, A.; Cooks, R. G.; Tabert, A. M.; Griep-Raming, J.; Guymon, A. J.; Cooks, R. G. *Anal. Chem.* **2003**, *75* (21), 5656–5664.

(52)   Schultze, K. P. Advanced System Components for the Development of a Handheld Ion

Trap Mass Spectrometer, University of North Carolina at Chapel Hill, 2014.

(53)   Ramsey, J. M.; Schultze, K. P. Miniature charged particle trap with elongated trapping region for mass spectrometry. US8878127B2, 2014.

(54)   Hampton, A. Improving the Selectivity of High Pressure Mass Spectrometry, University of North Carolina at Chapel Hill, 2016.

(55)   Baker, D. R. *Capillary electrophoresis*; Wiley, 1995.

(56)   Landers, J. P. *Handbook of capillary electrophoresis*; CRC Press, 1997.

(57)   Jorgenson, J.; Lukacs, K. *Science (80-.)*. **1983**, *222* (4621), 266–272.

(58)   Jorgenson, J. W.; Lukacs, K. D. *J. Chromatogr. A* **1981**, *218*, 209–216.

(59)   Jorgenson, J. W.; Lukacs, K. D. *Anal. Chem.* **1981**, *53* (8), 1298–1302.

(60)   Redman, E. A. Development of a Microfluidic Capillary Electrophoresis-Mass Spectrometry Platform for the Characterization of Biotherapeutic Proteins, University of North Carolina at Chapel Hill, 2016.

(61)   Manz, A.; Harrison, D. J.; Verpoorte, E. M. J.; Fettinger, J. C.; Paulus, A.; Lüdi, H.; Widmer, H. M. *J. Chromatogr. A* **1992**, *593* (1), 253–258.

(62)   Seiler, K.; Harrison, D. J.; Manz, A. *Anal. Chem.* **1993**, *65* (10), 1481–1488.

(63)   Harrison, D. J.; Manz, A.; Fan, Z.; Luedi, H.; Widmer, H. M. *Anal. Chem.* **1992**, *64* (17), 1926–1932.

(64)   Jacobson, S. C.; Koutny, L. B.; Hergenroeder, R.; Moore, A. W.; Ramsey, J. M. *Anal. Chem.* **1994**, *66* (20), 3472–3476.

(65)   Jacobson, S. C.; Hergenroder, R.; Koutny, L. B.; Warmack, R. J.; Ramsey, J. M. *Anal. Chem.* **1994**, *66* (7), 1107–1113.

(66)   Jacobson, S. C.; Hergenroeder, R.; Koutny, L. B.; Ramsey, J. M. *Anal. Chem.* **1994**, *66* (14), 2369–2373.

(67)   Jacobson, S. C.; Hergenroder, R.; Koutny, L. B.; Ramsey, J. M. *Anal. Chem.* **1994**, *66* (7), 1114–1118.

(68)   Lazar, I. M.; Ramsey, R. S.; Jacobson, S. C.; Foote, R. S.; Ramsey, J. M. *J. Chromatogr. A* **2000**, *892* (1–2), 195–201.

(69)   *Capillary Electrophoresis-Mass Spectrometry (CE-MS): Principles and Applications*; de Jong, G., Ed.; Wiley-VCH Verlag GmbH & Co. KGaA: Weinheim, Germany, 2016.

(70)   Manz, A.; Graber, N.; Widmer, H. M. *Sensors Actuators B Chem.* **1990**, *1* (1), 244–248.

(71)   Culbertson, C. T.; Jacobson, S. C.; Ramsey, J. M. *Anal. Chem.* **1998**, *70* (18), 3781–3789.

(72)   Griffiths, S. K.; Nilson, R. H. *Anal. Chem.* **2001**, *73* (2), 272–278.

(73)   Molho, J. I.; Herr, A. E.; Mosier, B. P.; Santiago, J. G.; Kenny, T. W.; Brennen, R. A.; Gordon, G. B.; Mohammadi, B. *Anal. Chem.* **2001**, *73* (6), 1350–1360.

(74)   Ramsey, R. S.; Ramsey, J. M. *Anal. Chem.* **1997**, *69* (6), 1174–1178.

(75)   Xue, Q.; Foret, F.; Dunayevskiy, Y. M.; Zavracky, P. M.; McGruer, N. E.; Karger, B. L. *Anal. Chem.* **1997**, *69* (3), 426–430.

(76)   Li, J.; Kelly, J. F.; Chernushevich, I.; Harrison, D. J.; Thibault, P. *Anal. Chem.* **2000**, *72* (3), 599–609.

(77)   Lazar, I. M.; Ramsey, R. S.; Sundberg, S.; Ramsey, J. M. *Anal. Chem.* **1999**, *71* (17), 3627–3631.

(78)   Svedberg, M.; Pettersson, A.; Nilsson, S.; Bergquist, J.; Nyholm, L.; Nikolajeff, F.; Markides, K. *Anal. Chem.* **2003**, *75* (15), 3934–3940.

(79)   Licklider, L.; Wang, X.-Q.; Desai, A.; Tai, Y.-C.; Lee, T. D. *Anal. Chem.* **2000**, *72* (2), 367–375.

(80)   Kameoka, J.; Orth, R.; Ilic, B.; Czaplewski, D.; Wachs, T.; Craighead, H. G. *Anal. Chem.* **2002**, *74* (22), 5897–5901.

(81)   Mellors, J. S.; Gorbounov, V.; Ramsey, R. S.; Ramsey, J. M. *Anal. Chem.* **2008**, *80* (18), 6881–6887.

(82)   Batz, N. G.; Mellors, J. S.; Alarie, J. P.; Ramsey, J. M. *Anal. Chem.* **2014**, *86* (7), 3493–3500.

(83)   Mellors, J. S.; Black, W. A.; Chambers, A. G.; Starkey, J. A.; Lacher, N. A.; Ramsey, J. M. *Anal. Chem.* **2013**, *85* (8), 4100–4106.

(84)   Redman, E. A.; Batz, N. G.; Mellors, J. S.; Ramsey, J. M. *Anal. Chem.* **2015**, *87* (4), 2264–2272.

(85)   Redman, E. A.; Mellors, J. S.; Starkey, J. A.; Ramsey, J. M. *Anal. Chem.* **2016**, *88* (4), 2220–2226.

(86)   Redman, E. A.; Ramos-Payan, M.; Mellors, J. S.; Ramsey, J. M. *Anal. Chem.* **2016**, *88* (10), 5324–5330.

(87)   Black, W. A.; Stocks, B. B.; Mellors, J. S.; Engen, J. R.; Ramsey, J. M. *Anal. Chem.* **2015**, *87* (12), 6280–6287.

(88)   Wilm, M.; Mann, M. *Anal. Chem.* **1996**, *68* (1), 1–8.

(89) El-Faramawy, A.; Siu, K. W. M.; Thomson, B. A. *J. Am. Soc. Mass Spectrom.* **2005**, *16* (10), 1702–1707.

(90) Schmidt, A.; Karas, M.; Dülcks, T. *J. Am. Soc. Mass Spectrom.* **2003**, *14* (5), 492–500.

(91) Smith, R. D.; Shen, Y.; Tang, K. *Acc. Chem. Res.* **2004**, *37* (4), 269–278.

(92) Ibrahim, Y.; Tang, K.; Tolmachev, A. V.; Shvartsburg, A. A.; Smith, R. D. *J. Am. Soc. Mass Spectrom.* **2006**, *17* (9), 1299–1305.

(93) Lin, B.; Sunner, J. *J. Am. Soc. Mass Spectrom.* **1994**, *5* (10), 873–885.

(94) Page, J. S.; Kelly, R. T.; Tang, K.; Smith, R. D. *J. Am. Soc. Mass Spectrom.* **2007**, *18* (9), 1582–1590.

(95) Cox, J. T.; Marginean, I.; Smith, R. D.; Tang, K. *J. Am. Soc. Mass Spectrom.* **2015**, *26* (1), 55–62.

(96) Kebarle, P.; Tang, L. *Anal. Chem.* **1993**, *65* (22), 972A–986A.

(97) Zook, D. R.; Bruins, A. P. *Int. J. Mass Spectrom. Ion Process.* **1997**, *162* (1), 129–147.

(98) Zhou, L.; Yue, B.; Dearden, D. V.; Lee, E. D.; Rockwood, A. L.; Lee, M. L. *Anal. Chem.* **2003**, *75* (21), 5978–5983.

(99) Page, J. S.; Tang, K.; Smith, R. D. *Int. J. Mass Spectrom.* **2007**, *265* (2), 244–250.

(100) Yu, Q.; Diao, Z.; Ni, K.; Qian, X.; Tang, F.; Wang, X. *Rapid Commun. Mass Spectrom.* **2015**, *29* (11), 1055–1061.

(101) Schneider, B. B.; Javaheri, H.; Covey, T. R. *Rapid Commun. Mass Spectrom.* **2006**, *20* (10), 1538–1544.

(102) Kelly, R. T.; Page, J. S.; Marginean, I.; Tang, K.; Smith, R. D. *Current* **2008**, *80* (14), 5660–5665.

(103) Jiang, L.; Moini, M. *Anal. Chem.* **2000**, *72* (1), 20–24.

(104) Pauly, M.; Sroka, M.; Reiss, J.; Rinke, G.; Albarghash, A.; Vogelgesang, R.; Hahne, H.; Kuster, B.; Sesterhenn, J.; Kern, K.; Rauschenbach, S. *Analyst* **2014**, *139* (8), 1856.

(105) Krutchinsky, A. N.; Padovan, J. C.; Cohen, H.; Chait, B. T. *J. Am. Soc. Mass Spectrom* **2015**, *26*, 659–667.

(106) Cox, J. T.; Marginean, I.; Kelly, R. T.; Smith, R. D.; Tang, K. *J. Am. Soc. Mass Spectrom.* **2014**, *25* (12), 2028–2037.

(107) Page, J. S.; Tang, K.; Kelly, R. T.; Smith, R. D. *Anal. Chem.* **2008**, *80* (5), 1800–1805.

(108) Marginean, I.; Page, J. S.; Tolmachev, A. V.; Tang, K.; Smith, R. D. *Anal. Chem.* **2010**, *82* (22), 9344–9349.

(109) Schaffer, S. A.; Tang, K.; Anderson, G. A.; Prior, D. C.; Udseth, H. R.; Smith, R. D. *Rapid Commun. Mass Spectrom.* **1997**, *11* (16), 1813–1817.

(110) Doroshenko, V. M.; Cotter, R. J. *Rapid Commun. Mass Spectrom.* **1993**, *7* (9), 822–827.

(111) Chambers, D. M.; Goeringer, E.; Mcluckey, S. A.; Glisht, G. L. *Anal. Chem.* **1993**, *65* (15), 14–20.

(112) McLuckey, S. A.; Van Berkel, G. J.; Goeringer, D. E.; Glish, G. L. *Anal. Chem.* **1994**, *66* (13), 689A–696A.

(113) Qin, J.; Chait, B. T. *Anal. Chem.* **1996**, *68* (13), 2102–2107.

(114) Louris, J. N.; Amy, J. W.; Ridley, T. Y.; Cooks, R. G. *Int. J. Mass Spectrom. Ion Process.* **1989**, *88* (2), 97–111.

(115) Cavanaugh, C. A. The Microionizer - A Solid State Ion Source for High Pressure Mass Spectrometry, University of North Carolina at Chapel Hill, 2016.

(116) Snyder, D. T.; Pulliam, C. J.; Ouyang, Z.; Cooks, R. G. *Anal. Chem.* **2016**, *88* (1), 2–29.

(117) Adam Keil; Nari Talaty; Christian Janfelt; Robert J. Noll; Liang Gao; Zheng Ouyang, and; Cooks*, R. G.; Keil, A.; Talaty, N.; Janfelt, C.; Noll, R. J.; Gao, L.; Ouyang, Z.; Cooks, R. G. *Anal. Chem.* **2007**, *79* (20), 7734–7739.

(118) Gao, L.; Sugiarto, A.; Harper, J. D.; Cooks, R. G.; Ouyang, Z. *Anal. Chem.* **2008**, *80* (19), 7198–7205.

(119) He, M.; Xue, Z.; Zhang, Y.; Huang, Z.; Fang, X.; Qu, F.; Ouyang, Z.; Xu, W. *Anal. Chem.* **2015**, *87* (4), 2236–2241.

(120) Chernookiy, D. Optimization of the Cylindrical Ion Trap Geometry for Mass Analysis at High Pressure, University of North Carolina at Chapel Hill, 2016.

Chapter 2: Initial Development of Electrospray Ionization Coupled with High Pressure Mass Spectrometry

2.1   Introduction

Since its initial development, electrospray ionization (ESI) has significantly expanded the range of mass spectrometric analysis from gas phase and volatile molecules to include biomolecules and other liquid-borne analytes.[1,2] ESI provides a facile method for coupling liquid phase separations, such as liquid chromatography (LC) or capillary electrophoresis (CE) with mass spectrometry (MS) detection.[3,4] As a result, LC-MS has become a widely used analytical tool in fields such as proteomics,[5] environmental monitoring,[6,7] drug discovery and development,[8] and clinical diagnostics.[9,10] Despite their usefulness, conventional LC-MS systems are usually confined to dedicated laboratories because they are large, expensive, complex, and require significant amounts of power. The development of a smaller, less expensive, and simpler liquid phase separation/MS analytical platform could be applied to many of the same fields as traditional LC-MS systems, with the added potential for on-site analysis. The miniaturization of LC systems is limited by the need for a rugged system of pumps, valves, and tubing, while mass spectrometers are limited by low pressure operation, which requires bulky, fragile, and expensive turbomolecular pumps. Many recent efforts have been made towards the miniaturization of both liquid phase separations and mass spectrometry,[11,12] including a miniature CE separation system coupled with a miniature MS system.[13] The combination of miniature separations platforms and mass spectrometry could be a low-cost, targeted alternative to conventional instrumentation.

With the goal of a fully miniature separation-MS analysis system, this chapter describes the first steps in coupling microfabricated ESI devices with high pressure mass spectrometry (HPMS).

Microfluidic-based ESI devices have small sample volumes, short analysis times, flow rates easily coupled to MS, and a small form factor that fits within the goal of a miniature analytical platform.[14] Previous work from the Ramsey lab produced glass microchips with high performance, monolithically integrated ESI emitters that are also simple to fabricate. These devices were used to perform CE separations for many biomolecule analyses, with the separation channel terminating at the corner of the device that acts as an ESI emitter, resulting in a microchip-MS interface with no detectable band broadening.[15–17] These microchips can be controlled with only DC voltage, have a small footprint (~2.5 x 6 cm), and give high efficiency separations, making them excellent candidates for a miniature CE-MS system.

Recently, high pressure mass spectrometry has been demonstrated as a viable method for the miniaturization of mass spectrometry.[18,19] The strategy for HPMS utilizes miniature cylindrical ion traps (CITs) with sub-mm critical dimensions operated at elevated drive frequencies compared to conventional ion traps. Previous HPMS work focused on gas phase analysis of small organic analytes or xenon, with the maximum m/z analyzed not extending beyond 150 m/z. Most analytes of interest (proteins, peptides, amino acids) for ESI are substantially larger in size, so mass range considerations of the CIT are important. The mass range for a quadrupolar ion trap can be expressed as the maximum m/z ion that can be ejected from the trap:[20]

$$\left(\frac{m}{z}\right)_{max} = \frac{8V_{max}}{q_{max}\Omega^2_{RF}(r_0^2 + 2z_0^2)} \qquad 2.1$$

where V_{max} is the maximum RF drive voltage, $q_{max} = 0.908$ is a trapping parameter and constant, Ω_{RF} is the drive frequency ($2\pi f$), r_0 is the radius of the trap, and z_0 is the axial dimension of the trap. If practical voltages are maintained (<1000 V$_{0\text{-p}}$), the drive frequency and the size of the trap can be adjusted to tune the mass range of the instrument.[21] This has been previously investigated where traps with r_0 of 500 μm and frequencies between 6 and 10 MHz were used resulting in a mass range of about 70 to 140 m/z.[18,19] With the goal of improving mass resolution, smaller traps ($r_0 < 500$ μm) have been used, but the frequency was increased simultaneously so the mass range was roughly maintained.[22] For many common analyses by ESI, the mass range may need to extend up to as much as 2000 m/z. The frequency of the trap may need to be adjusted, the trap size reduced, or both to generate the desired mass range.

One of the difficulties associated with coupling ESI sources with MS systems is that ions must be transported into vacuum for mass analysis.[23] The transmitted ion current from an ESI source can be reduced by up to three orders of magnitude when travelling through a capillary inlet. These losses occur mostly in transfer regions from a higher pressure to lower pressures (i.e. on either side of a capillary inlet),[24] and two or more of these regions are usually present for traditional ESI-MS. Operation at HPMS pressures with air as a buffer gas, however, should simplify the ESI-MS interface. Given that ions may be introduced from atmospheric pressure directly into the mass analysis chamber, high pressure MS operation reduces the number of differential pumping regions necessary to perform MS analysis. In addition, many conventional mass spectrometers use a desolvation gas or an inert bath gas for normal operation, so the use of ambient air as a buffer gas would prevent dilution of analytes from the addition of other gases. These simplifications have the potential to yield improvements in instrument sensitivity by limiting possible ion losses and dilution factors compared to conventional instruments that have

one or more regions of differential pressure.

In this chapter, the initial developments in coupling microchip ESI sources with high pressure mass spectrometry via an atmospheric inlet and direct current (DC) optics are explored. Initial work here focuses on small biomolecules including amino acids and peptides. These are of interest as one application of a CE-HPMS system could be monitoring of amino acids for process control of bioreactors used to produce biopharmaceuticals. Monitoring amino acid concentration can be used to optimize growth conditions and monitor cellular activity in a cell culture or bioreactor.[25] Analysis of peptides is of importance for QA/QC of biopharmaceuticals, identification and characterization of proteins, or to gain greater insight into cellular functions.[26] Parameters for miniature CIT operation are adjusted and optimized to create the desired mass range for the analysis of amino acids and peptides. CE-ESI-HPMS analysis is performed on peptide molecules and compared with CE-ESI-MS with a commercial mass spectrometer (Synapt G2). In addition, multiple stages of tandem mass spectrometry (MS/MS) up to MS^4 are investigated as a tool for increasing the selectivity of an ion trap mass spectrometer operated under HPMS conditions.

2.2   Experimental

2.2.1   Materials and Reagents

HPLC grade acetonitrile and formic acid (99.9%) were obtained from Fisher Scientific (Fairlawn, NJ). Purified deionized water was obtained using a Nanopure Diamond water purifier (Barnstead International, Dubuque, IA). APDIPES (3-Aminopropyl di-isopropylethoxysilane) was obtained from Gelest (Morrisville, PA). Amino acids used for analysis were obtained from Fisher Scientific. Peptides bradykinin, methionine-enkephalin, thymopentin, and angiotensin II

were obtained from American Peptide Company (Sunnyvale, CA). Leucine enkephalin and acetaminophen used for MS/MS experiments were obtained from Sigma (St. Louis, MO). The background electrolyte (BGE) for all experiments was 50% acetonitrile, 49.9% water, and 0.1% formic acid (v/v/v, pH = 3.1).

2.2.2 Microchip Design and Operation

Two microchip devices were used for this work: an infusion-ESI device and a CE-ESI device with a 46-cm serpentine separation channel, schematics of which are shown in Figure 2.1. Fabrication of these devices is described in detail in Appendix I. Channels for both devices were isotropically wet-etched to 10 μm deep and 70 μm wide. Devices were coated according to the coating procedures outlined in Appendix I. Briefly, devices were coated with APDIPES via chemical vapor deposition (CVD) using a LabKote CVD system (Yield Engineering Systems, Livermore, CA). The pumping (EO) channels for both devices were then functionalized with a 20 kDa polyethylene glycol (PEG) reagent (NanoCS, Boston, MA). The PEG reagent terminates with an N-hydroxysuccinimide ester that reacts with the primary amine of the APDIPES surface, forming a covalent bond between the PEG chain and the surface coating.

Devices were operated as described in Appendix II. All voltages were applied via platinum wire electrodes and controlled with a custom LabVIEW program. For the infusion device, voltages applied were +5 kV at the EO reservoir and +0.5 kV at the S reservoir. Voltages applied to each reservoir for the CE-ESI devices are shown in Table 2.1. Operational voltages are shown in the column labeled V_{run}. Injections were performed electrokinetically. To perform an injection, voltages were switched to the column labeled V_{inj} and then back to V_{run} after the injection was complete. The applied voltages produced an electric field strength of 400 V/cm with an approximate flow rate of 165 nL/min.

2.2.3 Microchip ESI-MS

Electrospray ionization-high pressure mass spectrometry (ESI-HPMS) experiments were performed with a custom atmospheric interface and differentially pumped vacuum system. A schematic of a typical experimental setup is shown in Figure 2.2.

The microchip-ESI device (CE or infusion) was mounted on an adjustable x-y-z stage and positioned approximately 5-10 mm from the HPMS inlet capillary (items 1 and 2 in Figure 2.2). A single-sided copper clad circuit board (M.G. Chemicals, Burlington, Ontario, Canada) was used to shield the ESI orifice on the chip from the voltages applied to the reservoirs (not shown). The corner of the microfluidic device extended about 5 mm through a slit in the board. The copper board was held at +1 kV for CE experiments and GND for infusion experiments.

The miniature CIT used for HPMS analysis was mounted in a custom differentially pumped vacuum chamber described previously.[18] Ions were conducted into vacuum using a custom capillary interface, consisting of a stainless steel capillary (2 in Figure 2.2) that had 0.01 in. ID, 0.0625 in. OD, and was 10 cm long (Valco Instruments Co., Inc., Houston, TX). The capillary was held in place by a Swagelok UltraTorr fitting (Solon, OH). Ions were typically accumulated for 5 ms before analysis. They were then scanned out of the trap and detected with an electron multiplier (6 in Figure 2.2) (Detech 2300, Detector Technology, Inc., Sturbridge, MA). A typical mass spectrum was an average of 30 to 1000 individual mass scans. Two sets of pumps were used for differentially pumping the chamber (7 in Figure 2.2). A dry scroll pump (SH-110, Agilent Technologies, Inc., Santa Clara, CA) was used on the mass analysis chamber (~1 Torr) and an Agilent TPS Bench turbomolecular pump (Model TV81M) backed by a dry scroll pump (SH-110) was used on the detector chamber (~10 mTorr).

Miniature CIT electrodes were wet etched by Towne Technologies, Inc. (Somerville, NJ). Dimensions for the CITs were $r_0 = 250$ μm, $z_0 = 325$ μm, and endcaps had 200 μm hole diameters. Each ring electrode contained a single trap. Traps were assembled by manual alignment using alignment pins and holes etched through the electrodes. Electrodes were mounted to a custom plate with 125 μm kapton (polyimide) spacers between them. Drive RF waveforms were applied by a Rohde and Schwarz SMB 100A signal generator and amplified using a Mini Circuits TVA-R5-13 preamplifier and AR 305 power amplifier. The signal was resonated with a tank circuit, and applied frequencies ranged from 7 to 12 MHz. For MS/MS experiments, a small supplementary RF voltage was applied to the endcap closest to the inlet capillary using an AFG 3022B Function generator (Tektronix, Beaverton, OR). Custom LabVIEW software was designed to monitor, control, and collect data. A National Instruments PXIe-1073 data acquisition chassis was used to interface the electronics and LabVIEW software.

For comparison of CE separation detection, a Synapt G2 quadrupole-ion mobility-time-of-flight mass spectrometer was used (Waters Corporation, Milford, MA). The Synapt G2 was operated at a rate of 90 ms per summed scan with an interscan delay of 24 ms (~9 Hz). The mass range was set to 300 to 1600 m/z. MassLynx software used to collect data was triggered by a custom LabVIEW program used to control voltages applied to the microchip.

2.3   Results and Discussion

2.3.1   Atmospheric Interface

Because the goal of this work is to develop an easy to operate, low-cost instrument, a simple interface to conduct ions from atmosphere into vacuum for HPMS analysis was designed. Typical atmospheric pressure interfaces for MS consist of capillary inlets or small apertures to

47

conduct ions into the first vacuum stage. Using this as a guide, a stainless steel capillary inlet was chosen for the initial atmospheric interface (2 in Figure 2.2). The ESI-HPMS interface developed here should have several advantages over conventional ESI-MS interfaces. Conventional ESI-MS interfaces consist of an atmospheric inlet, multiple regions of differential pressure, and complex ion optics – required due to the low-pressure operation of the mass analyzer. Because HPMS operates with pressures close to 1 Torr, the interface can introduce ions directly from atmosphere into the mass analyzer chamber via the capillary inlet with a simple vacuum fitting holding the capillary in place. In addition, minimal ion optics should be required to maximize ion transmission due to a shorter ion source-to-mass analyzer distance.

Four different capillary sizes, 0.005, 0.007, 0.01, and 0.02 in. ID were tested. No ions were observed with either the 0.005 or 0.007 in. ID capillaries. Pumping requirements proved too strenuous for the 0.02 in ID capillary, so a capillary with 0.01 in. ID was chosen for further development. A copper electrode (3 in Figure 2.2) was used to align the capillary with the entrance to the CIT and to accelerate ions toward the trap after exiting the capillary. The capillary and accelerating electrode were in electrical contact, and a voltage between +100 and +200 V was applied to the combination. In addition to alignment and acceleration, a focusing element was added to further improve sensitivity. A simple DC "gate" electrode (4 in Figure 2.2, $r = 250$ μm, 380 μm thick, spaced 125 μm from the endcap of the CIT) was inserted between the trap and the alignment electrode. The gate electrode focuses ions into the trap during the ion injection segment of the timing sequence and prevents ions from entering the trap during mass analysis. A timing diagram is shown in Figure 2.3. A positive voltage between +20 and +100 V is applied to the gate to focus ions into the trap during ion injection, and ground or a small negative DC voltage (-5 to -30 V) is applied to stop ions during the rest of the timing sequence.

The rest of the sequence contains a time for ions to cool in the trap, an instability scan (mass analysis) in which the RF amplitude is ramped to eject ions, and a clear step in which the RF amplitude is made very low so ions not ejected during the mass ramp are cleared from the trap before the next scan. If more ions enter the trap during the cool or mass ramp portions of the scan, they could interfere with mass analysis. The DC gate electrode efficiency was tested by gating of ions from BGE with the ion signal shown along with the RF voltage sequence in Figure 2.4. A pulse of ions is observed during the desired ion injection time (0 to 4 ms in the figure), and no ions are observed during the ramp. Note the ion signal observed is from ions that are not trapped during the ion injection period. This behavior is expected because the sample does not contain any analyte. If the sample contained analyte, ions from the sample would be trapped and we would expect ion signal during the RF ramp/mass analysis portion of the sequence. The observation of this pulse demonstrates that the DC gate electrode can be used to efficiently control ion entrance into the CIT.

The amino acid histidine was used as the initial model analyte for the development of the microchip-to-MS interface. The infusion-ESI microchip was used so a constant source of ions was present. After optimization of the RF frequency and voltage to create the desired mass range, all twenty amino acids were separately infused and detected, shown in Figure 2.5, in order of increasing mass from bottom to top. Mass analysis was performed at a pressure of 1.2 Torr with ambient air as the buffer gas at a drive frequency of 10.2 MHz. Each spectrum was an average of 1000 individual mass scans. The mass range was approximately 70 to 220 m/z. The $(M+H)^+$ peak for each amino acid is detectable, which should provide sufficient information for compound identification in a targeted analysis scenario. Many of the smaller amino acids have additional peaks in the spectra that have higher m/z than the protonated molecule. These peaks

49

likely correspond to either adducts or dimers of these amino acids, which is not unexpected due to the high concentration of the amino acids infused (100 μM). For most of the higher mass amino acids, additional peaks were observed below the (M+H)$^+$ peak. These peaks likely correspond to fragments of the amino acids. To more easily view the spectra of these amino acids, a sample of four of the same spectra from Figure 2.5 are shown in Figure 2.6: proline, glutamic acid, histidine, and arginine. The (M+H)$^+$ peaks in each of these spectra are easily identifiable and in the case of histidine and glutamic acids, fragments are also visible. ESI is a soft ionization technique, but operation at high pressures results in increased ion-buffer gas collisions, which can impart the energy required to induce fragmentation. In the future, these fragmentation patterns may aid in the identification of chemical species, including the differentiation of isobaric molecules. Detection of the twenty common amino acids demonstrates the ability to detect a range of analytes varying in size, polarity, and basicity.

Expanding the mass range of detectable analytes would increase the utility of an ESI-HPMS system. For instance, a low cost, high throughput method for the detection of peptides could be used for QA/QC of biopharmaceuticals. As shown in Equation 2.1, the mass range can be extended by decreasing the RF drive frequency for a given RF drive voltage and trap dimension. To test this, the RF drive frequency was decreased to 7.1 MHz from 10.2 MHz, giving a predicted mass range of 300 – 725 m/z compared to a mass range of 75 – 225 m/z for the amino acid analysis.

Using this strategy, an infusion-ESI-HPMS spectrum of a small peptide, thymopentin (RKDVY, (M+H)$^+$ m/z = 681), was collected (Figure 2.7). Mass analysis was performed at a pressure of 1.3 Torr with ambient air as the buffer gas. The spectrum shows a large peak at around m/z 341, corresponding to the doubly charged species, (M+2H)$^{2+}$. The protonated

molecule is also observed at *m/z* 681. There are a number of peaks that appear between *m/z* 360 and *m/z* 500, which likely correspond to fragments of thymopentin. The analysis and detection of this peptide demonstrates that the mass range of the CIT can be extended to at least *m/z* 681, with the potential to further extend the mass range by tuning the RF drive frequency, drive voltage, and trap size.

With respect to sensitivity, the signal-to-noise ratio (S/N) for thymopentin was significantly greater than the S/N observed for the amino acids, ~75x higher. One explanation for the smaller S/N observed for amino acids versus peptides could be due to less efficient capture of small molecules from scattering before entering the trap. The amino acids are much closer in mass to the buffer gas molecules than the peptide, so their trajectories are more likely to be altered by a collision with a buffer gas molecule than that of thymopentin. This experimental setup used very simple ion optics, consisting only of one accelerating electrode, and one DC gate lens. The discrepancy in S/N could be resolved with more complex ion optics for more efficient ion focusing and collection, such as an ion funnel.[24] Despite the difference in S/N between analytes of different mass, this simple inlet interface is an effective way of introducing ions from atmospheric pressure into vacuum for HPMS analysis.

2.3.2   CE-ESI-MS of Peptides

After demonstrating the viability of the atmospheric interface, the HPMS system was assessed as a detector for CE separations and compared with a commercial mass spectrometer, the Waters Synapt G2. Normalized base peak intensity (BPI) electropherograms of a standard peptide mixture (methionine enkephalin, angiotensin II, bradykinin, and thymopentin) detected with the HPMS system and the Synapt G2 are shown in Figure 2.8. Fluorescein was added to the mixture as a dead time marker.

The separation field strength was 400 V/cm with a flow rate of approximately

165 nL/min. About 7 fmol of peptide mixture was injected during a 0.5 s electrokinetically gated

injection. The CIT was operated at 1.2 Torr with an RF drive frequency of 7.1 MHz. As shown

in the traces in Figure 2.8, fluorescein and the four peptides in the standard mixture were

separated and detected. Comparing the two electropherograms, the average S/N of the four

peptides was 69 using HPMS and 437 using the Synapt G2. The calculated average separation

efficiencies were 445,000 theoretical plates using HPMS and 490,000 theoretical plates using the

Synapt G2. Both mass spectrometers were able to detect these fast and highly efficient

separations (average full-width at half maximum (FWHM) = 0.58 ± 0.04 s), with the discrepancy

resulting from differences in mass spectral sampling rate. The difference in sampling rate is

illustrated in Figure 2.9, showing individual data points collected over the peak in the

electropherogram corresponding to bradykinin (solid circles). The bottom trace shows the HPMS

system, where there were only about three data points collected over the width of the peak,

corresponding to a sampling rate of about 3 Hz. In contrast, the sampling rate for the Synapt G2

(top trace) was about three times as fast, or about 9 Hz, with nine points collected over the course

of the same peak. The HPMS system is limited by the time required to accumulate, analyze, and

clear ions from the trap as displayed in the timing sequence shown in Figure 2.3. In this case, a

typical sequence involved ion injection/accumulation times of about 4 to 5 ms, a cool time of

0.5 ms, a mass analysis scan of 5 ms, and a clear time of 1 ms. As shown in Figure 2.4, a typical

full scan function was about 11 ms. With improvements in sensitivity, the ion accumulation time

could be minimized, and the duty cycle, and therefore the sampling rate, increased. Detection of

these peptides shows that a miniature CIT based mass spectrometer operated at high pressure can

be used for detection of fast separations with narrow peak widths. Although the Synapt G2

showed about six times better S/N, this simple comparison demonstrates the viability of an

HPMS system using a mini-CIT as a detector for the separation of biomolecules.

For mixtures like these peptides, the HPMS system potentially offers a simple and

inexpensive alternative to a large commercial instrument like the Synapt G2. The miniature MS

system can provide useful mass spectral information for label-free detection and identification of

chemical species for targeted applications. A comparison of the mass spectra of bradykinin from

both mass spectrometers acquired during the CE separations is shown in Figure 2.10. Some

similar features can be observed in the two spectra, most notably the $(M+2H)^{2+}$ peak around

m/z 531. A feature corresponding to the $(M+3H)^{3+}$ peak is also observed around m/z 354. The

most obvious difference in the two spectra is the observed peak width (FWHM: 12.0 m/z with

HPMS; 0.026 m/z with the Synapt G2). Wider peaks are expected with HPMS due to increased

analyte-buffer gas collisions with higher pressure operation and a larger buffer gas (ambient air).

Even with increased peak widths, a mass spectrum combined with CE migration time provides

sufficient information for identification of chemical species, especially for an application where

the goal is detection of known target analytes. Note that if narrower peak widths are needed,

peak widths could be improved with higher RF frequency operation and the use of smaller traps

to maintain the mass range, and different trap geometries or arrays of CITs could make up for

lost charge capacity.[27,28] In the case of a miniature bench top instrument, it might be possible to

use helium buffer gas to further improve resolution. Resolution could also be improved by

applying a small RF voltage to one or both endcaps of the trap to perform resonant or double

resonant ejection.[29,30]

2.3.3   Tandem Mass Spectrometry

One of the advantages of quadrupolar trap analyzers is the ability to perform tandem mass spectrometry (MS/MS) with a single mass analyzer.[29] MS/MS analysis can significantly increase the selectivity of a mass spectrometer by performing multiple stages of fragmentation and mass analysis. With the loss of some resolution when using HPMS, tandem mass spectrometry would greatly increase the utility of the platform.

Tandem mass spectrometry in an ion trap is most often done by isolating a single peak in a mass spectrum and then fragmenting that peak with collision-induced dissociation (CID). Briefly, a small supplementary AC voltage is applied to one or both endcaps that excites ion motion in the trap. The excited ions collide with neutral buffer gas molecules, and the kinetic energy from those collisions is converted to internal energy, which can be sufficient to fragment those ions. MS/MS using CID under HPMS conditions has been shown previously with mostly small, organic molecules as targets to improve mass spectral selectivity.[31] MS/MS would also be useful for improving the identification of biologically relevant molecules analyzed by ESI-HPMS and is used frequently in conventional ESI analyses for the identification of proteins, peptides and other biological compounds of interest.[32]

Infusion ESI-MS/MS with tryptophan as an analyte is shown in Figure 2.11. The CIT was operated at 7 MHz and a pressure of 1.2 Torr, with ambient air as the buffer gas. The black trace (labeled MS) shows an MS scan where the protonated molecule of tryptophan is observed, along with what is presumed to be a proton bound dimer. The blue trace (labeled isolation) shows the isolation of the proton bound dimer. The isolation was performed using a partial instability scan. The RF amplitude was ramped to the point just before the ejection of the dimer, ejecting all species of lower mass and isolating species of higher mass, in this case, the proton bound dimer.

After isolation, the dimer was excited for 5 ms with an axial RF voltage on one of the endcaps at 0.5 MHz and an amplitude of 4.8 V_{p-p}. The red trace (labeled MS/MS) then shows the result after isolation and excitation of the dimer. With energy added from the supplementary RF, some of the parent ion (dimer) is fragmented to the monomer.

An advantage of ion traps is that they can perform multiple stages of tandem mass spectrometry, or MS^n with it having been shown in a conventional trap up to MS^{12}. This capability can further increase the selectivity of the instrument.[33] Different stages of isolation and excitation of clusters of acetaminophen from an infusion up to MS^4 are shown in Figure 2.12. The first stage (A) shows an MS scan of the acetaminophen clusters. In the second stage (B), the highest mass (latest ejecting) cluster (labeled 1) is isolated and fragmented. In the third stage (C), the highest mass fragment from the MS^2 scan (labeled 2) is isolated and fragmented. Finally, the fourth stage (D) shows the isolation of the highest mass ion from the MS^3 scan (labeled 3) and a small peak corresponding to the last fragment (labeled 4). The mass spectra and scan functions used to produce each stage of MS are shown in Figure 2.13. The same excitation frequency and voltage (0.3 MHz, 8.5 V_{p-p}) were used for each excitation, but for varying lengths. The ability to use the same frequency indicates that broadband excitation can be performed under HPMS conditions. This is likely due to the fact that the secular frequencies of the ions in the trap are not well defined because of the large number of ion-buffer gas collisions at high pressure.[31] It is important to note that only the highest mass ion was isolated in each case using a partial instability scan by ramping the drive RF amplitude to just below the ejection voltage of the highest mass ion. Ion traps also have the potential to target and isolate other peaks in the mass spectrum using techniques like apex isolation or SWIFT.[34,35] These types of isolation have been

55

performed with HPMS previously and could be implemented to further improve the selectivity of HPMS.

The discussion of tandem mass spectrometry has focused on fragmentation of loosely bound species, but molecules like peptides can be much more difficult to fragment because there are a larger number of bonds over which internal energy can be distributed. Leucine enkephalin (YGGFL) is an endogenous neurotransmitter often used as a mass spectral calibrant and prototype molecule to study peptide fragmentation[36] and was used to test CID of peptides under HPMS conditions. A full mass spectral scan of YGGFL (black trace) shown in Figure 2.14 with a spectrum of YGGFL after isolation and subsequent CID. The drive RF frequency was 7.1 MHz, and the pressure was 1.0 Torr of ambient air. The excitation voltage for the CID spectrum was 8 V_{p-p}, applied for 0.5 ms at 0.1 MHz. Both spectra are dominated by the protonated molecule, ejected at about 3 ms. Some of the fragments observed in the full spectrum are produced again after CID. There is also a shoulder on the protonated molecule that was not present in the full scan, indicating that MS/MS may provide new information to aid in identification of species. More efficient fragmentation would aid in peptide identification, but the fragmentation of YGGFL shows MS/MS of peptides under HPMS conditions is possible.

2.4   Conclusions

The first steps (capillary interface and DC gate electrode) in coupling ESI with HPMS have been demonstrated. A simple atmospheric interface was designed to conduct ions from atmosphere into the ion trap in vacuum. Microchip infusions and CE separations were performed using HPMS as a detector operated at pressures greater than 1 Torr with ambient air as the buffer gas, demonstrating the viability of a miniature CE-ESI-MS system. Finally, MS/MS under HPMS conditions with electrospray-infused analytes was performed. The next chapters discuss

improvements on the initial development of ESI-HPMS described here for specific analytes and

applications.

2.5   Figures and Tables
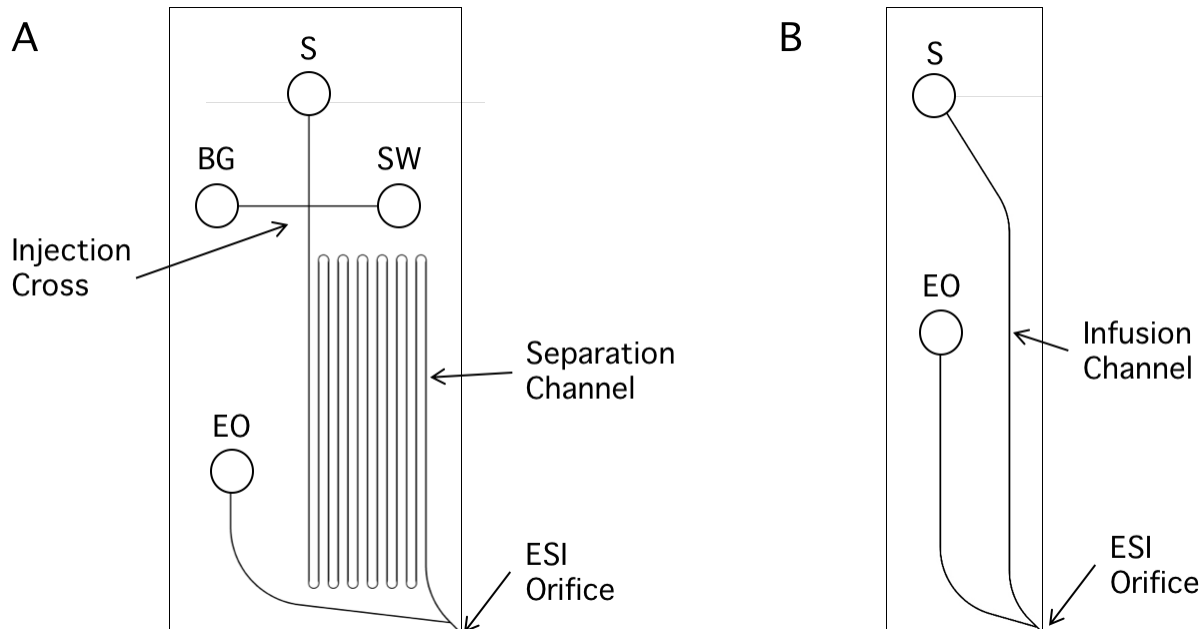
Figure 2.1: Schematics for capillary electrophoresis (A) and infusion (B) glass microfluidic devices. All channels were etched to a depth of 10 µm. Reservoirs are designated with circles and indicate sample (S), background electrolyte (BG), sample waste (SW), and electroosmotic pump (EO). The microchip in A consists of an injection cross, a 46-cm serpentine separation channel, and an electroosmotic pumping channel. The infusion device (B) consists of a 5.5-cm channel and an electroosmotic pumping channel, and both reservoirs are filled with the sample.
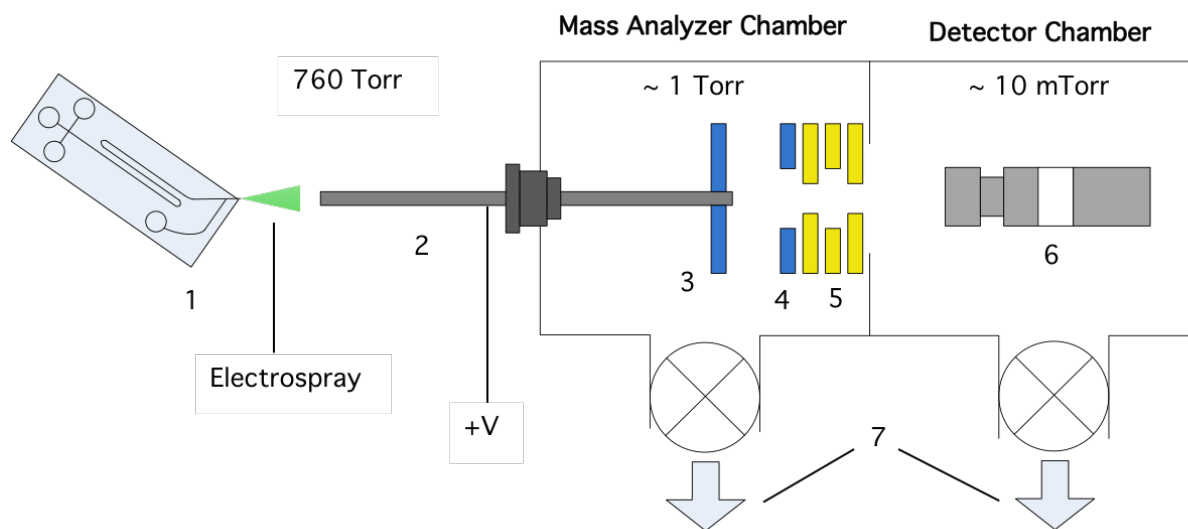
Figure 2.2: Experimental setup (not to scale) for ESI-HPMS with (1) Glass microchip with electrospray, (2) stainless steel capillary and UltraTorr fitting, (3) accelerating electrode, (4) gate electrode, (5) trap electrodes; two endcaps (BeCu) and ring (Cu), (6) electron multiplier detector, and (7) vacuum pumps.
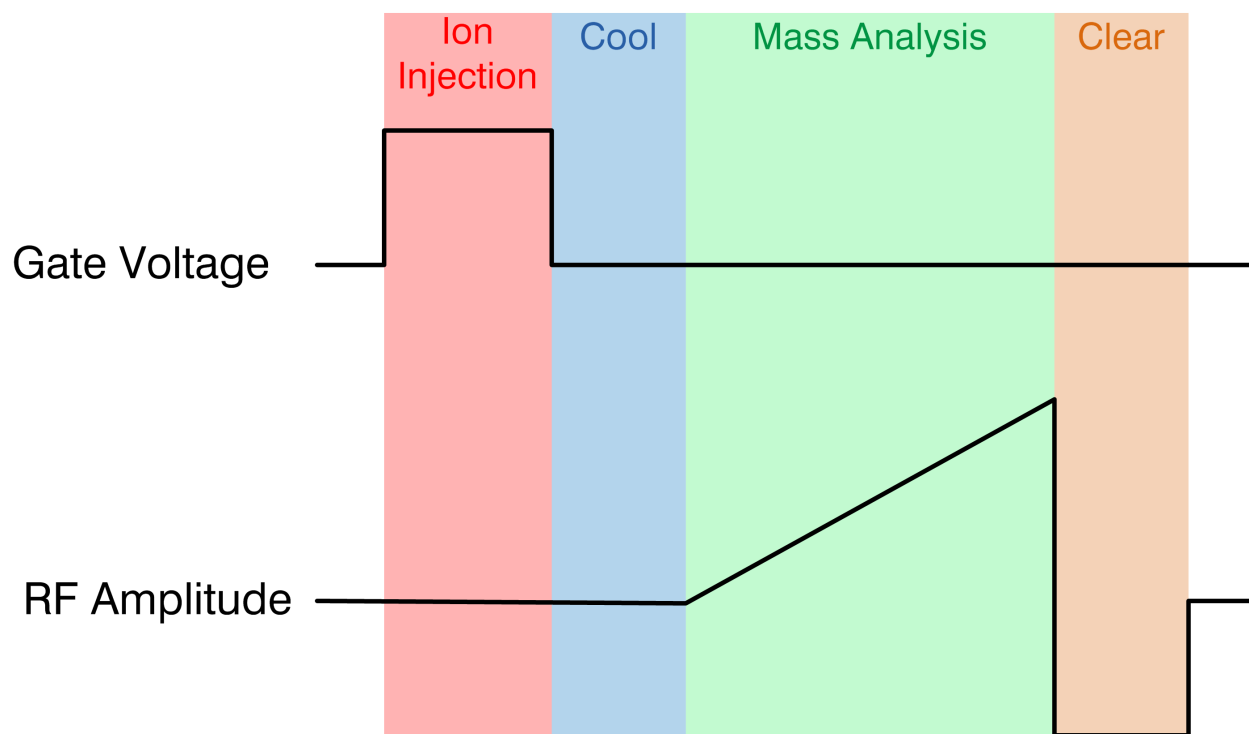
Figure 2.3: Timing diagram for HPMS experiments. The voltage applied to the gate electrode (gate voltage) is high during the ion injection portion and low during the rest of the scan. After ion injection, the RF amplitude is constant while the trapped ions are given time to cool. The RF amplitude is then ramped to perform the mass analysis scan. The RF amplitude is then reduced to near-zero and any ions remaining after the ramp are cleared from the trap before the next scan begins.
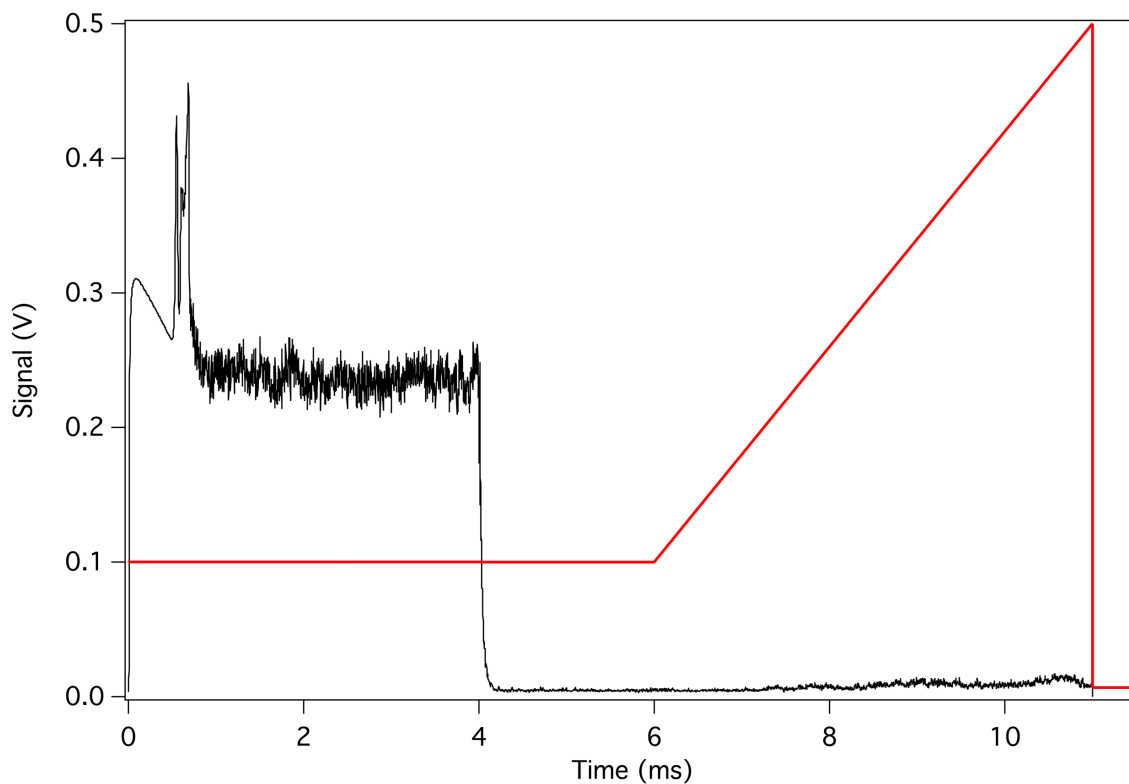
Figure 2.4: Ion gating with the gate electrode using background electrolyte as the sample. The black trace shows ion signal, and the red trace shows the RF ramp (arbitrary units). The signal from 0 to 4 ms shows that ions can be efficiently gated with the electrode; the voltage on the gate electrode is high during this point and low during the rest of the scan. The spikes at the beginning of the pulse are a turn-on feature from the detector.
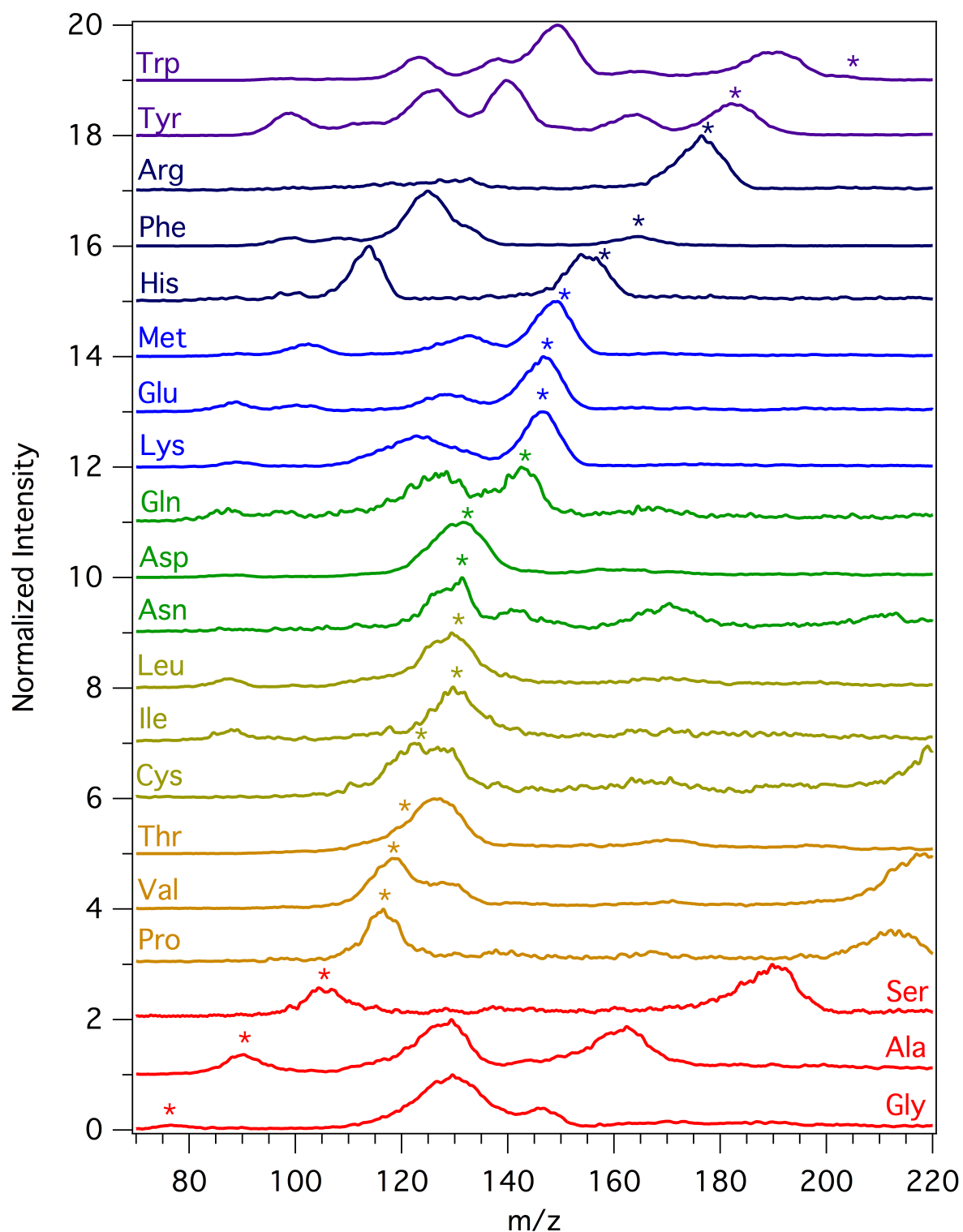
Figure 2.5: Infusion-ESI-HPMS spectra of the twenty common amino acids. Each amino acid was infused separately at 100 μM in BGE. The drive RF was 10.2 MHz, and the buffer gas was ambient air at 1.2 Torr. *indicates $(M+H)^+$
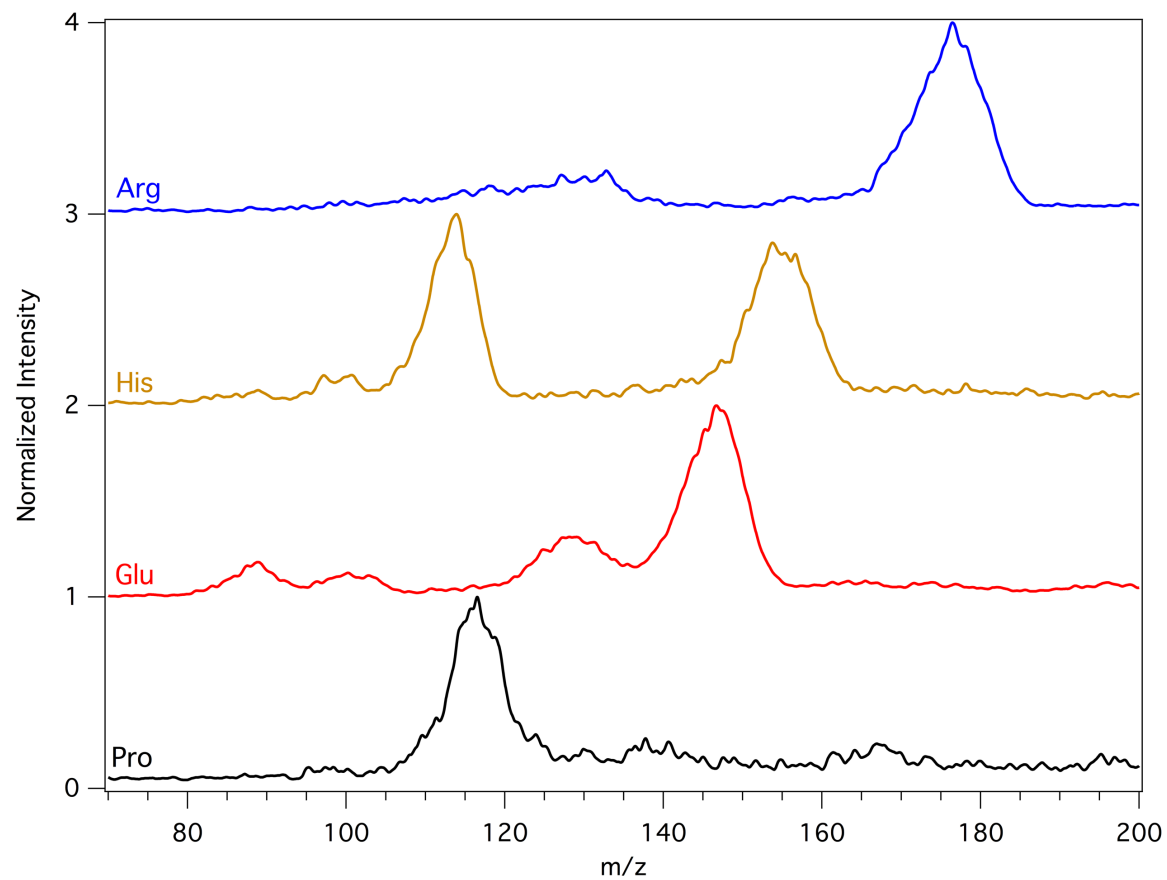
Figure 2.6: Infusion-ESI-HPMS spectra of four amino acids (100 µM) shown in Figure 2.5. The drive RF was 10.2 MHz, and buffer gas was ambient air at 1.2 Torr.
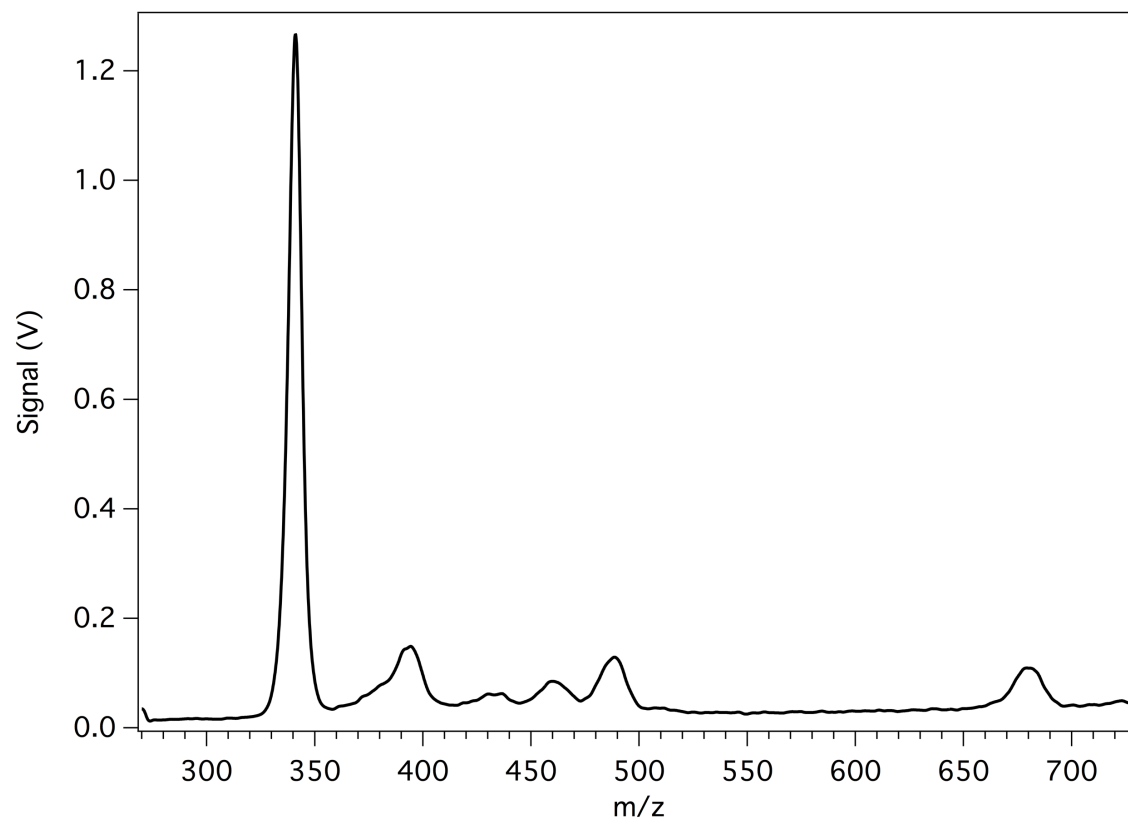
Figure 2.7: Infusion-ESI-HPMS spectrum of 5 μM thymopentin in BGE. The drive RF was 7.1 MHz, and the buffer gas was ambient air at a pressure of 1.3 Torr.
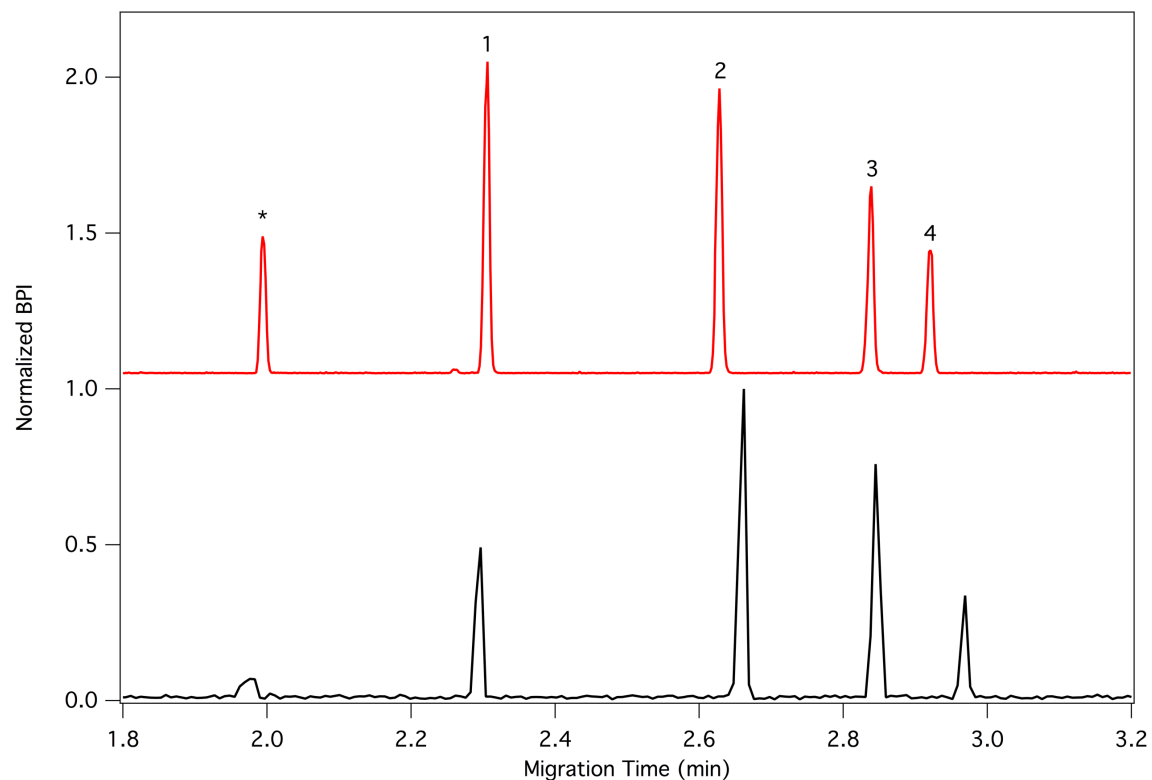
Figure 2.8: BPI electropherograms of a peptide mixture with a 46-cm long separation channel CE microchip with HPMS (black) and Synapt G2 (red) detection. Fluorescein (*), Methionine Enkephalin (1), Angiotensin II (2), Bradykinin (3), Thymopentin (4) were the analytes. Approximately 7 fmol of peptide mixture was injected during a 0.5 s gated injection. The separation field strength was 400 V/cm.
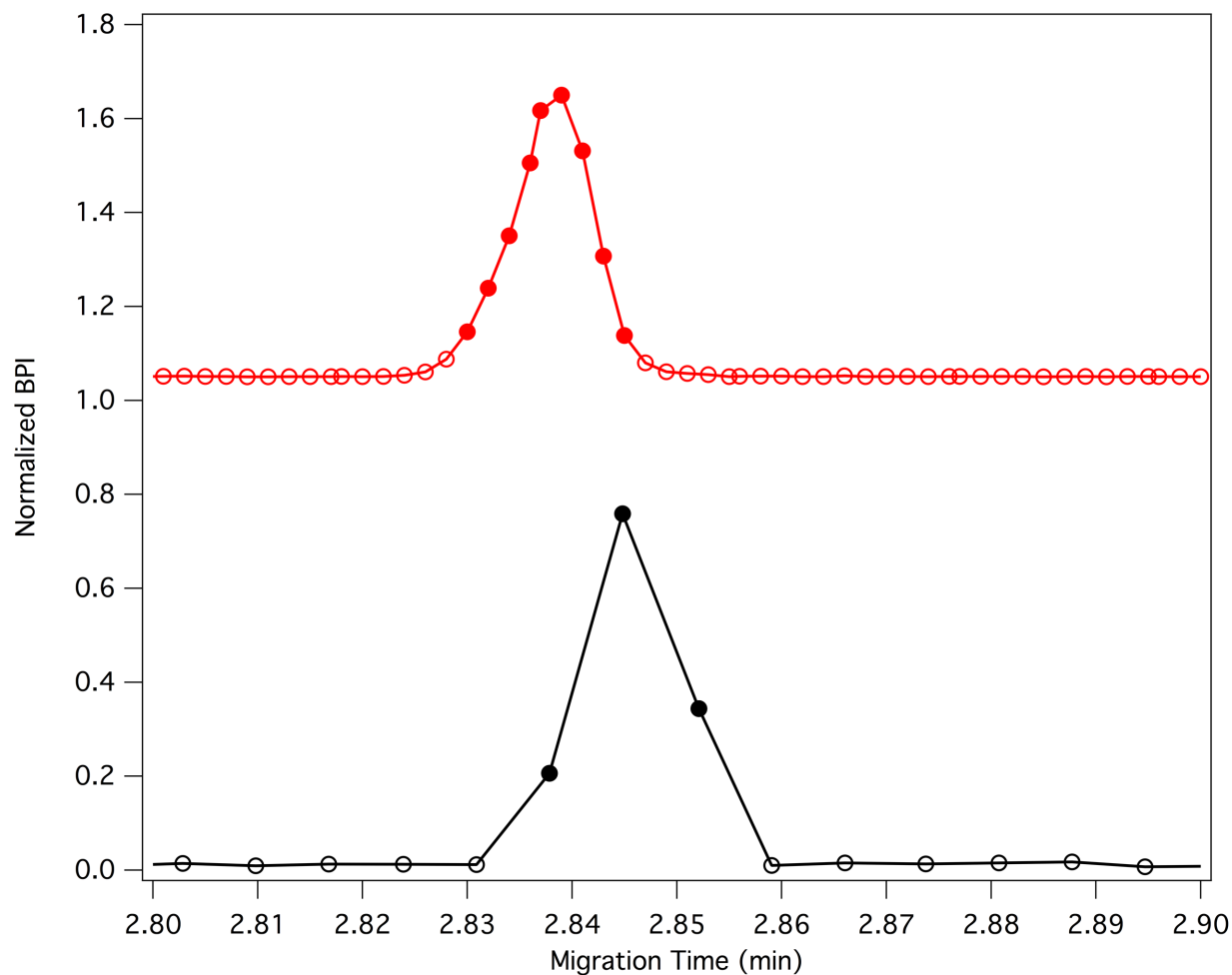
Figure 2.9: Sampling rate comparison of HPMS (black) and Synapt G2 (red) over the bradykinin peak shown in Figure 2.8 (peak 3). About 9 points per peak are observed with G2, and about 3 points per peak are observed with HPMS.
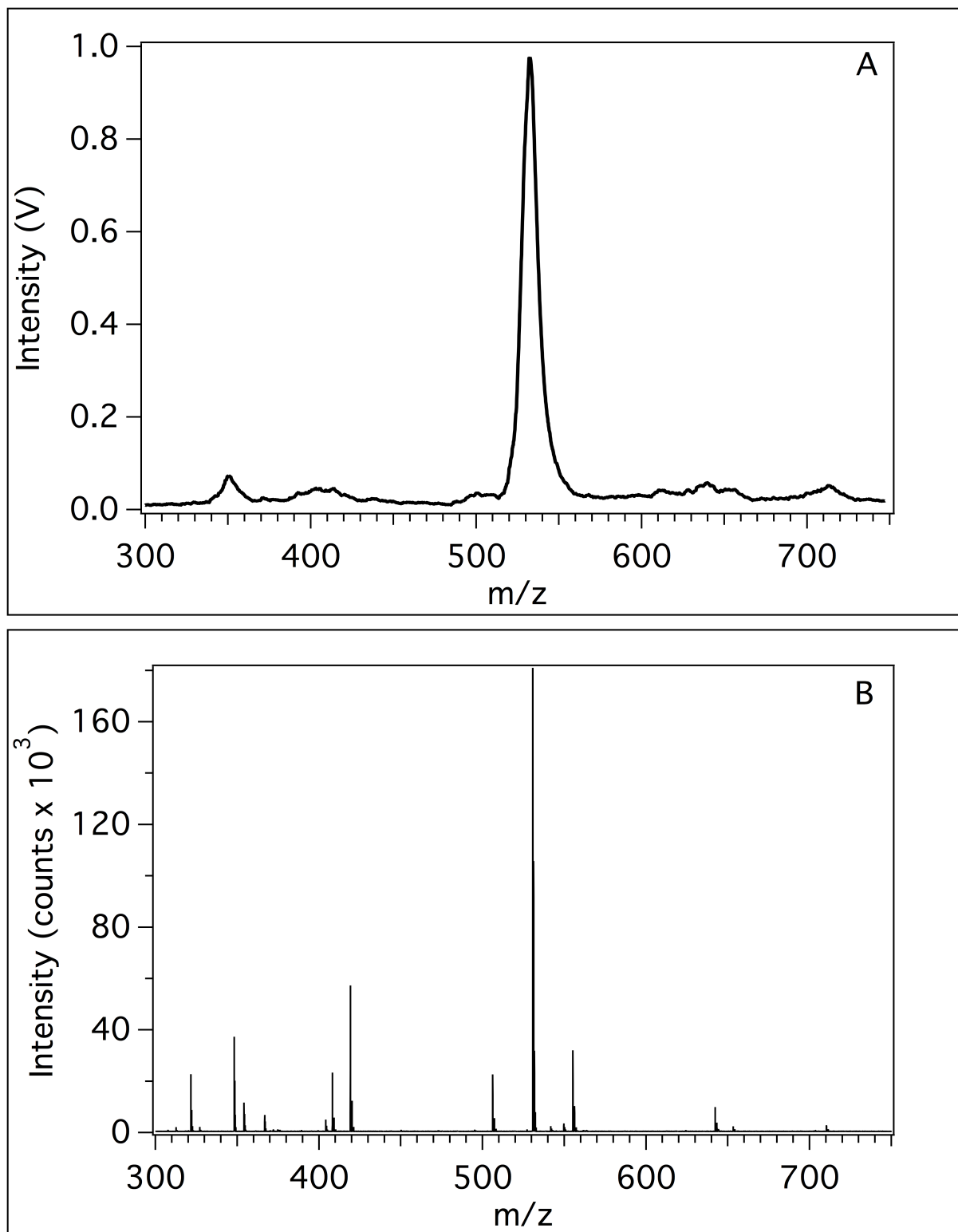
Figure 2.10: Sample mass spectra of bradykinin from A) HPMS and B) Synapt G2.
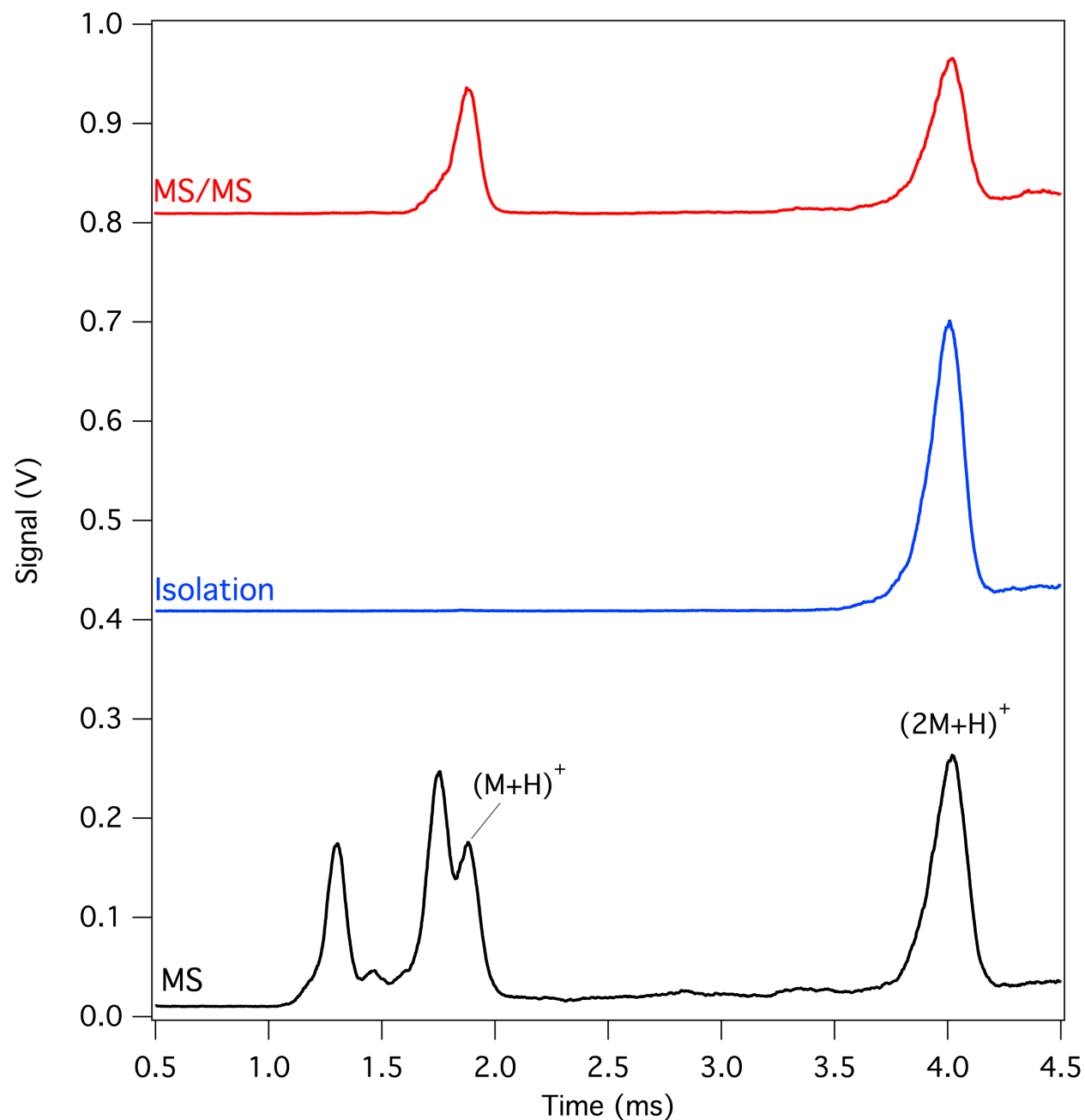
Figure 2.11: Infusion-ESI-HPMS, isolation, and MS/MS of tryptophan and tryptophan dimer. The black trace shows a full MS scan. The blue trace shows the isolation of the dimer. The red trace shows the HPMS scan result after isolation and excitation of the dimer with a small axial potential (4.8 V_{p-p}).
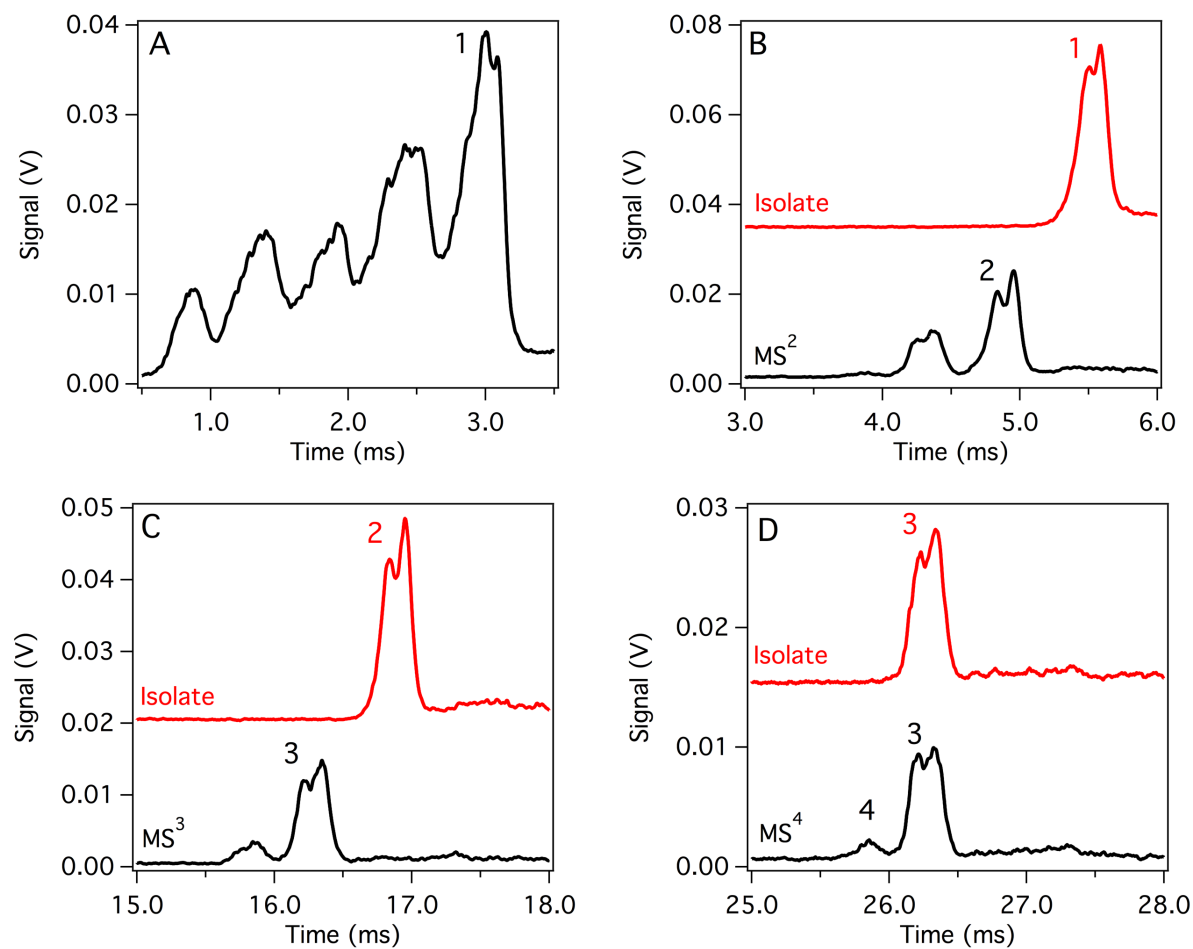
Figure 2.12: Isolation and excitation of acetaminophen clusters at MS stages up to MS^4.
A) Initial MS scan without isolation or excitation. B) Isolation of Peak 1 and fragmentation.
C) Isolation of Peak 2 and fragmentation. D) Isolation of Peak 3 and fragmentation to Peak 4.
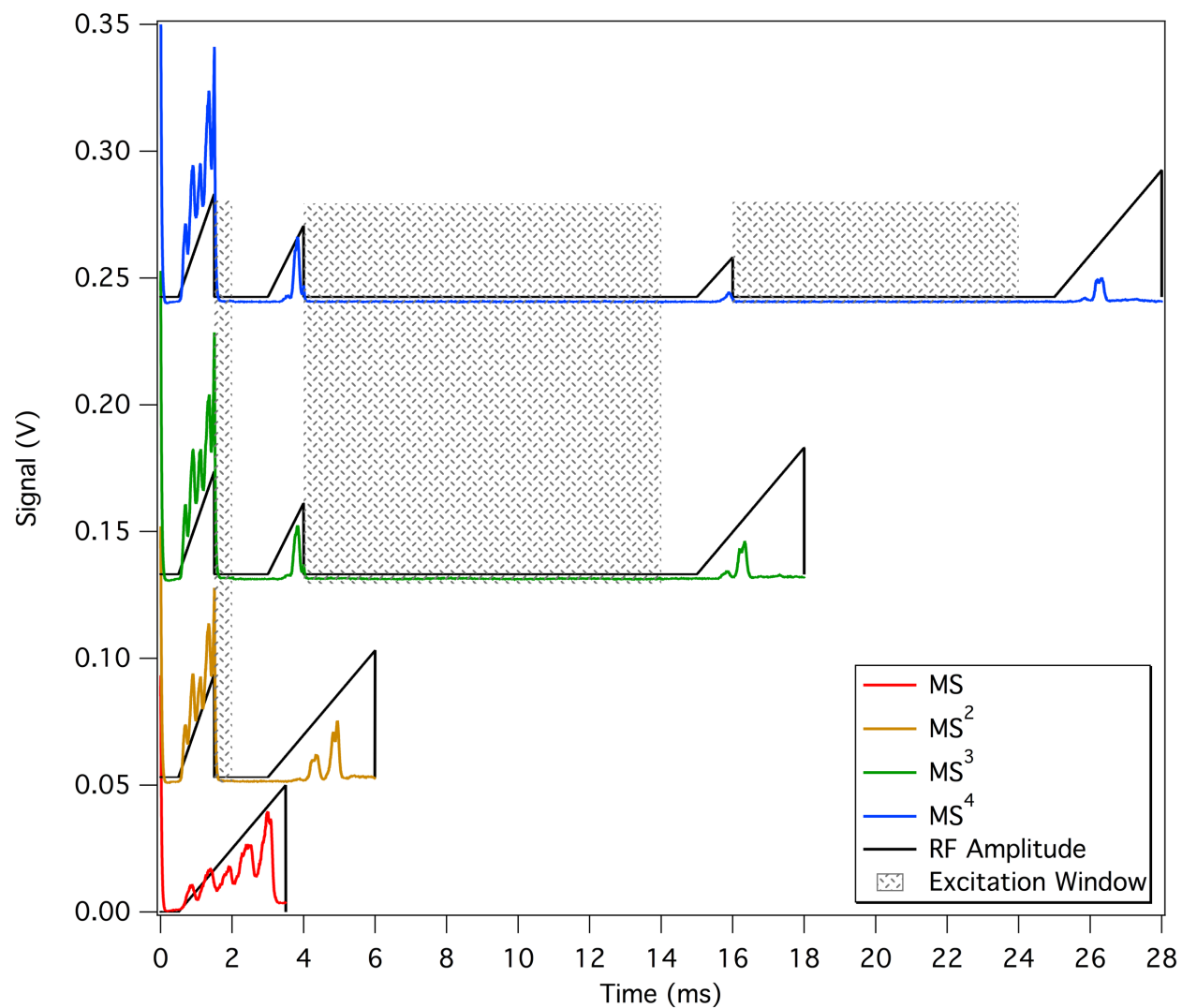
Figure 2.13: Stages of MS and scan functions for acetaminophen clusters/adducts up to MS^4. The last ramp in each sequence is the mass analysis scan, and the previous ramps (partial instability scans) are used to isolate the highest mass ion.
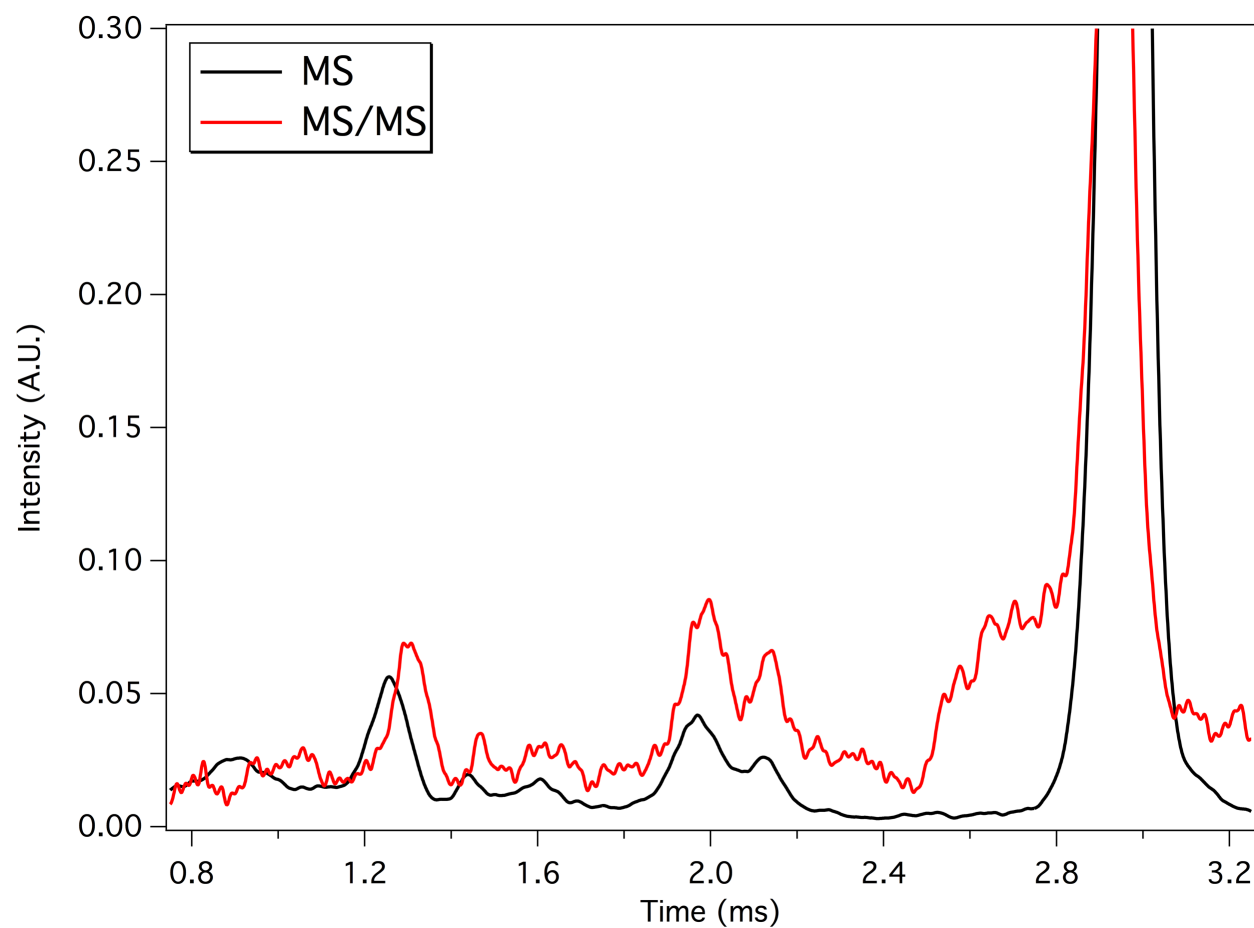
Figure 2.14: Infusion-ESI-HPMS and MS/MS of leucine enkephalin. Some of the fragment features in the MS scan (black trace) are reproduced after the protonated molecule is isolated and fragmented. A shoulder on the protonated molecule also appears after excitation.

Table 2.1: Operational voltages for CE-ESI device at each reservoir during CE run and injections.

	V_{run} (kV)	V_{inj} (kV)
S	-14	-14
BG	-14	-13
SW	-12	-13
EO	+6	+6

2.6   REFERENCES

(1)   Whitehouse, C. M.; Dreyer, R. N.; Yamashita, M.; Fenn, J. B. *Anal. Chem.* **1985**, *57* (3), 675–679.

(2)   Smith, R. D.; Loo, J. A.; Loo, R. R. O.; Busman, M.; Udseth, H. R. *Mass Spectrom. Rev.* **1991**, *10* (5), 359–452.

(3)   Mehlis, B.; Kertscher, U. *Anal. Chim. Acta* **1997**, *352* (1), 71–83.

(4)   Smith, R. D.; Barinaga, C. J.; Udseth, H. R. *Anal. Chem.* **1988**, *60* (18), 1948–1952.

(5)   Bantscheff, M.; Schirle, M.; Sweetman, G.; Rick, J.; Kuster, B. *Anal. Bioanal. Chem.* **2007**, *389* (4), 1017–1031.

(6)   Hernández, F.; Sancho, J. V.; Ibáñez, M.; Guerrero, C. *TrAC Trends Anal. Chem.* **2007**, *26* (6), 466–485.

(7)   González, S.; Barceló, D.; Petrovic, M. *TrAC Trends Anal. Chem.* **2007**, *26* (2), 116–124.

(8)   Pioch, M.; Bunz, S.-C.; Neusüss, C. *Electrophoresis* **2012**, *33* (11), 1517–1530.

(9)   Honour, J. W. *Ann. Clin. Biochem.* **2003**, *40* (Pt 6), 628–638.

(10)   Ho, C. S.; Lam, C. W. K.; Chan, M. H. M.; Cheung, R. C. K.; Law, L. K.; Lit, L. C. W.; Ng, K. F.; Suen, M. W. M.; Tai, H. L. *Clin. Biochem. Rev.* **2003**, *24* (1), 3–12.

(11)   Tetala, K. K. R.; Vijayalakshmi, M. A. *Anal. Chim. Acta* **2016**, *906*, 7–21.

(12)   Snyder, D. T.; Pulliam, C. J.; Ouyang, Z.; Cooks, R. G. *Anal. Chem.* **2016**, *88* (1), 2–29.

(13)   He, M.; Xue, Z.; Zhang, Y.; Huang, Z.; Fang, X.; Qu, F.; Ouyang, Z.; Xu, W. *Anal. Chem.* **2015**, *87* (4), 2236–2241.

(14)   Baker, C. A.; Duong, C. T.; Grimley, A.; Roper, M. G. *Bioanalysis* **2009**, *1* (5), 967–975.

(15)   Mellors, J. S.; Gorbounov, V.; Ramsey, R. S.; Ramsey, J. M. *Anal. Chem.* **2008**, *80* (18), 6881–6887.

(16)   Batz, N. G.; Mellors, J. S.; Alarie, J. P.; Ramsey, J. M. *Anal. Chem.* **2014**, *86* (7), 3493–3500.

(17)   Redman, E. A.; Batz, N. G.; Mellors, J. S.; Ramsey, J. M. *Anal. Chem.* **2015**, *87* (4), 2264–2272.

(18)   Blakeman, K. H.; Wolfe, D. W.; Cavanaugh, C. A.; Ramsey, J. M. *Anal. Chem.* **2016**, *88* (10), 5378–5384.

(19)   Blakeman, K. H.; Cavanaugh, C. A.; Gilliland, W. M.; Ramsey, J. M. *Rapid Commun. Mass Spectrom.* **2016**, *31* (1), 27–32.

(20)   R. E. March and J. F. J. Todd. *Practical Aspects of Ion Trap Mass Spectrometry, Volume 1*; CRC Press, 1995.

(21)   Pau, S.; Pai, C. S.; Low, Y. L.; Moxom, J.; Reilly, P. T. A.; Whitten, W. B.; Ramsey, J. M. *Phys. Rev. Lett.* **2006**, *96* (12), 120801.

(22)   Blakeman, K. Development of High Pressure Mass Spectrometry for Handheld Instruments, University of North Carolina at Chapel Hill, 2015.

(23)   Page, J. S.; Kelly, R. T.; Tang, K.; Smith, R. D. *J. Am. Soc. Mass Spectrom.* **2007**, *18* (9), 1582–1590.

(24)   Schaffer, S. A.; Tang, K.; Anderson, G. A.; Prior, D. C.; Udseth, H. R.; Smith, R. D. *Rapid Commun. Mass Spectrom.* **1997**, *11* (16), 1813–1817.

(25)   Hong, P.; Wheat, T. E.; Mazzeo, J. R.; Diehl, D. M. Monitoring Cell Culture Media with the Waters Amino Acid Analysis Solution http://www.waters.com/webassets/cms/library/docs/720002381en.pdf (accessed May 27, 2015).

(26)   Domon, B.; Aebersold, R. *Science* **2006**, *312* (5771), 212–217.

(27)   Badman, E. R.; Cooks, R. G. *Anal. Chem.* **2000**, *72* (14), 3291–3297.

(28)   Amy M. Tabert; Jens Griep-Raming; Andrew J. Guymon, A.; Cooks, R. G.; Tabert, A. M.; Griep-Raming, J.; Guymon, A. J.; Cooks, R. G. *Anal. Chem.* **2003**, *75* (21), 5656–5664.

(29)   March, R. E. *J. Mass Spectrom.* **1997**, *32* (4), 351–369.

(30)   Moxom, J.; Reilly, P. T. A.; Whitten, W. B.; Ramsey, J. M. *Rapid Commun. Mass Spectrom.* **2002**, *16* (8), 755–760.

(31)   Hampton, A. Improving the Selectivity of High Pressure Mass Spectrometry, University of North Carolina at Chapel Hill, 2016.

(32)   Mann, M. *Nat. Rev. Mol. Cell Biol.* **2016**, *17* (11), 678–678.

(33)   Louris, J. N.; Brodbelt-Lustig, J. S.; Graham Cooks, R.; Glish, G. L.; van Berkel, G. J.; McLuckey, S. A. *Int. J. Mass Spectrom. Ion Process.* **1990**, *96* (2), 117–137.

(34)   March, R. E.; Todd, J. F. J. *Practical aspects of ion trap mass spectrometry*; CRC Press, 1995.

(35)   Guan, S.; Marshall, A. G. *Int. J. Mass Spectrom. Ion Process.* **1996**, *157*, 5–37.

(36) Sztáray, J.; Memboeuf, A.; Drahos, L.; Vékey, K. *Mass Spectrom. Rev.* **2011**, *30* (2), 298–320.

Chapter 3: Investigation of ESI-HPMS for Small Molecule Analysis

3.1   Introduction

While small, volatile, and gas phase molecules were the targets for initial HPMS development using an electron ionization or glow discharge ion source, there are many applications where small, nonvolatile molecules are of interest. Drug characterization and validation for both production and forensics/screening,[1–4] environmental monitoring,[5,6] and many metabolomics applications[7–10] necessitate detection of small, nonvolatile chemical species. These targets are often in complex matrices and necessitate a separation step prior to mass spectrometry (MS) analysis, usually by liquid chromatography (LC) or capillary electrophoresis (CE) coupled to MS via electrospray ionization (ESI). Many of these applications involve targeted (rather than discovery) analysis and would benefit from analysis on-site, making microchip CE-HPMS a good alternative to conventional LC and CE-MS methods.

Initial developments of ESI-HPMS were discussed in Chapter 2 and involved the analysis of small molecules, including amino acids, but there are many improvements that can be made to enhance the performance of the platform. The mass resolution of peaks shown in Chapter 2 could be improved by increasing the drive frequency applied to the ion trap. Equation 1.6, reproduced here as Equation 3.1, shows the proportional relationship between resolving power ($m/\Delta m$), pressure (P), and frequency (Ω).[11]

$$\frac{m}{\Delta m} \propto \frac{\Omega}{P} \qquad\qquad 3.1$$

If the pressure remains constant, an increase in drive frequency will improve the resolving

power. However, if the frequency is increased, the mass range is decreased if all other

parameters remain constant. Equation 1.7 shows the maximum mass that can be ejected from a

trap and is reproduced as Equation 3.2:[12]

$$\left(\frac{m}{z}\right)_{max} = \frac{8V_{max}}{q_{max}\Omega^2(r_0^2+2z_0^2)} \qquad\qquad 3.2$$

where m/z is the mass-to-charge ratio, V_{max} is the maximum amplitude of the drive RF voltage,

q_{max} is the trapping parameter and constant (usually 0.908), and r_0 and z_0 are the dimensional

parameters of the trap. In order to maintain the mass range when increasing the RF drive

frequency and maintain practical voltages, the size of the trap must be decreased. For the work in

this chapter, the drive frequency was increased up to 30 MHz, about three times higher than

previous work, and the trap size was decreased to critical dimensions of about 100 μm.

With a decrease in trap size, there is a corresponding decrease in the number of ions that

can be stored in the trap without loss in performance. In order to make up for the loss of trapping

capacity of miniature cylindrical ion traps (CITs), arrays of CITs have been used.[13–15] However,

heterogeneity in the performance of the elements of the array may lead to decreased resolution.

An alternative to CIT arrays to improve trap capacity is the stretched length ion trap, or

SLIT.[16,17] The SLIT operates in the same manner as a CIT, but the volume of the trap is stretched

in one dimension. For the smallest trap dimensions (~100 µm), SLIT traps were used to increase the ion storage capacity.

While changes to the mass analyzer geometry and operation can improve performance of the instrument, the transmission of ions to the mass analyzer is equally important to overall instrumental utility. One method to increase ion transmission is to improve the inlet geometry. Capillaries of different inner diameters and lengths can be used, or orifice inlets can be used in place of capillaries. Aperture or orifice inlets can use a smaller ID than capillaries and produce the same conductance limit, but their smaller length reduces the possibility of ion collisions with the wall of the inlet and may improve ion transmission. Both types of inlets are regularly implemented in mass spectrometry instruments,[18] so both inlets were investigated to optimize ion transmission. Another way to increase ion transmission is improved ion optics. An electrode or "gate" lens with approximately the same dimensions as the ring electrode was used for focusing and gating ions in the previous chapter, but different optics could produce better ion focusing. Tube lenses have been used previously to focus ions from the inlet capillary in the first region of a commercial mass spectrometer,[19] which operates at approximately the same pressure as HPMS. Therefore, using a tube lens in an HPMS system, ion focusing can be improved while still maintaining simple operation (i.e. only DC voltages). To help guide the design process, simulations were performed to optimize tube lens geometry before implementing the tube lens experimentally.

Two applications were chosen for proof-of-concept demonstration of the platform to take advantage of the improved sensitivity and resolution. These include monitoring the components of cell growth media for bioreactor monitoring and detection of opiates in urine for forensics or screening.

Biotherapeutics, particularly monoclonal antibodies (mAbs), represent a growing portion of clinical drugs and much work has been done to characterize the drug product.[20–22] The production of mAbs is a complex process involving cell growth followed by a series of purification and filtration steps.[23] Proper cell growth is critical for many applications, including biotherapeutics to maximize protein yield, so monitoring the cell growth process is important.[23–27] Therefore, monitoring the composition of the medium as cells consume the various components is a way for monitoring cell growth progress. Being able to monitor the process on the production plant floor would be advantageous as it would eliminate the need for transport to a central laboratory. This could also decrease reaction times for adding key nutrients to the bioreactor to maintain optimal growth conditions by providing information in a timely manner. A compact microchip CE-ESI-HPMS system could provide an inexpensive and rapid strategy to monitor the components in growth media at the source. The time scale for cell growth is on the order of hours, while the typical analysis time for CE-HPMS is usually under 5 min, presenting the opportunity for real-time monitoring of cell growth. Thus, microchip CE-HPMS was explored here for monitoring cell growth via measurement of components, specifically amino acids, contained in the growth medium.

Another potential application of a miniature CE-HPMS platform is the detection of drugs of abuse in a forensic or screening setting, where rapid results are critical. Traditional drug analysis is performed in a "two-tiered" system where field measurements are performed before sending samples to a central lab.[28,29] In the lab, analysis is typically performed by gas chromatography (GC) or LC methods coupled to MS, which are well characterized and considered the standard for many of these analyses.[28,30] A microchip CE-HPMS platform may provide an inexpensive alternative to the standard LC and GC-MS analyses, and if made portable

enough for use in the field, the platform could eliminate the need for the "two-tiered" system. There are many possible drug targets for this analysis. Opiates are a commonly abused class of drugs, with over 2 million Americans having a substance abuse disorder related to prescription drugs in 2016.[31] Because of their prevalence and high rate of abuse, opiates were chosen as the target analytes for this work.

This chapter outlines improvements in the CE-HPMS platform for the analysis of small molecules presented in Chapter 2 along with a demonstration of two potential applications for the technology. A tube lens was evaluated with SIMION simulations before experimental validation. Amino acid standards were then analyzed before attempting to monitor their consumption as a function of cell growth. Finally, opiate standards were analyzed before extracting and analyzing codeine in a urine sample.

3.2   Experimental

3.2.1   Materials and Reagents

HPLC grade acetonitrile, methanol, and formic acid (99.9%) were obtained from Fisher Scientific (Fairlawn, NJ). Purified deionized water was obtained using a Nanopure Diamond water purifier (Barnstead International, Dubuque, IA). (3-Aminopropyl)di-isopropylethoxysilane (APDIPES) was obtained from Gelest (Morrisville, PA). NHS-PEG$_{450}$ was obtained from NanoCS (Boston, MA). Individual amino acids were obtained from Fisher Scientific, and the mix of amino acid standards was obtained from Promega (Madison, WI). Drug standards were obtained from Cerilliant (Round Rock, TX). The background electrolyte (BGE) for most experiments was 49% methanol, 2% formic acid, and 49% water (v/v/v pH = 2.8). For analysis

of the drug standards, the BGE was 50% acetonitrile, 1% formic acid, and 49% water
(v/v/v pH = 3.1).

The cells used for amino acid consumption experiments were *Escherichia coli* K-12
MG1655 strain. The cells were grown for varying amounts of time in Luria-Bertani growth
medium prepared in-house and stirred in an incubator at 37 °C. Optical density measurements
were made at 600 nm (OD_{600}) using a Biomate 3S UV-Vis spectrophotometer (Thermo
Scientific, Waltham, MA).

3.2.2   Microchip Design and Operation

Three different microchip devices were used for this work: an infusion-ESI device and two
CE-ESI devices with either a 10-cm or a 23-cm separation channel. Device fabrication and
coating details are outlined in Appendix I. Briefly, the devices were wet etched to a depth of
10 μm and full width of 70 μm. The devices were then coated with APDIPES via chemical vapor
deposition (CVD). All APDIPES coated channels were then functionalized with 20 kDa PEG in
order to suppress the EOF.

Operation of the devices is described in detail in Appendix II. All voltages were applied
with platinum wire electrodes controlled by a custom LabVIEW program. Pressure to the devices
was applied with 2 psi of air gated by 3-way valves from Clippard (Cincinnati, OH). For infusion
devices, +5 kV was applied to one reservoir along with 2 psi pressure to facilitate electrospray.
No voltage (GND) was applied to the other reservoir. For analysis of the opiate standards, a
23-cm CE-ESI device was used, and injections were performed electrokinetically as described in
Chapter 2. Run voltages of +20 kV were applied to the top (sample) and waste, +18 kV was
applied to the BGE reservoir, and +2 kV was applied to the pumping channel reservoir. For all
other experiments, a 10-cm CE-ESI device was used and injections were performed

81

hydrodynamically. To perform injections, voltages were turned off, and pressure was applied to the sample reservoir and a reservoir containing BGE for 5 to 40 s, then pressure was applied only to the reservoir containing BGE for 1 second. The voltages were then turned on, and normal zone electrophoresis began. Voltages were operated at up to +16.5 kV for the BGE reservoir and up to +2 kV for the pumping reservoir. Pressure was provided to the pumping reservoir to provide the flow necessary for electrospray.

3.2.3 Microchip ESI-HPMS

Electrospray ionization-high pressure mass spectrometry (ESI-HPMS) experiments were performed with a custom atmospheric interface and differentially pumped vacuum system adapted from the system described in Chapter 2, but redesigned with a chamber with much smaller form factor, approximately 2.5 x 2.5 x 12 cm compared to 10 x 10 x 20 cm used previously. A CAD drawing of the vacuum chamber and MS components is shown in Figure 3.1. Two different inlets and two types of optics were used: a capillary or an aperture inlet and a "gate lens" or tube lens for optics. For simplicity, only the aperture as the inlet and tube lens as the optic element are shown in Figure 3.1.

The microchip-ESI device (CE or infusion) was mounted on an adjustable x-y-z stage and positioned approximately 5-10 mm from the HPMS inlet aperture or capillary. A single-sided copper clad circuit board (M.G. Chemicals, Burlington, Ontario, Canada) was used to shield the ESI orifice on the chip from the voltages applied to the reservoirs (not shown). The corner of the microfluidic device extended about 5 mm through a slit in the board. The copper board was held at +0.5 kV for all experiments.

Ions were conducted into the chamber using either a 250 μm ID capillary (Valco Instruments Co., Inc., Houston, TX) or a 50 μm ID aperture (Lenox Laser, Glen Arm, MD). DC

voltages up to +265 V were applied to the capillary. The ions were then focused into the trap using either a 560 μm ID "gate lens" or a 3 to 6 mm ID tube lens, both spaced 140 μm from the entrance of the front endcap of the trap using a teflon spacer. Only DC potentials were used to focus ions. A positive voltage between +20 and +265 V was applied to the gate or tube during ion accumulation, and a negative voltage of -50 V or GND was applied during other parts of the scan to prevent ions from entering the trap during mass analysis.

Miniature CIT and SLIT electrodes were wet etched by Towne Technologies, Inc. (Somerville, NJ). Dimensions for the CITs were $r_0 = 280$ μm, $z_0 = 330$ μm, and endcaps with 210 μm hole diameters. Dimensions for the SLITs were $x_0 = 100$ μm, $z_0 = 117$ μm, and SLIT aperture endcaps had full widths of 165 μm. Each ring electrode contained a single trap. Traps were assembled by manual alignment using alignment pins and holes etched in the electrodes. Electrodes were mounted to a custom plate with 140 μm (CIT) or 55 μm (SLIT) teflon (PTFE) spacers between them. Drive RF waveforms were applied by a Rohde and Schwarz SMB 100A signal generator and amplified using a Mini Circuits TVA-R5-13 preamplifier and AR 305 power amplifier. The signal was resonated with a tank circuit, and applied frequencies ranged from about 7 to 31 MHz. A small supplementary RF voltage was applied to the endcap closest to the inlet using an AFG 3022B Function generator (Tektronix, Beaverton, OR) to perform resonant or double resonant ejection. Custom LabVIEW software was designed to monitor, control, and collect data. A National Instruments PXIe-1073 data acquisition chassis was used to interface the electronics and LabVIEW software.

Ions were accumulated between 1 and 30 ms before analysis. They were then scanned out of the trap and detected with an electron multiplier (Detech 2300, Detector Technology, Inc., Sturbridge, MA) connected to a current preamplifier (SR570, Stanford Research Systems,

Sunnyvale, CA). A typical mass spectrum was an average of 10 to 1000 individual mass scans.

Two sets of pumps were used for differentially pumping the chamber. A dry scroll pump

(SH-110, Agilent Technologies, Inc., Santa Clara, CA) was used on the mass analysis chamber

(~1 Torr) and an Agilent TPS Bench turbomolecular pump (Model TV81M) backed by a dry

scroll pump (SH-110) was used on the detector chamber (~30 mTorr).

For comparison of the separation and detection of the drug standards, a Synapt G2

quadrupole-ion mobility-time-of-flight mass spectrometer was used (Waters Corporation,

Milford, MA). The Synapt G2 was operated at a rate of 90 ms per summed scan with an

interscan delay of 24 ms (~9 Hz). The mass range was set to 50 to 1000 *m/z*. MassLynx software

used to collect data was triggered by a custom LabVIEW program used to control voltages

applied to the microchip.

3.3   Results and Discussion

3.3.1   SIMION Simulations of Tube Lens

Ion simulations performed by collaborators at 908 Devices, Inc. motivated the use of a

tube lens to focus ions into the trap. Ion trajectories were modeled with SIMION 8.1 software

(Scientific Instrument Services, Inc. Ringoes, NJ) using a hard-sphere collision model with SDS

(statistical diffusion simulation) program to predict the interaction of ions with background

nitrogen gas at 1 Torr. All ions were set to have a mass of 120 Da and a +1 charge. The ions

were generated at the exit of an electrode representing a capillary inlet with either a gate

electrode or a tube lens. Only DC voltages were applied to the capillary and the ion optics.

The simulation results are shown in Figure 3.2. The first set of simulations used a capillary

and a gate lens. The capillary was held at +50 V, the gate was held at +30 V, and the other

electrodes are grounded. A potential energy (PE) surface generated by SIMION is shown in Figure 3.2a with these parameters. There is an initial downhill field emanating from the capillary, but then it rises back uphill on approach to the gate electrode. In addition to collisions with buffer gas molecules, this field might impede ions traversing from the capillary to the trap. Upon exiting the gate electrode, there is a downhill and slight focusing field going towards the trap, indicating that the element should focus ions into the trap if they persist through the hole in the electrode. Figure 3.2b shows ion trajectories when no gas flow is present and where ions will only move in the presence of an electric field. In this case, the electric field created by the voltage applied to the capillary is not strong enough to drive ions through collisions with buffer gas molecules towards the gate electrode and the trap, and instead they turn around toward the inlet. Figure 3.2c shows ion trajectories with the same voltages applied in Figure 3.2b but with gas flow of 350 m/s applied in the y direction toward the trap. With the gas flow, ions are conducted from the capillary, through the gate lens, and into the trap. The magnitude of this gas flow is unrealistic over this distance, but it demonstrates that the primary driving force conducting ions from the capillary into the trap in previous experiments was not the electric field but the gas flow from the capillary through the chamber.

An alternative to gate lenses are tube lenses into which the outlet of the capillary can be inserted. A PE surface of the capillary with a tube lens of 5 mm length and 5 mm ID is shown in Figure 3.2d. The voltage applied to the capillary was +50 V, the voltage applied to the tube was +30 V, and the other electrodes were held at GND (the same voltages as Figure 3.2a). With the addition of the tube lens, there is a downhill or flat path spanning from the capillary to the trap. The inward slope of the potential surface at the edges and the exit of the tube lens suggest that it will act as a focusing element as well. Figure 3.2e shows ion trajectories with the new geometry

and no gas flow. In this case, the electric field is sufficient to drive ions to the trap, and no gas flow is necessary. In addition, the tube lens provides a focusing effect for the ions into the trap, giving them a narrower dispersion than the simulation of the gate electrode with gas flow in Figure 3.2c. While some gas flow is present in reality, these simulations indicate that, with a tube lens, the primary driving force for ion transport will be the electric fields. The results of these simulations suggest that a tube lens would be an improved optic element over a shorter "gate lens," and still only require DC voltages. This motivated a switch in instrumentation implementation to use of the tube lens as the primary ion optic element.

3.3.2   Tube Lens ID Characterization

Based on the simulation results, a set of tube lenses was characterized to assess their performance. Tube lenses 5 mm in length with diameters of 3, 4, 5, and 6 mm were tested. Histidine was infused into the mass spectrometer at 100 μM as the test analyte. The pressure in the mass analyzer chamber was 1 Torr with ambient air as the buffer gas. The RF applied to the CIT was 14.4 MHz, and a small axial potential was applied to the endcap nearest the inlet at 4.8 MHz and 5 V_{p-p}. A voltage of +130 V was applied to the capillary and the tube lenses were pulsed from +230 V during ion injection to GND during other parts of the scan.

The results from each of the tube lenses tested are shown in Figure 3.3. Figure 3.3a shows a sample histidine mass spectra for each of the tube lenses. The protonated molecule is clearly visible in each spectrum at *m/z* 156, along with a fragment at *m/z* 110 (loss of carboxylic acid). Although ESI is a relatively soft ionization technique, it is not surprising to see some fragmentation under HPMS conditions. The high pressure (1 Torr) results in more collisions of analyte molecules with buffer gas, which can lead to the conversion of kinetic energy to internal energy and cause fragmentation. As the tube lens diameter is increased, there is a clear increase

in signal for both peaks in the spectrum. Figure 3.3b shows the signal-to-noise ratio (S/N) for the protonated molecule in each of the spectra. While each tube lens generates spectra with high enough S/N for quantitation, there is a clear advantage of the 6 mm ID lens over the other three. The S/N is roughly double that of the 4 and 5 mm lenses, and almost five times that of the 3 mm lenses. An ID of 6 mm is the practical upper limit due to space constraints in the high pressure mass spectrometer, so larger ID lenses were not tested. With the clear advantage of the 6 mm ID lens over the others for histidine, a 6 mm ID lens was used for all further analysis of amino acids by HPMS.

3.3.3   Amino Acid Standards

After optimization of the tube lens ID, several other changes were made for the analysis of amino acids compared to initial efforts presented in Chapter 2. First, according to Equation 3.1, the resolution can be improved by increasing the drive frequency applied to the ring electrode. In order to improve the resolution under HPMS conditions, the drive frequency was increased to close to 30 MHz from less than 10 MHz implemented previously. In order to implement HPMS at 30 MHz, according to Equation 3.2, the trap size must be decreased to maintain practical voltages. In this case, the trap size was decreased from critical dimensions around 280 μm to 100 μm. With the decrease in trap size comes a decrease in trapping capacity, so a SLIT geometry was used instead of a CIT to increase the number of ions that can be trapped and improve sensitivity. Finally, an aperture inlet was found to have similar ion transmission and flow rates to a capillary but was simpler to implement in the mechanical design, so an aperture inlet was used for amino acid analysis.

Each of the 20 common amino acids was infused separately into the mass spectrometer at a concentration of 50 μM. The spectra for each amino acid are shown in Figure 3.4, in order of

increasing mass from bottom to top. The RF frequency applied to the ring electrode was 30.6 MHz, and axial RF was applied to the endcap at 7.67 MHz and 4.0 V_{p-p}. A 50 μm ID aperture was used, +35 V was applied constantly to the inlet. The 6-mm ID tube lens had +20 V applied during ion accumulation and -50 V during all other parts of mass analysis. Each spectrum is an average of 1000 individual mass scans. The mass range was the same as previous analyses, approximately 70 to 220 m/z. The protonated molecule (($M+H)^+$) for each compound is easily detectable, which should provide enough information for compound identification in many scenarios, especially those that are targeted. The aberrations in the baselines of glycine and alanine are artifacts from filtering and show the lower S/N of those molecules. They were detected at lower S/N likely because of their small size and can be scattered more easily than amino acids of larger mass by collisions with the buffer gas. Most spectra only contain the protonated molecule, but the aspartic acid and cysteine spectra have additional features. These features are probably adducts of the analytes with solvent molecules. Even with these adducts and other features, a peak for the protonated molecule is easily detectable.

Significant improvements for these spectra were observed over the infusions performed during the initial development of the platform discussed in Chapter 2. Comparisons of two sample spectra of proline and arginine are shown in Figure 3.5a and b, respectively. For proline (Figure 3.5a), the same features are observed in each spectrum, including a prominent $(M+H)^+$ peak and some other minor peaks at higher m/z. However, the new spectrum (top, red) shows several improvements over the previous spectrum (bottom, black) including in S/N and reduced peak width (full-width half maximum, FWHM). The S/N increased from 14.5 to 407.9, and the FWHM was narrowed from 7.1 to 3.4 m/z. Similar improvements are seen with the arginine spectra in Figure 3.5b. The largest peak in each arginine spectrum is the protonated molecule,

and some smaller features are observed at lower *m/z*. As with the proline spectrum, there are significant enhancements in S/N and FWHM in the new arginine spectrum over the previous spectrum. The S/N increased from 50.1 to 618.5, and the FWHM narrowed from 9.6 to 3.2 *m/z*. A complete list of improvements in S/N and FWHM for each of the amino acids over previous analyses is shown in Table 3.1. There was an average of 28-fold increase in S/N, and the FWHM narrowed 2.6-fold on average.

With detectability of each amino acid shown, a separation of a mixture of the twenty common amino acids was performed to demonstrate the viability of a CE-ESI-HPMS platform for small molecule analysis. The results of the separation and detection are shown in Figure 3.6. The same RF frequencies and voltages, DC voltages, and pressure (1 Torr) as the amino acid infusions were used. A 10-cm CE-ESI device was used with a separation channel field strength of about 1000 V/cm. Hydrodynamic injections were performed for 5 s each. A BPI electropherogram from the analysis is shown in Figure 3.6a with amino acid labels for each peak. The separation is performed in under 1.8 min, and 18 of the 20 common amino acids are detected, with the two smallest amino acids, glycine and alanine, going undetected. Species that might overlap in an HPMS spectrum are separated in the CE dimension. For example, leucine (L) and isoleucine (I) have exactly the same mass and are completely separated with microchip CE. There are some components that are unresolved in the CE domain, namely the co-migrating pairs methionine (M) and threonine (T), asparagine (N) and proline (P), tryptophan (W) and glutamine (Q), and glutamic acid (E) and cysteine (C). However, each of these pairs is easily distinguished in the mass spectral domain. This is readily seen in the 2D plot showing the migration times and *m/z* in Figure 3.6b. In this case, each of the spots corresponds to an amino acid, and it is easy to see where each amino acid is detected and separated. For example,

glutamine (Q) and tryptophan (W) co-migrate in the CE domain, but their protonated molecules (147 and 206 m/z, respectively) are clearly resolved in the mass domain. Even though some resolution is lost due to the operation at HPMS conditions, coupling with a CE separation makes up for some of that loss and enhances the potential for compound separation and identification.

3.3.4 Amino Acid Consumption and Cell Growth

In order to simulate consumption of amino acids from growth medium in a bioreactor, bacterial cells were grown in LB medium in flasks. The workflow for the experiment is shown in Figure 3.7. Cells were incubated in LB (Step 1), then samples of growth medium were taken and centrifuged to eliminate cell debris. The supernatant was then filtered with a 0.22 μm syringe filter (Step 2). Samples were then diluted 100X in BGE (49% methanol, 2% formic acid) and spiked with valine-d_8 as an internal standard (Step 3). Finally, each of the samples were loaded onto a 10-cm CE-ESI device for analysis by CE-HPMS (Step 4). The field strength for the separations was about 1000 V/cm, and hydrodynamic injections were performed for between 30 and 40 s. The pressure in the mass spectrometer was 1 Torr with ambient air as the buffer gas, and all other mass spectral parameters were the same as listed in the previous section for the infusions of amino acids.

To determine the components in growth medium to monitor, samples of growth medium before and after cell growth were analyzed. Figure 3.8 shows electropherograms of the growth medium before any cell growth and after 24 hours of cell growth. The numbered peaks indicate the same components in each electropherogram: arginine (1), isoleucine (2), and phenylalanine (3); the migration times were slightly different due to slight differences in electric field strength. The peaks marked with an asterisk indicate amino acids that were consumed over this time period. Those peaks correspond to serine, proline and asparagine (same peak), and tryptophan.

Some other components were consumed over this time period, but these amino acids were chosen as the primary targets for this analysis. Many of the other components, including other amino acids, remained unchanged over this time period of cell growth.

After determining which amino acids were consumed, another batch of cells were grown, and samples of the growth medium were acquired every 30 min for 9 h and one time point at 24 hours. Sample electropherograms from 0 h, 5.5 h, and 24 h are shown in Figure 3.9. The migration times were adjusted to align with the 0 hour time point for easy visualization of the changes between them. The peaks with asterisks indicate compounds that are completely consumed over this time period. The peak corresponding to isoleucine was overloaded intentionally to monitor other amino acids at lower concentrations. Based on the data in Figure 3.8, isoleucine was not expected to be consumed over this time period. Some amino acids are consumed at different rates than others, and some only partially consumed. Arginine, for example, is only partially consumed over the 24 hour time period. Figure 3.10 shows mass spectra of arginine at the three time points shown in Figure 3.9. The primary peak, the protonated molecule at m/z 175, drops in intensity over this time period, and the other smaller peaks in the spectrum decline in intensity as well.

In order to quantify the consumption of the targeted amino acids, their peak intensities were compared with that of the internal standard, valine-d_8. Their intensities at different time points relative to the internal standard and normalized to the time zero point are shown in Figure 3.11, along with the cell growth curve, as measured by the OD_{600}. Cell growth enters the exponential phase around 2 hours of cell growth, and begins to level off around after 6 hours of growth. As the cells grow, the amino acids are consumed at different rates with some not consumed at all. Valine, as shown in Figure 3.11, is an example of a component that is not

consumed in the 24 h time period. Serine, proline, and tryptophan were all completely consumed over this time period, albeit at different rates. Serine was consumed at the fastest rate, followed by tryptophan, and finally proline. Utilization of certain amino acids and their consumption at different rates could indicate factors affecting cell growth. For example, a lack of serine has been shown to induce stress and inhibit cell growth in certain types of cancer cells.[32]

The ability to track the components in growth medium in such a short time presents an opportunity for real-time monitoring of cell growth. Using the microchip CE platform, the amino acids in LB growth medium can be separated in under 3 minutes, and HPMS detection offers a simple and less expensive alternative to conventional mass spectrometry methods. Thus, there is potential for a CE-HPMS platform to be used as an on-line monitoring and screening tool to inform cell growth for biopharmaceutical or other applications. For example, if the concentration of serine is known at all times and is necessary for cell growth, the concentration can be adjusted in real-time to ensure the proper development of cells.

3.3.5 CE-HPMS of Opiate Standards

Opiate standards were dissolved in BGE at 5 μg/mL each. They were separated on a 23-cm microchip CE device before ESI into the mass spectrometer. Electrokinetic injections of 0.2 s were performed, and the field strength was about 675 V/cm. For HPMS detection, the pressure was 1 Torr with ambient air as the buffer gas, and the trap was operated with a drive RF of 8.1 MHz and no axial RF. The capillary was operated at +75 V, and the gate lens was pulsed from +30 V during ion injection to GND. The separation and detection of a mix of 13 standards with HPMS detection (red, bottom) and a commercial mass spectrometer (Synapt G2, black, top) is shown in Figure 3.12. All 13 components are detected with the Synapt G2, and 11 of the 13 components were detected with the HPMS system. The opiates were detected with similar

efficiencies and S/N in each electropherogram. The two components that were undetected with HPMS were methadone and *cis*-tramadol. Because of the high pressure of the HPMS system, it is likely that methadone and *cis*-tramadol are fragmenting in the mass spectrometer, and the subsequent fragments are outside the current mass range and therefore undetected. There are also different intensity ratios of the drug standard peaks. The most intense peak in the HPMS electropherogram corresponds to buprenorphine, while the most intense peak in the Synapt G2 electropherogram corresponds to three co-migrating compounds: hydromorphone, codeine, and methadone. As this particular method is targeting identification and not quantitation, differences in intensity are not important, but an internal standard could be used if quantitation was necessary in the future.

The separation and detection of the opiate standards with HPMS is shown in the 2D plot in Figure 3.13 to view both CE and mass spectral data, and to highlight the importance of each technique. Each spot on the 2D plot corresponds to a compound or one of its fragments. In this case, fragmentation was minimal. Three spots are labeled to highlight the advantage of both electrophoretic and mass spectral information. First, codeine and hydrocodone are labeled and have the same mass, but are separated in the CE domain. Without the CE separations, these two components could not be distinguished by HPMS. Second, hydromorphone and codeine co-migrate, but have distinct masses. Without HPMS, hydromorphone and codeine could not be distinguished. There are several other compounds in the mixture that would overlap in either domain, demonstrating the need for both steps for an effective analytical platform.

3.3.6   CE-HPMS of Codeine in Urine Samples

To demonstrate the viability of CE-HPMS for the analysis of opiates in complex matrices, codeine was spiked into urine at varying concentrations. The workflow for the experiment is

shown in Figure 3.14. Codeine was spiked into 1 mL urine samples (Step 1). The urine samples were then loaded onto a solid phase extraction (SPE) column (Waters HLB, Step 2). The samples were then eluted off the column with 100 μL of BGE, giving a 10x concentration factor (Step 3) before analysis by CE-HPMS (Step 4). Microfluidic platforms offer the integration of many elements onto one device, so it is possible that an SPE bed could be incorporated onto the microchip in the future. However, for this proof-of-concept experiment, all SPE was performed off-line. A CE device with a 10-cm separation channel was used, and the field strength was about 1000 V/cm. Injections were performed hydrodynamically for 5 s each. The mass spectrometer was operated at 1 Torr pressure with ambient air as the buffer gas, and all other mass spectral parameters were the same as described above for the analysis of the opiate standards.

Two sample electropherograms are shown in Figure 3.15. The bottom trace (black) shows a blank urine sample, and the top trace shows a sample spiked with codeine at a concentration of 100 ng/mL. The separation is performed in less than 2.1 min. Urine is a complex matrix, and the blank trace contains many peaks corresponding to various metabolites and other compounds in urine. When codeine is spiked in the sample at 100 ng/mL, there is a clear peak that appears in the electropherogram corresponding to codeine, labeled in the figure. Codeine can be identified as a spot in a 2D plot as well. Figure 3.16 shows 2D plots of codeine spiked into urine at two concentrations: 100 ng/mL (Figure 3.16a) and 10 ng/mL (Figure 3.16b). The spots corresponding to codeine are labeled in the figure. In both cases, codeine is separated from components of similar mass in the CE domain. Likewise, at the lower concentration in Figure 3.16b, codeine would not be distinguishable from other co-migrating components, further demonstrating the power of performing a separation step with HPMS detection. According to information from the Mayo Clinic, the necessary limit of quantitation (LOQ) to determine exposure for most opiates is

25 ng/mL.[33] The detection of codeine in urine at 10 ng/mL is within that LOQ, indicating that CE-HPMS could be viable alternative to LC/MS or GC/MS methods to detect opiates in urine.

3.4   Conclusion

Improvements and applications for ESI-HPMS analysis of small molecules have been demonstrated. SIMION simulations were used to guide the development of DC ion optics in the form of a tube lens to increase ion transmission over the initial design. The platform was used for the analysis of amino acid standards at 50 μM, and significant improvements were shown in both S/N and peak width. Amino acid content in LB growth medium was monitored and correlated with cell growth, demonstrating the viability of CE-HPMS for real-time measurements of bioreactor content. Finally, opiate drug standards were detected and compared with a commercial mass spectrometer. After SPE, codeine was detected in a urine sample as low as 10 ng/mL, showing a possible small molecule target for forensic application of CE-HPMS.

3.5   Figures and Tables
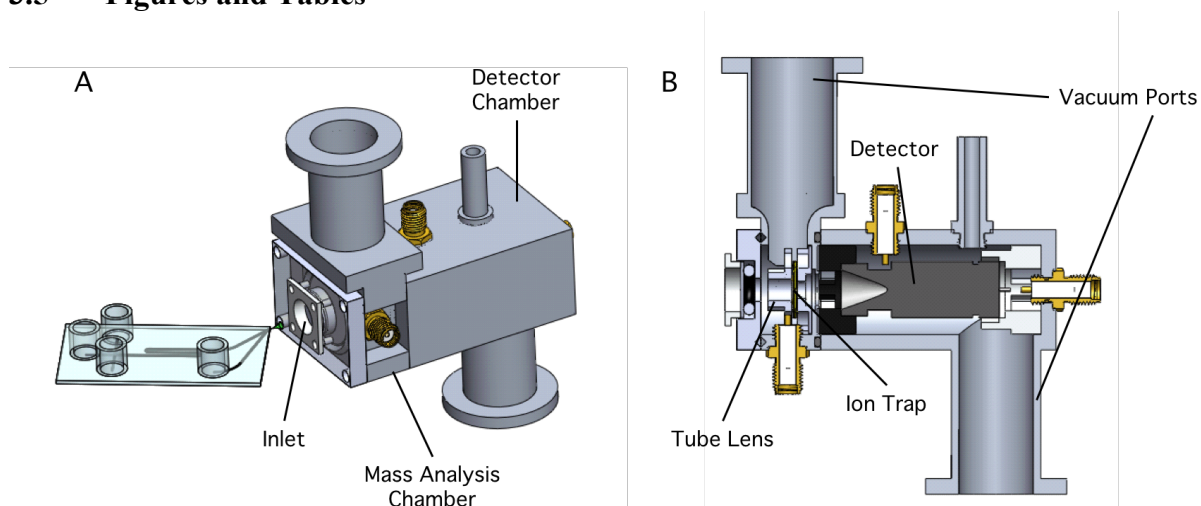
Figure 3.1: Instrument diagram (CAD) in A) isometric and B) cross-section view. Similar to the previous instrument design, there are two vacuum chambers, one for mass analysis at >1 Torr, and one for detection at <50 mTorr. The trap resides in the mass analysis chamber and acts as the conductance limit between the chambers.
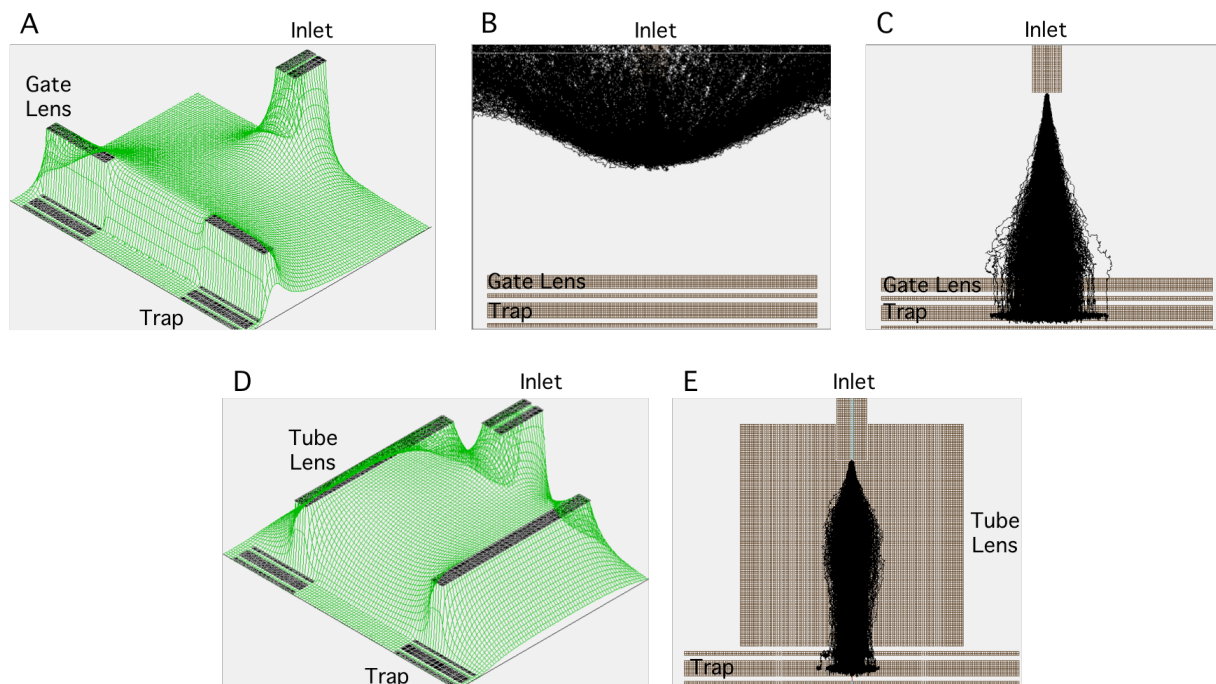
Figure 3.2: Results of SIMION simulations. A) Potential energy surface with capillary and gate lens. B) Ion trajectories using voltages applied to the capillary and gate lens without gas flow. C) Ion trajectories with 300 m/s gas flow in the y-direction (toward the trap). D) Potential energy surface with capillary and tube lens. E) Ion trajectories using voltages applied to the capillary and tube lens without gas flow.
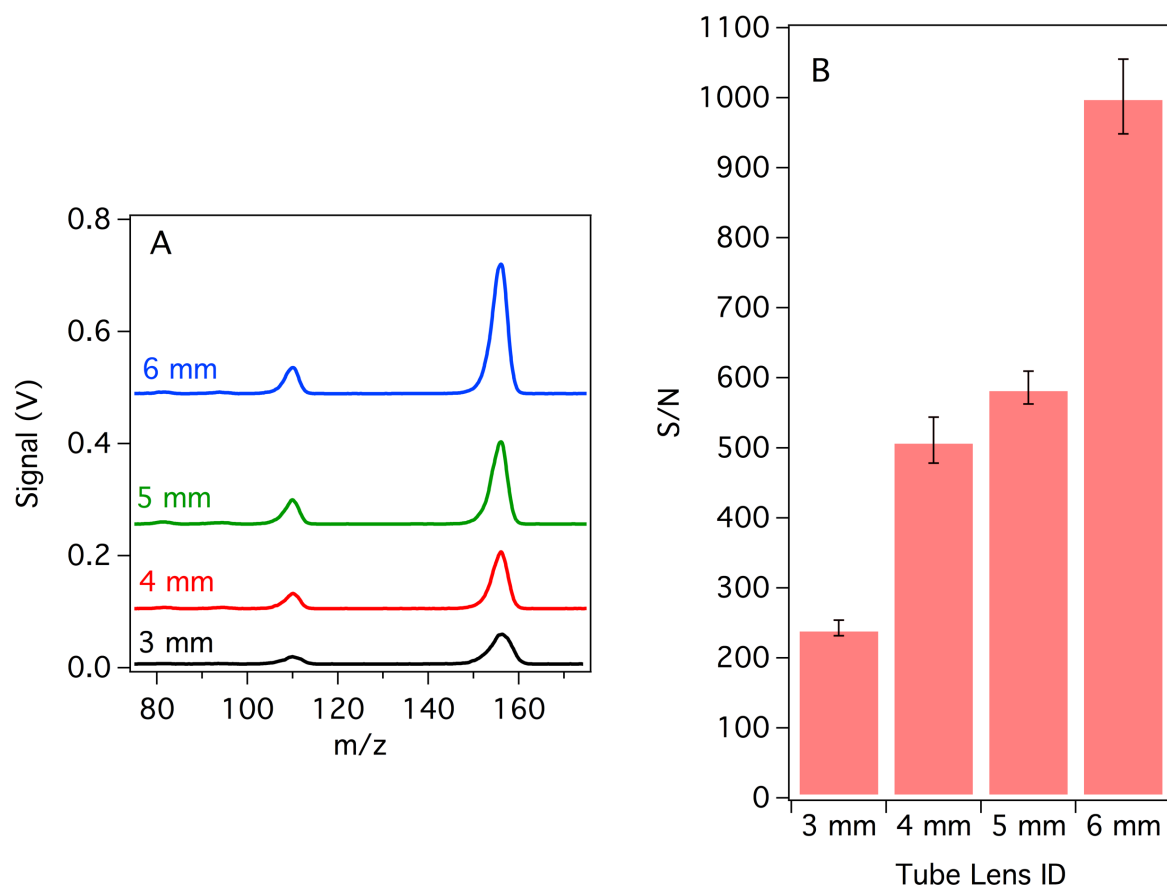
Figure 3.3: Effects of tube lens ID on mass spectra with A) Sample mass spectra of histidine and B) S/N of histidine protonated molecule at various tube lens IDs.
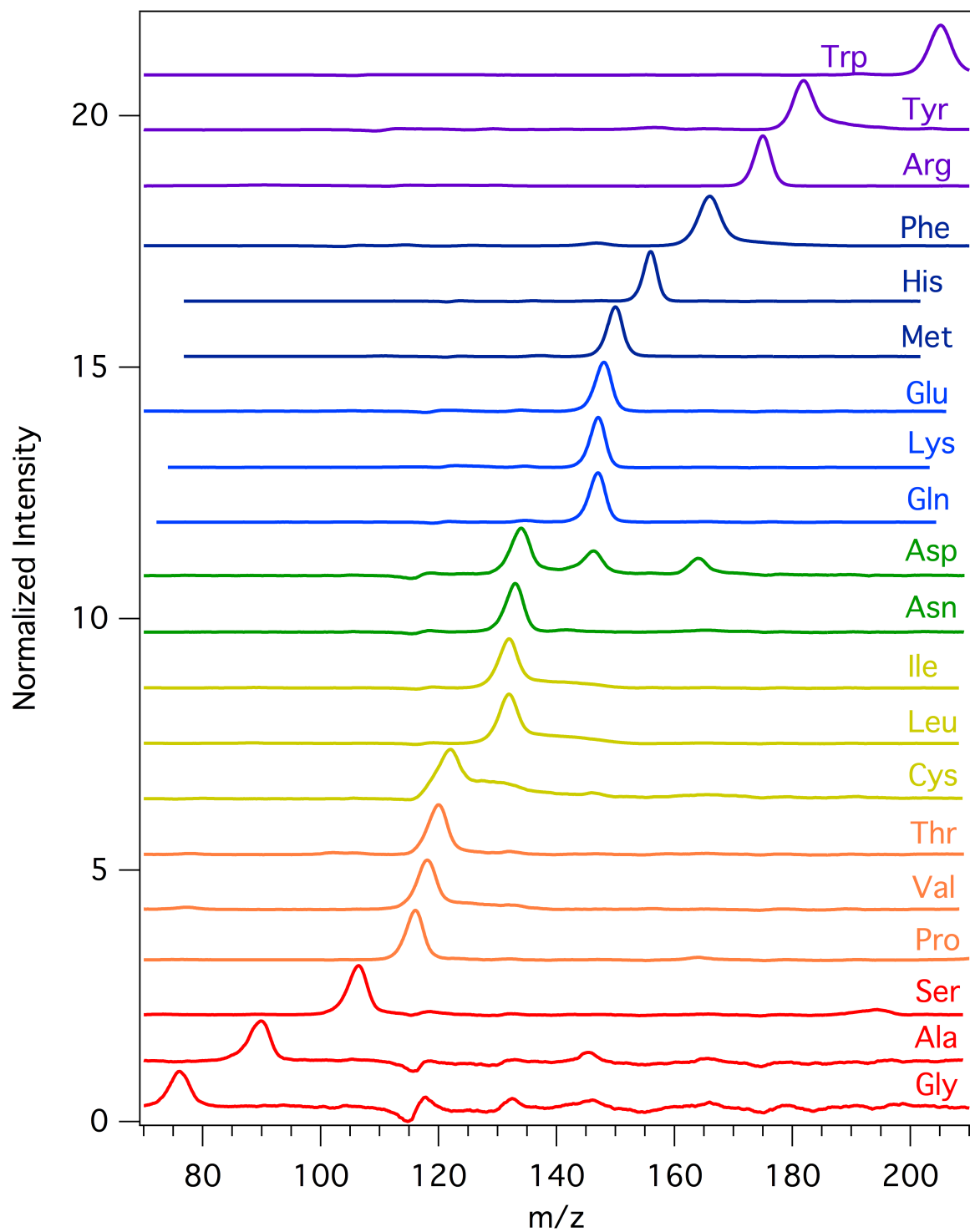
Figure 3.4: Infusion-ESI-HPMS spectra of each of the twenty common amino acids at 50 μM.
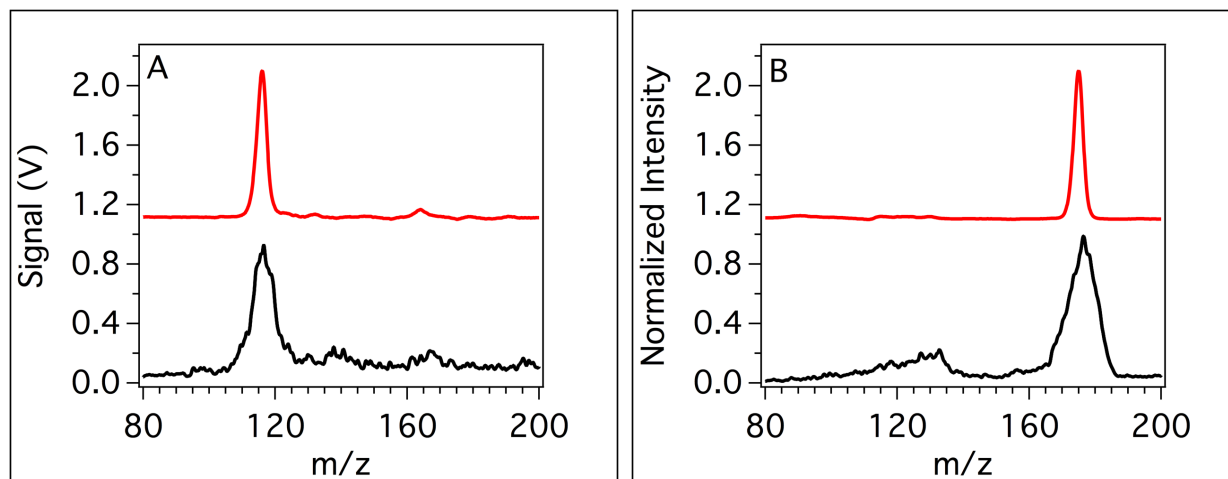
Figure 3.5: Sample amino acid mass spectra taken with a tube lens (red, top) compared to a gate lens (spectra from Chapter 2; black, bottom) of A) proline and B) arginine.

Table 3.1: HPMS improvements in S/N and FWHM for the 20 common amino acids before and after system optimization.

Amino Acid	S/N Before	S/N After	FWHM Before	FWHM After
Ala	6.9	7.9	7.4	4.1
Arg	50.1	618.5	9.6	3.2
Asn	18.8	525.2	8.6	3.4
Asp	48.1	435.3	12.0	3.8
Cys	7.3	345.3	14.8	5.2
Gln	17.7	978.3	11.4	3.2
Glu	42.4	500.4	8.5	3.2
Gly	6.5	7.6	7.9	4.0
His	36.1	1008.2	9.1	2.6
Ile	11.3	820.2	9.7	3.8
Leu	21.2	679.5	10.8	3.8
Lys	59.6	843.3	7.6	3.0
Met	100.0	1756.2	8.5	3.0
Phe	42.1	986.2	8.6	4.4
Pro	14.5	407.9	7.1	3.4
Ser	9.7	649.2	7.1	3.8
Thr	23.1	318.2	11.5	3.8
Trp	17.8	1030.1	10.8	4.6
Tyr	87.5	101.4	9.9	4.1
Val	18.1	665.7	9.8	4.2
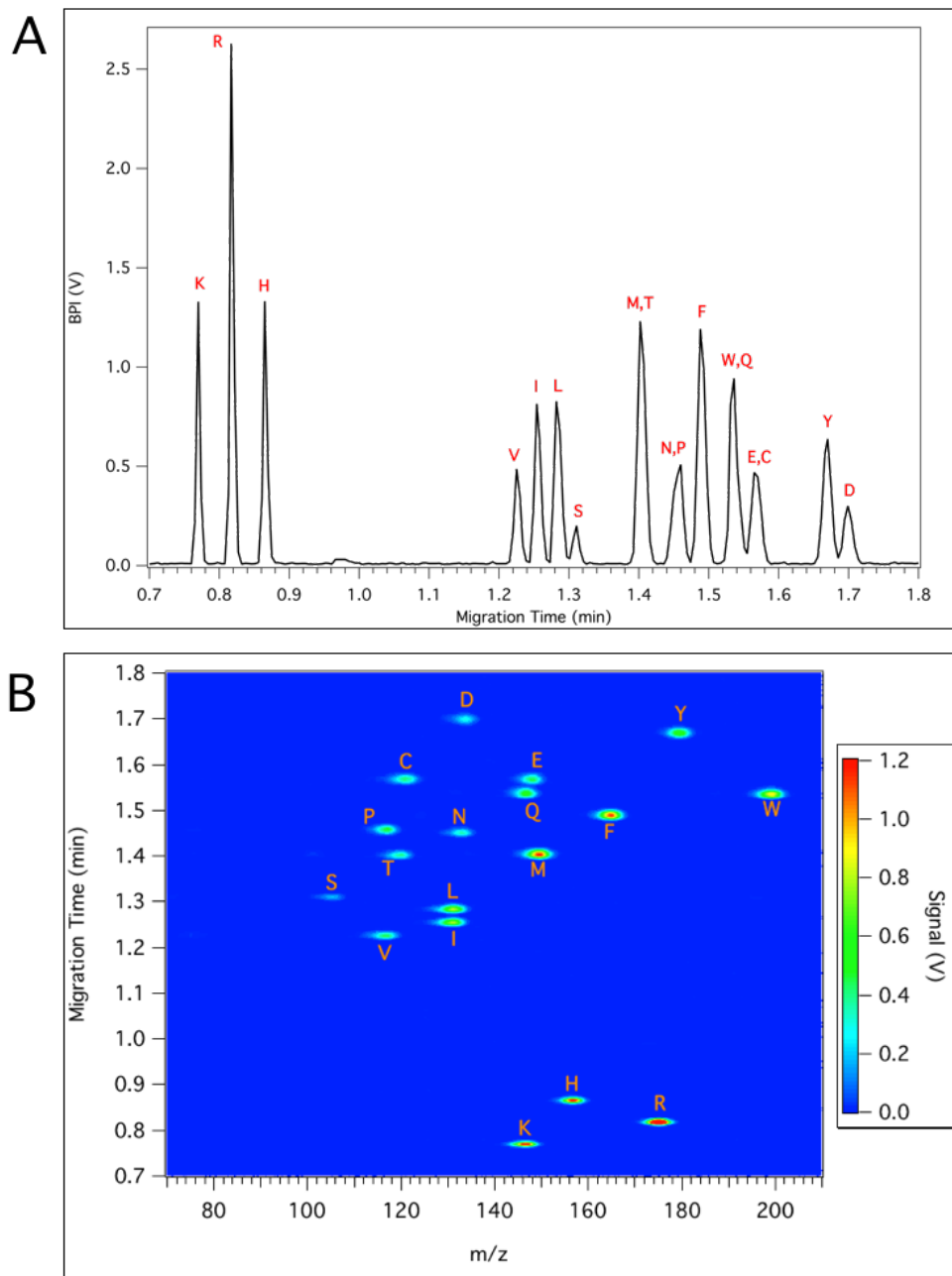
Figure 3.6: CE-HPMS separation and detection of amino acid standards in A) a standard electropherogram and B) a 2D plot showing both migration time and *m/z*.
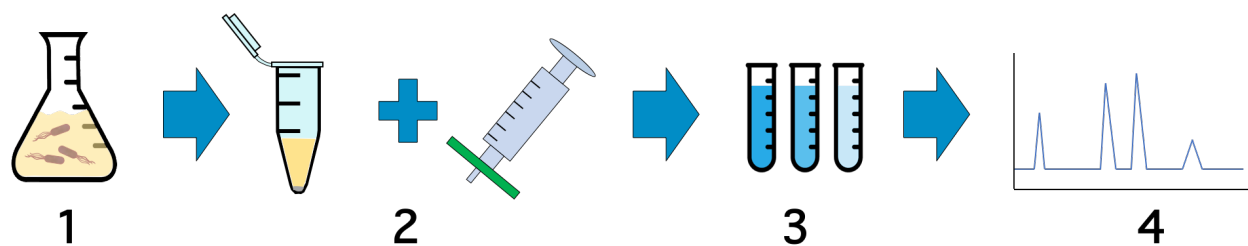
Figure 3.7: Workflow for growth medium sample experiments. 1) *E. coli* are incubated at 37 °C in LB growth medium. 2) Samples are centrifuged and subsequently filtered with 0.22 μm syringe filter. 3) Samples are then diluted 100X in BGE and an internal standard added and 4) analyzed by CE-HPMS.
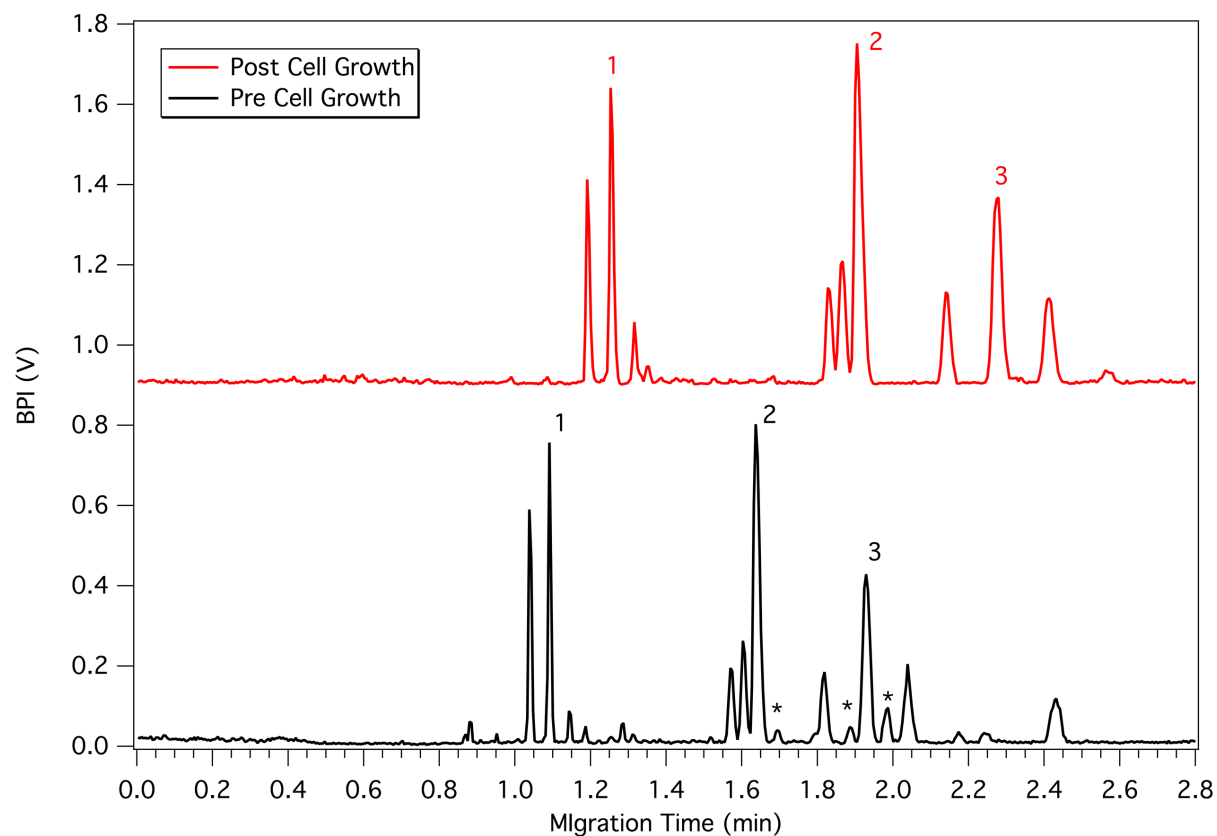
Figure 3.8: CE-HPMS electropherograms pre (black, bottom) and post (red, top) cell growth. The numbered peaks correspond to the same components, and the starred peaks are amino acids that are consumed over this time period.
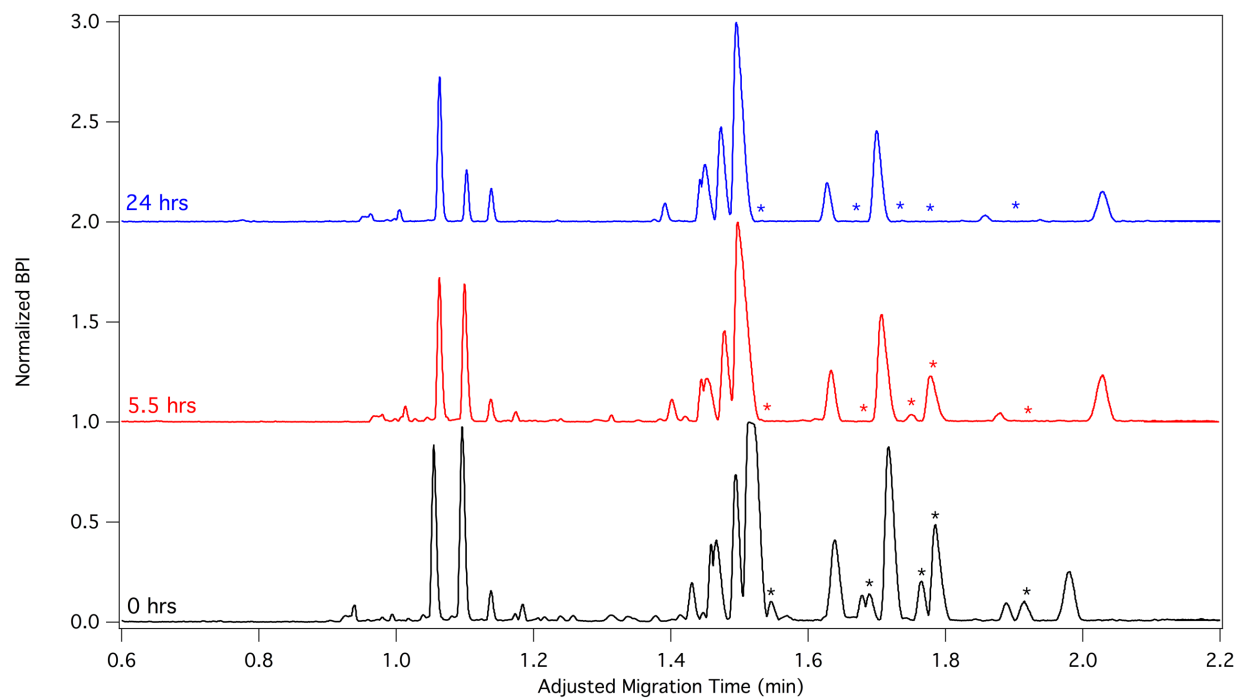
Figure 3.9: Sample electropherogram time points over the course of cell growth. The migration times were adjusted to correspond with the 0 h time point for visualization. The starred peaks represent components that were consumed of the course of this experiment.
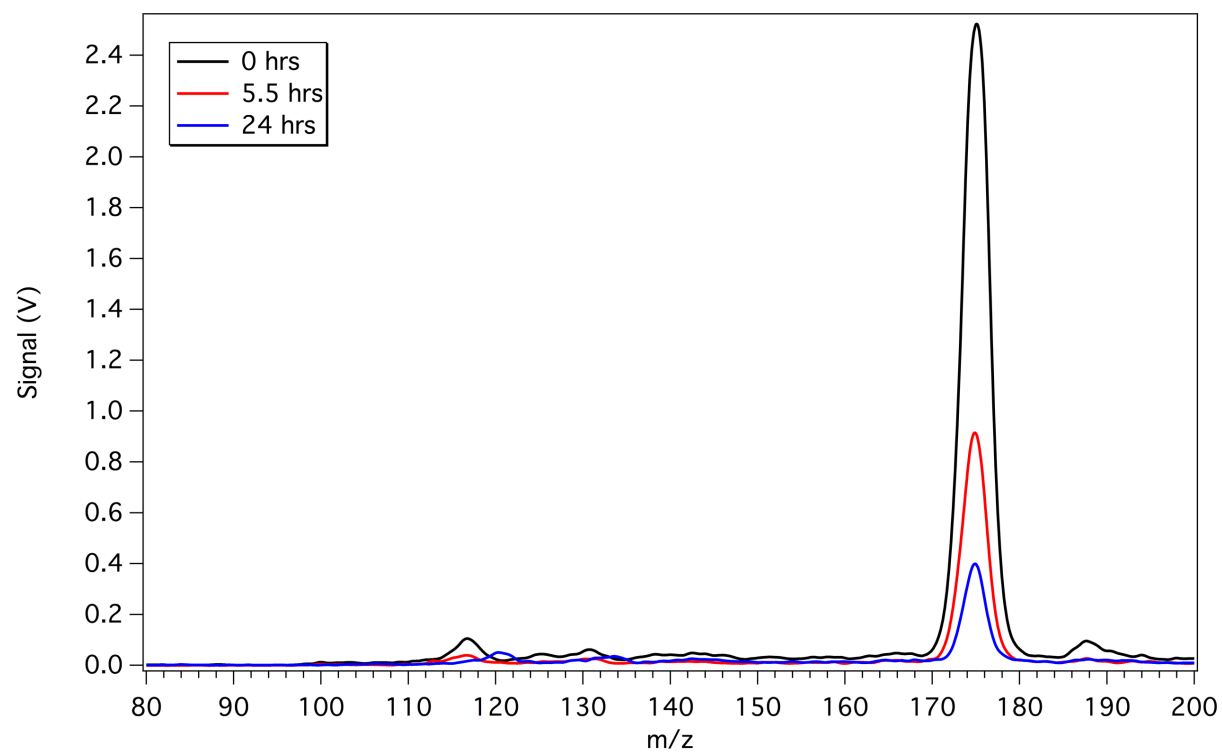
Figure 3.10: Sample arginine mass spectra over the time points shown in Figure 3.9.
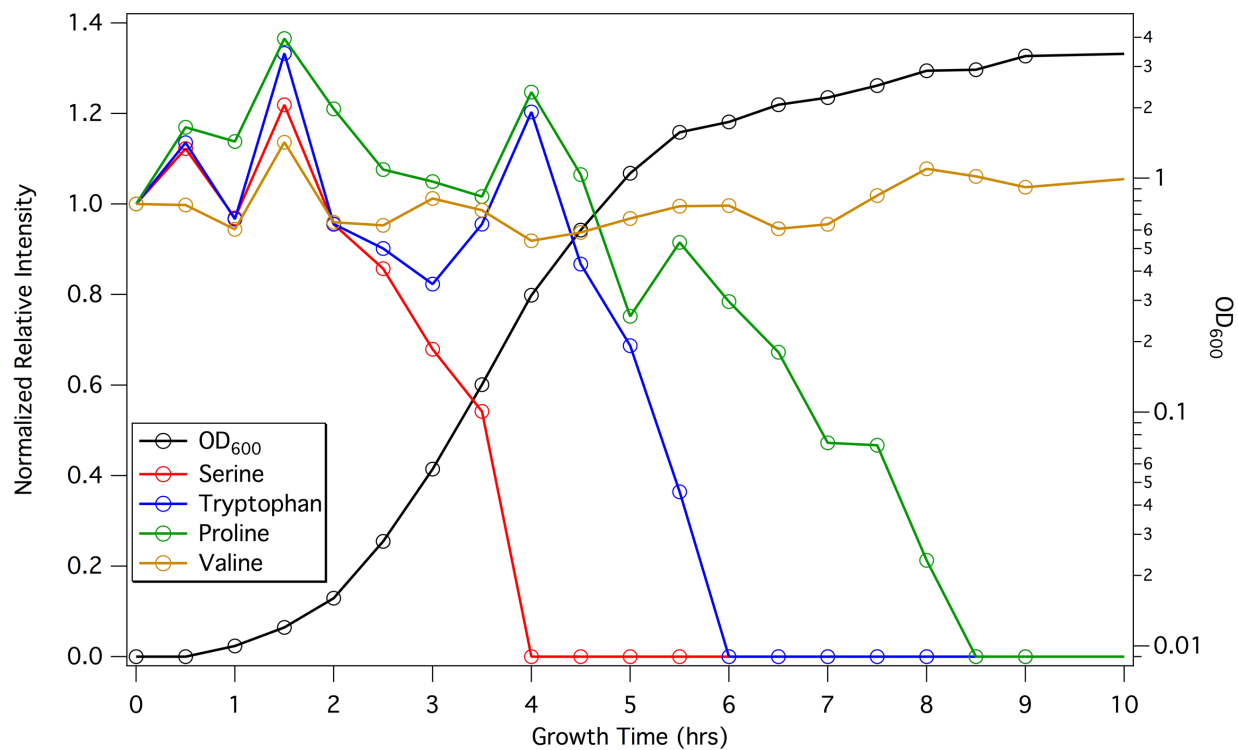
Figure 3.11: Relative peak areas of four amino acids referenced to the internal standard shown with the cell growth as measured by OD_{600}.
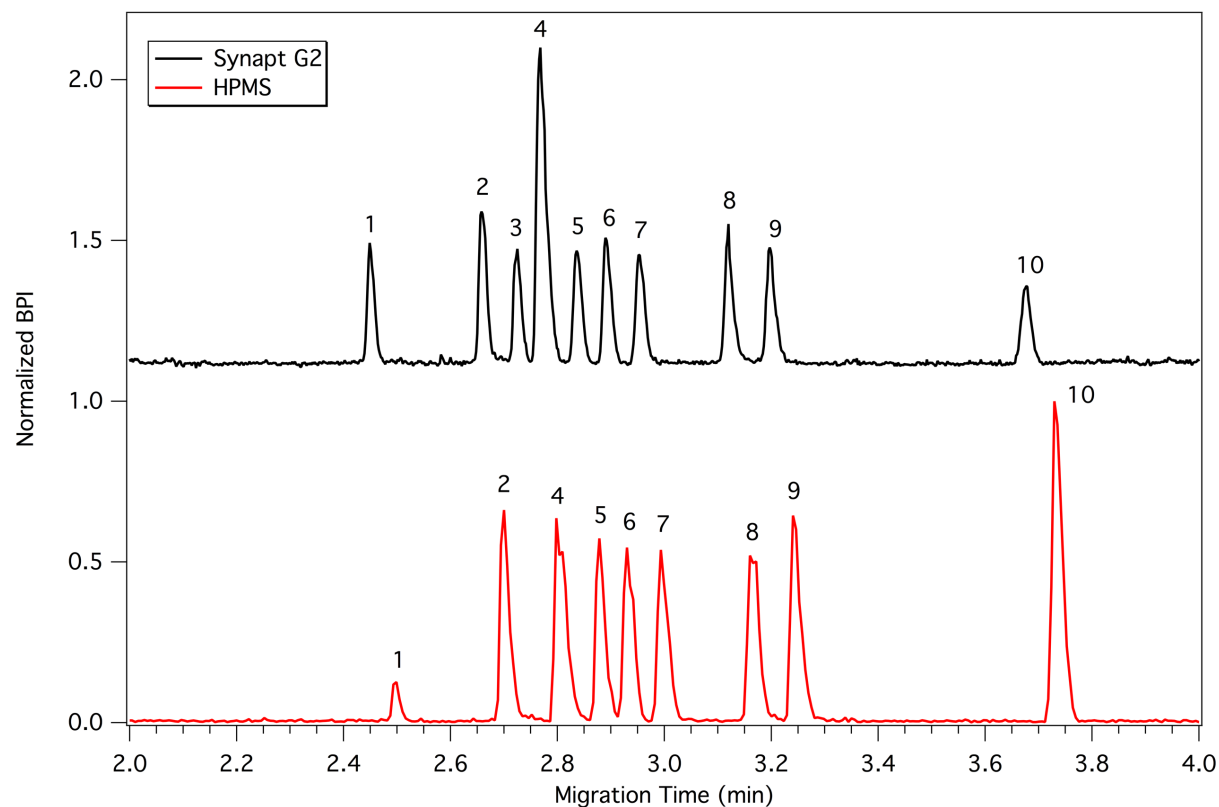
Figure 3.12: Electropherograms of opiate standards (5 µg/mL) detected on Synapt G2 (black, top) and HPMS (red, bottom). 1 – meperidine, 2 – hydrocodone, 3 – *cis*-tramadol* ,4 – hydromorphone, codeine, methadone*, 5 – oxycodone, 6 – morphine, 7 – oxymorphone, 8 – naloxone, fentanyl (0.5 µg/mL), 9 – naltrexone, 10 – buprenorphine. Starred components were not detected with HPMS.
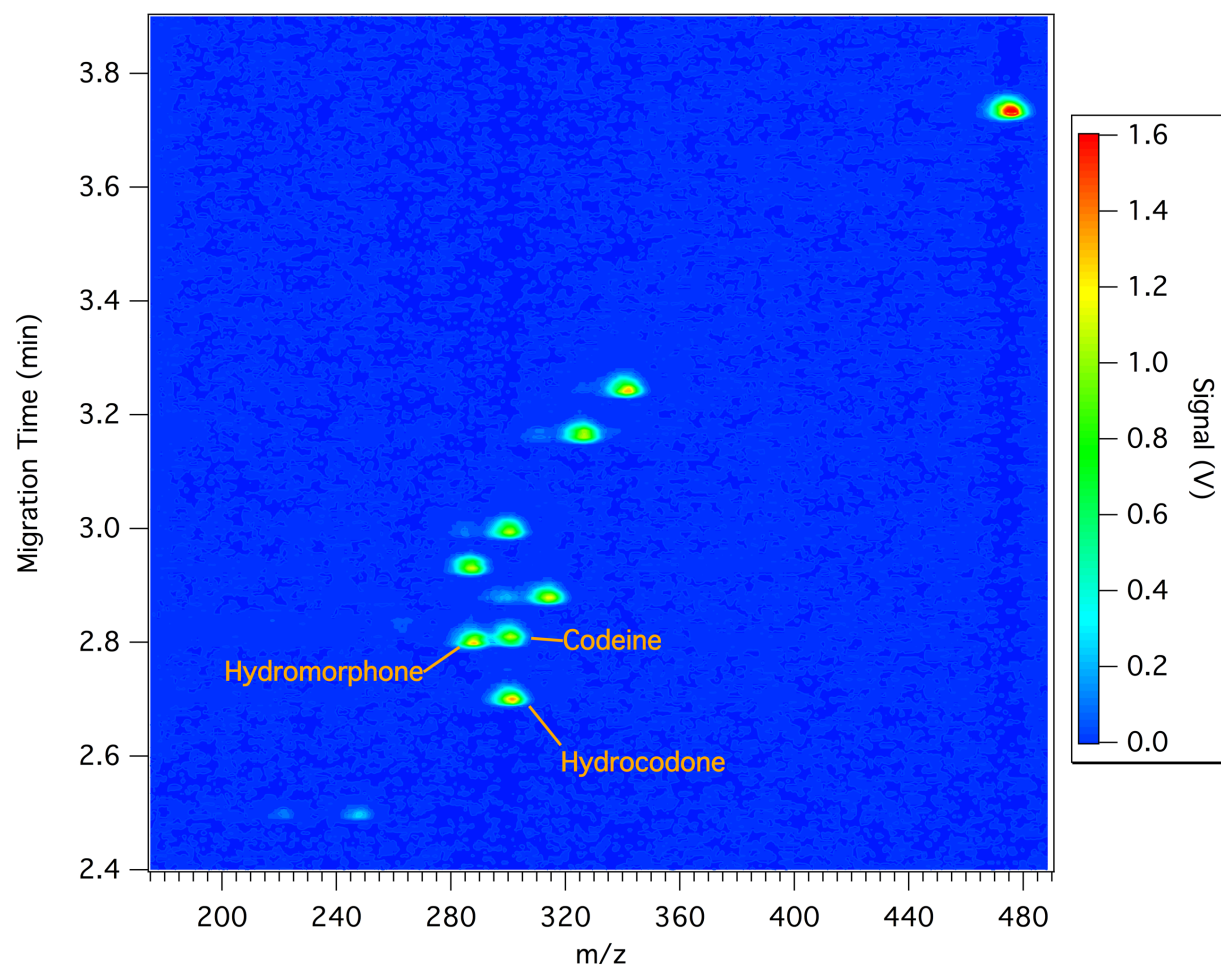
Figure 3.13: 2D plot of CE-HPMS of opiate standards. Codeine, hydrocodone, and hydromorphone are labeled to highlight the need for both CE separation and MS detection.
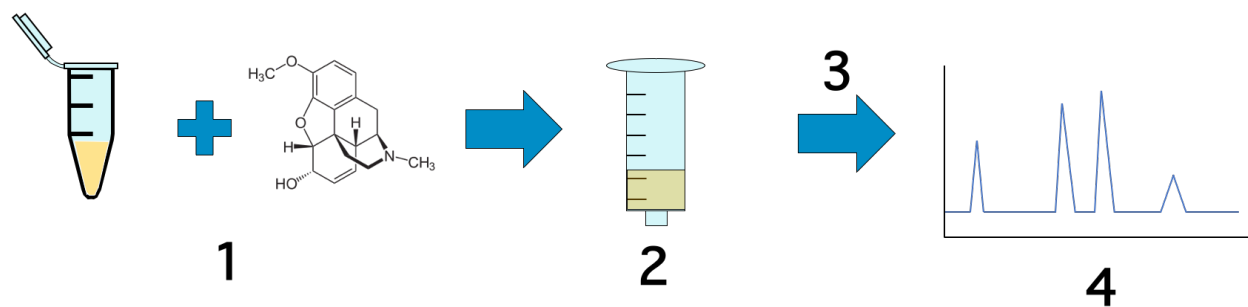
Figure 3.14: Workflow for detection of codeine in urine. 1) 1 mL of urine is spiked with codeine. 2) Spiked urine sample is loaded onto to Waters HLB SPE cartridge. 3) Sample is eluted from SPE cartridge in 100 µL of BGE. 4) Analysis by CE-HPMS.
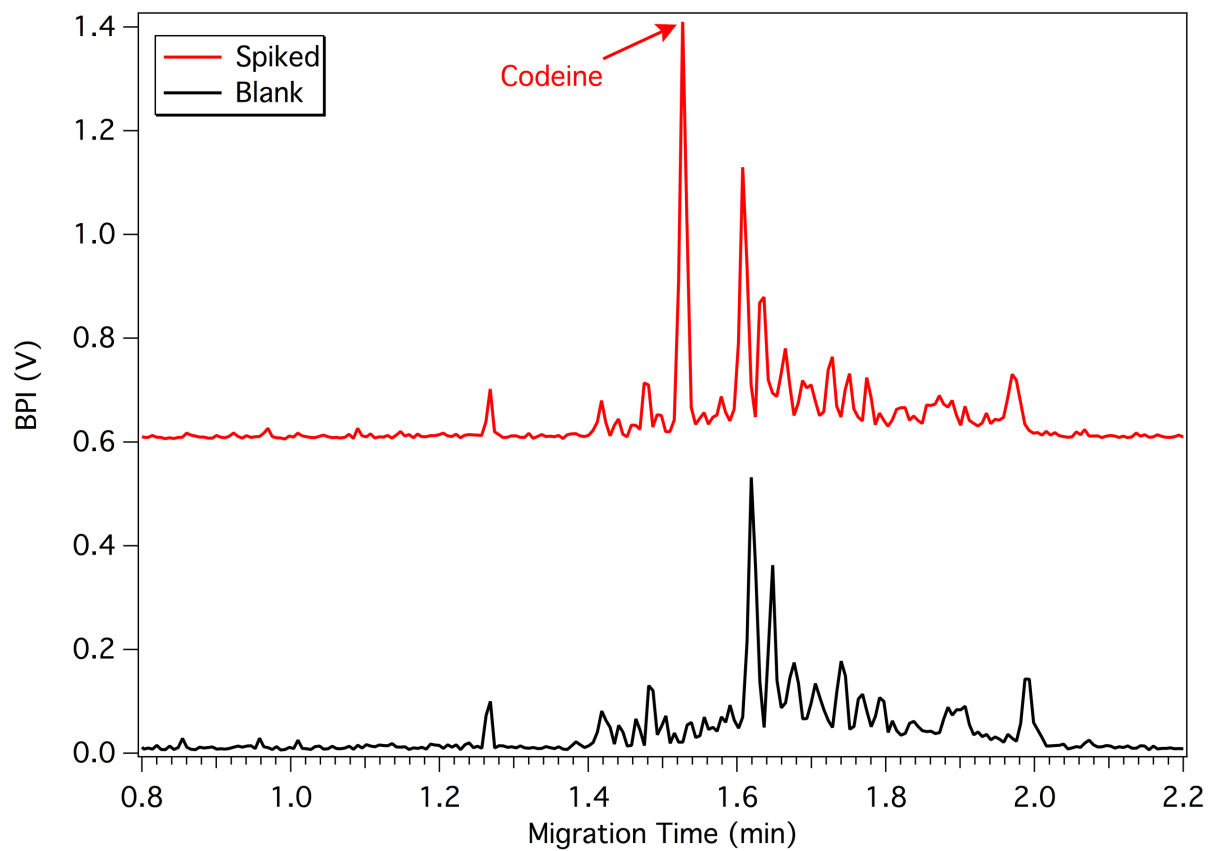
Figure 3.15: Sample electropherograms of urine blank (black, bottom) and spiked with 100 ng/mL codeine (red, top).
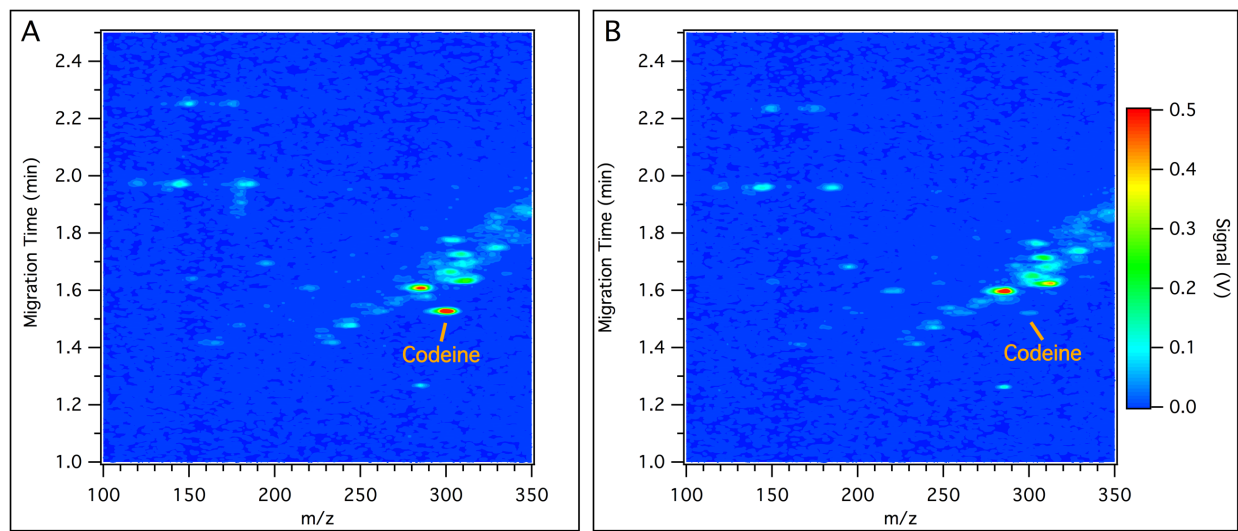
Figure 3.16: 2D plots of CE-HPMS of codeine spiked urine at A) 100 ng/mL and B) 10 ng/mL.

3.6   REFERENCES

(1)   Hoffmann, W. D.; Jackson, G. P. *Annu. Rev. Anal. Chem.* **2015**, *8* (1), 419–440.

(2)   Fernández, F. M.; Cody, R. B.; Green, M. D.; Hampton, C. Y.; McGready, R.; Sengaloundeth, S.; White, N. J.; Newton, P. N. *ChemMedChem* **2006**, *1* (7), 702–705.

(3)   Thevis, M.; Schänzer, W. *Mass Spectrom. Rev.* **2007**, *26* (1), 79–107.

(4)   Li, L.-P.; Feng, B.-S.; Yang, J.-W.; Chang, C.-L.; Bai, Y.; Liu, H.-W. *Analyst* **2013**, *138* (11), 3097.

(5)   Lebedev, A. T. *Annu. Rev. Anal. Chem.* **2013**, *6* (1), 163–189.

(6)   Petrović, M.; Hernando, M. D.; Díaz-Cruz, M. S.; Barceló, D. *J. Chromatogr. A* **2005**, *1067* (1), 1–14.

(7)   Wang, Y.; Liu, S.; Hu, Y.; Li, P.; Wan, J.-B. *RSC Adv.* **2015**, *5* (96), 78728–78737.

(8)   Beger, R.; D., R. *Metabolites* **2013**, *3* (3), 552–574.

(9)   Viant, M. R.; Sommer, U. *Metabolomics* **2013**, *9* (S1), 144–158.

(10)   Mastrangelo, A.; Armitage, E. G.; Garcia, A.; Barbas, C. *Curr Top Med Chem* **2014**, *14* (23), 2627–2636.

(11)   Goeringer, D. E.; Whitten, W. B.; Ramsey, J. M.; McLuckey, S. A.; Glish, G. L. *Anal. Chem.* **1992**, *64* (13), 1434–1439.

(12)   March, R. E. *Mass Spectrom. Rev.* **2009**, *28* (6), 961–989.

(13)   Badman, E. R.; Cooks, R. G. *Anal. Chem.* **2000**, *72* (14), 3291–3297.

(14)   Amy M. Tabert; Jens Griep-Raming; Andrew J. Guymon, A.; Cooks, R. G.; Tabert, A. M.; Griep-Raming, J.; Guymon, A. J.; Cooks, R. G. *Anal. Chem.* **2003**, *75* (21), 5656–5664.

(15)   Chaudhary, A.; van Amerom, F.; Short, R. T. *J. Microelectromechanical Syst.* **2009**, *18* (2), 442–448.

(16)   Schultze, K. P. Advanced System Components for the Development of a Handheld Ion Trap Mass Spectrometer, University of North Carolina at Chapel Hill, 2014.

(17)   Ramsey, J. M.; Schultze, K. P. Miniature charged particle trap with elongated trapping region for mass spectrometry. US8878127B2, 2014.

(18)   Manisali, I.; Chen, D. D. Y.; Schneider, B. B. *TrAC Trends Anal. Chem.* **2006**, *25* (3), 243–256.

(19)   Mylchreest, I. C.; Hail, M. E.; Herron, J. R. Method and apparatus for focusing ions in viscous flow jet expansion region of an electrospray apparatus. US5157260, 1991.

(20)   Redman, E. A.; Batz, N. G.; Mellors, J. S.; Ramsey, J. M. *Anal. Chem.* **2015**, *87* (4), 2264–2272.

(21)   Gagnon, P. Technology trends in antibody purification. *Journal of Chromatography A*, 2012, *1221*, 57–70.

(22)   Gronemeyer, P.; Ditz, R.; Strube, J. *Bioengineering* **2014**, *1* (4), 188–212.

(23)   Shukla, A. A.; Thömmes, J. *Trends Biotechnol.* **2010**, *28* (5), 253–261.

(24)   Gloeckner, H.; Jonuleit, T.; Lemke, H.-D. *J. Immunol. Methods* **2001**, *252* (1), 131–138.

(25)   Taya, M.; Hegglin, M.; Prenosil, J. E.; Bourne, J. R. *Enzyme Microb. Technol.* **1989**, *11* (3), 170–176.

(26)   Guo, M.; Chen, J.; Yun, X.; Chen, K.; Nie, L.; Yao, S. *Biochim. Biophys. Acta - Gen. Subj.* **2006**, *1760* (3), 432–439.

(27)   Butler, M.; Spearman, M.; Braasch, K. *Methods Mol. Biol.* **2014**, *1104*, 169–192.

(28)   Kirby, A. E.; Lafrenière, N. M.; Seale, B.; Hendricks, P. I.; Cooks, R. G.; Wheeler, A. R. *Anal. Chem.* **2014**, *86* (12), 6121–6129.

(29)   Bush, D. M. *Forensic Sci. Int.* **2008**, *174* (2), 111–119.

(30)   *Clinical Applications of Mass Spectrometry*; Garg, U., Hammett-Stabler, C. A., Eds.; Methods in Molecular Biology; Humana Press: Totowa, NJ, 2010; Vol. 603.

(31)   Opioid Addiction 2016 Facts and Figures http://www.asam.org/docs/default-source/advocacy/opioid-addiction-disease-facts-figures.pdf (accessed Feb 2, 2017).

(32)   Maddocks, O. D. K.; Berkers, C. R.; Mason, S. M.; Zheng, L.; Blyth, K.; Gottlieb, E.; Vousden, K. H. *Nature* **2012**, *493* (7433), 542–546.

(33)   Drugs of Abuse: Opiates - Mayo Medical Laboratories http://www.mayomedicallaboratories.com/test-info/drug-book/opiates.html (accessed Feb 2, 2017).

Chapter 4: Investigation of ESI-HPMS for the Analysis of Proteins

4.1   Introduction

4.1.1   Background and Motivation

The identification and structural determination of proteins has been incredibly important to life sciences research because the study of proteins gives "insights into the composition, structure, function, and control of the proteome, shedding light on complex biological processes and phenotypes."[1] In addition, proteins have increasingly been developed and characterized as therapeutic agents for various human diseases.[2] In recent years, mass spectrometers have been the primary driving force in characterizing proteins both for scientific discovery and screening drug products. Initially, however, the primary applications of mass spectrometers focused on the analysis of small gas phase and volatile compounds because MS analysis requires charged, gas phase molecules. The advent of electrospray ionization (ESI)[3,4] and matrix assisted laser desorption/ionization (MALDI)[5,6] provided methods for the ionization and volatilization of large biomolecules and have driven much of the development of mass spectrometer technology.

Much like commercial MS development, the initial steps in the development of high pressure mass spectrometry (HPMS) focused on the study of gas phase and volatile analytes.[7,8] The previous chapters have shown that ESI and HPMS can be coupled efficiently, both with CE separations and direct infusions of analytes. However, the analytes have all been small molecules under about 1000 Da, and most of those below 400 Da. Expanding CE-HPMS analyses to

include proteins and species of much higher mass (10 kDa and higher) would greatly increase the number of potential applications for the miniature analytical platform.

4.1.2 Mass Range Extension

The first step for HPMS analysis of proteins is extending the mass range. Previous ESI-HPMS analyses only had a mass range from 70 to about 700 m/z. For most protein species of interest, the mass range will need to be extended to at least 2000 m/z, and higher for certain proteins. Equation 1.7, reproduced here as Equation 4.1, shows the relationship between m/z, voltage, frequency and trap size:[9]

$$\left(\frac{m}{z}\right)_{max} = \frac{8V_{max}}{q_{max}\Omega^2(r_0^2+2z_0^2)} \tag{4.1}$$

where z is the charge, m is the ion mass, V_{max} is the maximum amplitude of the RF voltage, q_{max} is the trapping parameter and constant (usually 0.908), and r_0 and z_0 are the dimensional parameters of the trap. In order to extend the mass range, reducing or maintaining the RF frequency and reducing the trap size are options that can be explored. For illustration, the mass analyzer in Chapter 2 was operated at about 10 MHz with a trap size of $r_0 = 250$ μm, which produced a maximum mass of about 220 m/z. If the frequency were cut in half to 5 MHz, and the trap size were reduced to $r_0 = 100$ μm, with constant voltage, the result would be a roughly 25-fold increase in the maximum mass, to around 5500 m/z. This strategy, reducing or maintaining a low frequency and reducing the size of the trap, is presented here to produce a mass range suitable for the analysis of intact proteins.

4.1.3 Printed Circuit Board Ion Funnel

Another consideration for HPMS of proteins is the transfer of ions through vacuum to the mass analyzer. A DC tube lens was used for small molecules, but more complex optics such as

ion funnels have been shown to have near 100% transmission efficiency for protein-sized molecules.[10] Ion funnels consist of a stack of concentric ring electrodes, narrowing in diameter to an exit orifice, and 180 degrees out-of-phase RF signals are applied to adjacent electrodes, which provides a restoring force to the center of the rings. A DC gradient is applied along the length of the funnel to drive ions toward the exit orifice in the axial dimension. Ion funnels are traditionally used in commercial mass spectrometers in the first vacuum stage (0.1 to 30 Torr), an ideal operational pressure range for HPMS. For HPMS operation, the ion funnel and the mass analyzer can be operated at the same pressure, and thus, in the same vacuum chamber, reducing instrument complexity. Traditional ion funnels can consist of as many as 100 electrodes,[11] but a smaller, shorter design would fit better within the goal of a miniature analytical platform. Printed circuit board (PCB) technology has been used previously to produce ion funnels, which reduces the complexity of assembly and fabrication.[12,13] Here, after first using SIMION simulations to optimize the funnel geometry, a small (20 electrodes) ion funnel is produced from PCB material to improve ion transport for HPMS applications.

4.1.4 High *m/z* Applications of a CE-ESI-HPMS Platform

The analysis of biotherapeutic drugs is one possible application for an HPMS system capable of measuring high *m/z* molecules. Biotherapeutics have grown as a treatment strategy in the past decades, especially monoclonal antibodies (mAbs), which have become a multibillion dollar industry.[14] They are attractive candidates for many therapeutic applications because of their high specificity and low side effects.[14,15] While mAbs have been extremely successful as drugs, it is important to characterize them prior to their administration in order to predict the effects they may have on human health and ensure the safety of patients. However, mAbs are often difficult to characterize due to their size (~150 kDa) and complexity.[16] Much antibody

characterization is performed using LC/MS methods,[2] and recently, characterization of charge variants of intact mAbs and mAb drug conjugates were performed using microchip CE-MS.[17,18] The possibility of a high pressure mass spectrometry platform used for process characterization of biopharmaceuticals was discussed in Chapter 3. That HPMS system could be adapted for product (mAb) characterization and provide a targeted approach to screen for the proper production of protein therapeutics.

Another possible application for measuring proteins by HPMS is monitoring glycated hemoglobin (HbA1c) in diabetic patients. As of 2015, diabetes affected 415 million people worldwide and is estimated to affect 642 million by 2040.[19] HbA1c consists of a hemoglobin molecule to which a glucose group has been added nonenzymatically to one of the amino acid residues.[20] While blood glucose has traditionally been used to monitor diabetes, blood glucose levels only give a snapshot of glycemic control and can vary greatly in the short term, which can lead to irreproducible measurement and misdiagnosis. HbA1c provides a way to measure longer term glycemic control, about 120 days, or the average lifetime of human erythrocytes.[20–22] Many mass spectrometric methods have been developed to measure HbA1c,[23–25] including a method from the Ramsey lab using microchip CE-MS.[26] These methods all use conventional mass spectrometry instrumentation, which would limit them to use outside of clinical settings because of cost, size, complexity, and the need to be run by specialists. If a microchip CE-MS method could be adapted to run with HPMS rather than a commercial mass spectrometry, the simplicity and reduced cost of HPMS makes it a good potential candidate as a diagnostic tool in a clinical setting.

4.1.5 Summary

HPMS is explored for the analysis of high mass and *m/z* species, specifically proteins. A PCB ion funnel is simulated, constructed, and characterized to improve ion transmission. Small and large proteins are investigated to demonstrate the viability of HPMS to measure these species. A proof-of-concept analysis of a mAb is demonstrated for applications in biopharmaceutical characterization. Finally, hemoglobin glycation is characterized using a microchip CE-HPMS method adapted from previous work[26,27] to show the potential of the system as a diagnostic tool.

4.2 Experimental

4.2.1 Materials and Reagents

HPLC grade acetonitrile, isopropanol, acetic acid (99.9%) and formic acid (99.9%) were obtained from Fisher Scientific (Fairlawn, NJ). Purified deionized water was obtained using a Nanopure Diamond water purifier (Barnstead International, Dubuque, IA). (3-Aminopropyl)di-isopropylethoxysilane (APDIPES) was obtained from Gelest (Morrisville, PA). NHS-PEG$_{450}$ was obtained from NanoCS (Boston, MA). Myoglobin, cytochrome c, and bovine serum albumin were obtained from Sigma (St. Louis, MO). The mAb (IgG2) was supplied by Pfizer (St. Louis, MO). The background electrolyte (BGE) for all non-mAb protein infusion experiments was 50% acetonitrile, 49.9% water, and 0.1% formic acid (v/v/v, pH = 3.1). The BGE for the mAb infusion was 10% isopropanol, 89.8% water, and 0.2% acetic acid (v/v/v, pH = 3.2).

Deidentified whole blood samples were obtained from McLendon Clinical Laboratories (Chapel Hill, NC). The samples were analyzed by McLendon for HbA1c levels using a Vitros 5600 immunoassay (Ortho Clinical Diagnostics, Inc.). The fifteen samples had clinical HbA1c

values ranging from 5.0% to 13.0%. Samples were refrigerated at 4 °C prior to analysis. For

analysis by CE-HPMS, 10 μL of whole blood (without any further processing) was added to

990 μL of 50% acetonitrile, 47% water, and 3% acetic acid, for a 100X dilution. After that,

100 μL of the 100X solution was added to 900 μL of the acetonitrile/water/acetic acid BGE, for

a final dilution of 1000X. The 1000X sample was filtered using a Costar Spin-X 0.45 μm

centrifugal filter prior to CE-HPMS analysis.

4.2.2   Microchip Design and Operation

Two microchip devices were used for this work: an infusion-ESI device and a CE-ESI

device with a 23-cm separation channel. Device fabrication and coating details are outlined in

Appendix I. Briefly, the devices were wet etched to a depth of 10 μm and full width of 70 μm.

The devices were then coated with APDIPES via chemical vapor deposition. All of the

APDIPES coated channels were then functionalized with 20 kDa PEG in order to suppress the

EOF.

Devices were operated as described in Appendix II. All voltages were applied with

platinum wire electrodes controlled by a custom LabVIEW program. Pressure to the devices was

applied with 2 psi of air gated by 3-way valves from Clippard (Cincinnati, OH). For infusion

devices, +5 kV was applied to one reservoir along with 2 psi pressure to facilitate electrospray. A

voltage of +0.5 kV was applied to the other reservoir. For CE-ESI, injections were performed

hydrodynamically. Voltages were turned off, and pressure was applied to the sample reservoir

and a reservoir containing BGE for 3 seconds, then pressure was applied only to the reservoir

containing BGE for 1 second. The voltages were then turned on, and normal zone electrophoresis

began. Voltages were operated at +20 kV for the BGE reservoir and +1.2 kV for the pumping

reservoir. Pressure was provided to the pumping reservoir to provide the flow necessary for electrospray.

4.2.3   Microchip ESI-HPMS

Electrospray ionization-high pressure mass spectrometry (ESI-HPMS) experiments were performed with a custom atmospheric interface and differentially pumped vacuum system adapted from the system described in Chapter 3. A CAD drawing of the vacuum chamber and MS components is shown in Figure 4.1.

The microchip-ESI device (CE or infusion) was mounted on an adjustable x-y-z stage and positioned approximately 5-10 mm from the HPMS inlet aperture. A single-sided copper clad circuit board (M.G. Chemicals, Burlington, Ontario, Canada) was used to shield the ESI orifice on the chip form the voltages applied to the reservoirs (not shown). The corner of the microfluidic device extended about 5 mm through a slit in the board. The copper board was held at +0.5 kV for all experiments.

Ions were conducted into the vacuum chamber via a 100 μm ID aperture (Lenox Laser, Glen Arm, MD) mounted to the chamber and sealed with Viton o-rings (McMaster-Carr, Atlanta, GA). A potential of +265 V was typically applied to the inlet aperture. After traveling through the aperture, ions were conducted to the trap via a custom-built ion funnel made using printed circuit boards (PCBs). The PCB ion funnel consisted of 20 electrodes and 19 PCB spacers, each 0.5 mm thick (Advanced Circuits, Inc., Aurora, CO). The electrodes were designed using EAGLE PCB circuit board design software (Cadsoft, Pembroke Pines, FL). The first and last electrodes of the funnel, along with two spacers, are shown in Figure 4.2a. The spacers contain copper traces to make electrical connection between the electrodes of the funnel. Surface mount capacitors (1 nF) and resistors (180 kΩ) were used for the ion funnel. Electrical connections

121

were made to the funnel via SMA feedthroughs mounted on the main vacuum chamber. The funnel was fixed to the mounting bulkhead (Figure 4.1) to which the CIT was also mounted via another custom circuit board (PCB mounting plate in Figure 4.1) shown in Figure 4.2b and c. The bottom (blue, c), top (red, b), and inner (green) layers of the board are shown, and the inner layer traces on the board act as vacuum feedthroughs to make electrical connection to the trap. The circuit board is sealed into vacuum with a face-sealed o-ring on either side of the board.

Miniature CIT electrodes were wet etched by Towne Technologies, Inc. (Somerville, NJ). Dimensions for the CITs were $r_0 = 100$ μm, $z_0 = 125$ μm, and endcaps with 165 μm hole diameters. Each ring electrode contained a single trap. Traps were assembled by manual alignment using alignment pins and holes etched in the electrodes. Electrodes were mounted to a custom plate with 55 μm teflon (PTFE) spacers between them. Drive RF waveforms were applied by a Rohde and Schwarz SMB 100A signal generator and amplified using a Mini Circuits TVA-R5-13 preamplifier and AR 305 power amplifier. The signal was resonated with a tank circuit, and applied frequencies ranged from about 5 to 10 MHz. A small supplementary RF voltage was applied to the endcap closest to the inlet using an AFG 3022B function generator (Tektronix, Beaverton, OR) to perform resonant or double resonant ejection. Custom LabVIEW software was designed to monitor, control, and collect data. A National Instruments PXIe-1073 data acquisition chassis was used to interface the electronics and LabVIEW software.

Ions were accumulated between 0.05 and 20 ms before analysis. They were then scanned out of the trap and detected with an electron multiplier (Detech 2300, Detector Technology, Inc., Sturbridge, MA) connected to a current preamplifier (SR570, Stanford Research Systems, Sunnyvale, CA). A typical mass spectrum was an average of 10 to 1000 individual mass scans. Two sets of pumps were used for differentially pumping the chamber. A dry scroll pump (SH-

110, Agilent Technologies, Inc., Santa Clara, CA) was used on the mass analysis chamber

(~1 Torr) and an Agilent TPS Bench turbomolecular pump (Model TV81M) backed by a dry

scroll pump (SH-110) was used on the detector chamber (~10 mTorr).

4.3   Results and Discussion

4.3.1   SIMION Simulations of PCB Ion Funnel

Ion simulations were performed prior to the design of the PCB ion funnel in order to guide

its design. Ion trajectories were modeled with SIMION 8.1 software (Scientific Instrument

Services, Inc. Ringoes, NJ). A hard-sphere collision model with SDS (statistical diffusion

simulation) user program was used to predict the interaction of ions with background nitrogen

gas. The funnel consisted of 20 cylindrical electrodes, each 0.5 mm in width, spaced by 0.5 mm.

The first 10 electrodes had a diameter of 6 mm, and the next 9 decreased linearly to 2 mm in

diameter. The last electrode had a diameter of 2 mm. A solid electrode was placed 2 mm from

the exit of the funnel to mimic the location of the ion trap. RF and DC potentials were applied to

the first 19 electrodes, and only a DC potential was applied to the last electrode. The solid

electrode was maintained at GND.

Simulations were performed with ions of 3 different masses and a range of charge states, in

order to mimic protein and peptide molecules. The parameters used for the simulations are

shown in Table 4.1. The only parameters adjusted between each of the masses were the collision

cross-section and the charge states of the molecule. The DC potentials applied result in a gradient

of about 67 V/cm between the first and last electrodes. Trajectories for ions of 1700 *m/z* with

three different masses are shown in Figure 4.3 along with cross-sections of the electrodes: A)

17000 Da with +10 charge, B) 8500 Da with +5 charge, and C) 1700 Da with +1 charge. An

isometric view with a few ion trajectories is shown in Figure 4.3d. For ions of 8500 and 1700 Da, the trajectories are more disperse throughout the funnel than the 17000 Da ions, but there is still 100% transmission. The trajectories are also slightly more disperse at the exit of the funnel for the lower masses, but all of the ions are focused significantly more at the exit than at the entrance of the funnel, from a beam of 4 mm in diameter to a beam of less than 1 mm in diameter.

Transmission efficiencies of 100% were observed for all three masses at 1700 *m/z*, but transmission could vary as a function of *m/z*. To test this, ion trajectories were simulated under the same conditions with ions of the same masses but varying the charge state. The ranges of charge states were chosen based on reasonable charge states for molecules of similar size. Charge states of +10 to +30 were tested for mass 17000 (1700 to 567 *m/z*), +5 to +20 for mass 8500 (1700 to 432.5 *m/z*), and +1 to +5 for mass 1700 (1700 to 340 *m/z*). Transmission efficiency as a function of *m/z* is shown in Figure 4.4 for each of the different masses. Transmission efficiency was 100% for all charge states of the 17000 Da species, and for all *m/z* over 600. Ions of mass 8500 drop off in transmission efficiency at lower *m/z* (< 500), though transmission efficiency remained above 95%. Transmission efficiency dropped off more dramatically for ions of higher charge states for mass 1700. At 340 *m/z*, transmission efficiency was only about 25%. In the simulation, transmission loss was due to ions hitting the funnel electrodes. This was likely due to a combination of increased collisional scattering for ions of lower mass and the high effective potential experienced by ions of low mass and high charge. The effective potential experienced by an ion in an oscillating electric field is inversely proportional to the ions mass and directly proportional to its charge.[12,28] All else being equal, ions of lower mass and higher charge will experience a greater effective potential. This could

result in better control of the ions, but near the exit of the funnel where the apertures narrow, this resulted in collisions with the electrodes inside the funnel. Experimental parameters could be adjusted to increase efficiency for lower mass ions. For example, the RF frequency and voltage could be adjusted to improve ion focusing and the pressure could be decreased to reduce scattering from collisions. Since our initial target molecules are small proteins close to mass 17000, the ion funnel was designed based on the simulation parameters. For the analysis of peptides or smaller molecules (<1700 Da), experimental parameters may need to be changed or new optics may need to be designed.

The ion funnel was constructed from PCB materials with the fully assembled ion funnel shown in Figure 4.5 from a side view (A) and down the axis of the funnel (B). The funnel was about 2.5 cm in length, and the last electrode was about 2 mm from the entrance of the ion trap. The compact form factor of the funnel fits within the goal of a miniature analytical platform. The funnel was held together with metal screws and fixed to the mounting bulkhead shown in Figure 4.1. The PCB mounting plate from Figure 4.2 is also shown with the o-ring used for sealing and SMA connectors for electrical connection to the trap. This ion funnel was used for all ESI-HPMS protein experiments.

4.3.2 HPMS Analysis of Small Proteins

After the initial design, the experimental setup in Figure 4.1 and ion funnel in Figure 4.5 were used for the analysis of small proteins. Infusions of 2.5 μM cytochrome c (MW ~12.3 kDa) and 2.5 μM myoglobin (MW ~17 kDa) were performed. The pressure was 1.5 Torr with ambient air as the buffer gas and the background gas for the ion funnel. The ion funnel was operated at 1.12 MHz with a voltage of 90 V_{p-p}, with a DC gradient from +175 V to +50 V. The last electrode was held at +25 V during the ion injection period and pulsed to -50 V during mass

analysis to gate ions. The drive RF for the trap was 6.3 MHz, ramped from 70 to 270 V_{p-p}. The axial RF was applied continuously to the end cap nearest the inlet at 1.97 MHz and 1.5 V_{p-p}. Using Equation 4.1, the expected mass range under these conditions would be roughly from *m/z* 500 to 2000.

HPMS spectra of the two proteins compared with spectra from a commercial mass spectrometer (Waters Synapt G2) are shown in Figure 4.6. In Figure 4.6a, the charge states of cytochrome c are clearly visible and a distribution similar to the commercial mass spectrum was observed. Peaks from *m/z* 600 up to 1400 are observed, corresponding to charge states +20 (~*m/z* 615) down to +9 (~*m/z* 1367), with an average charge state of +16.4, calculated according to methods reported previously.[29] The FWHM for the most abundant charge state was 13.4 *m/z*.

Figure 4.6b shows the HPMS spectrum of myoglobin. The charge states observed agree with the charge states seen on the commercial mass spectrometer, with the exception of the peak at ~ *m/z* 618. That peak corresponds to the free heme group lost from myoglobin under our electrospray conditions. The heme group was not easily detectable by ESI-HPMS under these conditions. Nonetheless, peaks over the same mass range as cytochrome c are observed, corresponding to charge states +26 down to +12, with an average charge state of +20.6. The FWHM of the most abundant charge state was 14 *m/z*. The HPMS charge state distribution looks slightly different than that of the Synapt G2. Rather than a steady decrease at *m/z* above the most abundant charge state (~*m/z* 740), there was an increase around *m/z* 1000. This behavior might be due to two distinct conformations of myoglobin that exist under these conditions. With two conformations, the mass of myoglobin remains unchanged, but the conformations may favor different amounts of charging, resulting in two distinct charge state distributions. Even with two

charge state distributions, the *m/z* values remain unchanged, so the mass of myoglobin could still be identified with mass spectral information presented.

The spectra shown in Figure 4.6 demonstrate that HPMS can be performed on small proteins, extending the mass range of HPMS analysis to at least about *m/z* 1500, while previous HPMS work focused only on small molecules and did not exceed about *m/z* 200. Given the correlation with spectra from a commercial mass spectrometer, the HPMS spectra with the charge state distributions of the proteins could likely be used to identify them with a targeted approach. In addition, the spectra show that the PCB ion funnel works effectively for proteins of this size and can efficiently conduct ions into the trap for analysis.

The ion funnel improved ion transmission over previously used DC optics. Figure 4.7 shows two HPMS myoglobin spectra run with the PCB ion funnel and with the DC tube lens used for small molecules in Chapter 3. All conditions were kept the same between the two spectra with only the ion optics changed. The spectrum with the ion funnel gives about an 8-fold increase in signal intensity over the spectrum with the DC tube lens. There are also more peaks corresponding to additional charge states of myoglobin visible in the ion funnel spectrum, 14, compared to 10 for the tube lens spectrum. Better sensitivity and more charge states should aid in the identification of protein species. Another interesting effect of the ion funnel spectrum is the center of the charge state distribution shifts to lower *m/z* compared to the tube lens spectrum. The trap is the same and operated under the same conditions, so this shift is likely due to differences in ion transmission of the ion optics for species of different *m/z*.

To more fully characterize the performance of the ion funnel and the trap, a limit of detection (LOD) experiment was performed with myoglobin as the analyte. Starting at 2.5 μM, serial dilutions of myoglobin in BGE were performed down to 1 nM, and the solutions were

infused into the mass spectrometer. The same conditions for the ion funnel and trap were used as the infusions of cytochrome c and myoglobin in Figure 4.6. As the concentration was decreased, the fill time for the ion trap was adjusted to maintain signal quality. At high concentrations, long fill times would result in overloading of the ion trap, leading to space charging effects and decreasing the quality of the mass spectra. At low concentrations, the fill time can be increased to attempt to maintain the total number of ions in the trap and maintain signal intensity. Techniques like automatic gain control can be implemented in conventional ion traps to adjust the fill time dynamically and maintain consistent signal across a wide range of concentrations. The ion fill time was adjusted in order to mimic this function and produce a practically viable LOD. As interfacing CE with HPMS is a goal of this project, the fill times of the trap were capped at 20 ms to maintain a reasonable duty cycle for detection of CE separations.

The LOD was calculated using the signal-to-noise ratio (S/N) from the most abundant charge states of myoglobin in each spectrum. The S/N was then normalized to 20 ms by multiplying the S/N at each concentration by 20 ms/[current fill time]. Fill times ranged from 0.05 ms (the lower limit of fill times due to timing constraints in the LabVIEW software) up to 20 ms, and are shown as a function of concentration in Table 4.2. A plot of the "adjusted S/N" as a function of concentration is shown in Figure 4.8. The adjusted S/N rolls off on the high end of the concentrations, indicating the end of the linear dynamic range. The low concentrations are more important for determining LOD and are also more practical for target analytes. An inset of the large graph shows the adjusted S/N plotted against concentration for 150 nM down to 1 nM. A linear fit of these points is shown on the graph with an R^2 of 0.996, indicating good linearity over about two orders of magnitude concentration. Using an adjusted S/N of 3 as a cutoff, the LOD was determined to be 4.9 nM for myoglobin under these conditions.

4.3.3 HPMS Analysis of Large Proteins

Extending the analysis of ESI-HPMS to include large proteins would greatly increase its possible areas of application. Myoglobin and cytochrome c are useful standards for characterizing mass spectral performance, but there are many proteins of interest of much greater mass (>50 kDa), including monoclonal antibodies (mAbs) used in the biotherapeutic industry. Bovine serum albumin (BSA) and a mAb were investigated with ESI-HPMS.

BSA is a common protein standard of about 66 kDa, so it was chosen as an intermediate step to the analysis of mAbs, which have masses around 150 kDa. An infusion-ESI-HPMS spectrum of BSA is shown in Figure 4.9. The pressure of the ion funnel and the mass analyzer was 2.0 Torr with ambient air as the background gas. The ion funnel was operated at 1.072 MHz and 75 V_{p-p}, with a DC gradient from +175 V to +50 V. The last ion funnel electrode was pulsed from +30 V to -50 V to gate ions. The drive RF for the trap was 6.6 MHz, ramped from 100 to 560 V_{p-p}. An axial RF voltage was applied constantly to the endcap closest to the funnel at 2.05 MHz and 3.0 V_{p-p}.

The mass range in Figure 4.9 was about 600 to 1800 *m/z*, slightly more than the mass range in Figure 4.6, due to the increased RF voltage applied to the trap ring electrode. Many charge states of BSA were observed over this mass range, with the maximum of the distribution around *m/z* 1125. The inset shows a deconvolution performed on the charge state distribution to predict the mass of the protein. The deconvolution was performed using a custom LabVIEW program and an algorithm based on the z-score algorithm developed by Zhang and Marshall.[30] The deconvolution produces a peak with its center at 66.3 kDa, which agrees well with the accepted value of the mass of BSA at 66.4 kDa.[31] The pressure had to be increased to 2 Torr in order to detect BSA when infused. While the increase in pressure could affect the ion transfer, it is more

likely that the increased pressure aids in trapping species of large mass. Ions of significant mass may be difficult to trap in the shallow potential well of the miniature ion traps, so the increase in pressure will result in more ion-neutral collisions and reduce the kinetic energy of the large molecules. With this increase in pressure, BSA was trapped and analyzed effectively, demonstrating that HPMS could be used to characterize proteins up to this size.

To further investigate the possibility of high mass protein analysis, a mAb, specifically a γ-immunoglobulin (IgG), was infused into the HPMS system. A normalized spectrum of the mAb is shown in Figure 4.10 compared with a spectrum acquired on a commercial mass spectrometer (Waters LCT Premier). In order to produce the desired mass range, the RF drive frequency on the trap was lowered to 5.1 MHz, and the voltage was ramped from 270 to 800 V_{p-p}. The axial RF was operated at 1.8 MHz and 4 V_{p-p}. The pressure was increased to 6.1 Torr with ambient air as the background gas, about three times higher than necessary with BSA. Just as the pressure was increased in order to trap BSA, the pressure needed to be increased further to accommodate the higher mass of the analyte (~150 kDa).

The reduction in RF frequency and increase in voltage results in a mass range significantly higher than used for any previous HPMS analysis. The final mass range was about m/z 2500 to 7000. There are three distinct charge state distribution observed in the HPMS spectrum of the mAb. The highest m/z distribution (~m/z 4500 – 5500) corresponds to the intact, fully folded antibody. The other two distributions at lower m/z (~3400 to 4400) likely correspond to a partial unfolding of the mAb. In an unfolded conformation, more sites on the protein are accessible for protonation by ESI, which results in greater charging and peaks at lower m/z corresponding to increased charge states. The set of charge state distributions seen is due to protein degradation of the sample over time. Nonetheless, the location of the peaks in the highest m/z charge state

distribution agree well with the spectrum from the LCT Premier, confirming that these charge states correspond to the intact, fully folded protein. When a deconvolution was performed on the same set of peaks, the center of the deconvoluted peak was about 149 kDa (Figure 4.10 inset), which agrees with the expected mass of about 150 kDa.

4.3.4   Analysis of Whole Blood Lysate by CE-HPMS

Microfluidic CE-MS analysis of whole blood lysate was performed previously with a commercial mass spectrometer with a target application of diabetes diagnostics.[26] A similar study was performed here with CE-HPMS. The small size and lower cost of a CE-HPMS system would make operation of the platform feasible in a clinical setting, where the cost, size, and/or complexity of a commercial mass spectrometer may not be a reasonable possibility. CE-ESI-HPMS analysis was performed on blood samples in order to measure glycation of the β subunit of hemoglobin.

For CE-HPMS analysis of whole blood, the mass spectrometer and ion funnel were operated at 1.5 Torr, with ambient air as the background gas. The trap was operated at 8.59 MHz, ramped from 110 to 520 V_{p-p}. A small axial potential of 2.65 MHz at 2.0 V_{p-p} was applied to the endcap nearest the ion optics. The RF frequency on the ion funnel was 1.12 MHz at 70 V_{p-p}. The DC voltages were +175 V on the entrance electrode, +50 V on the second to last electrode, and pulsed from +30 during ion injection to -50 V at all other times on the last electrode.

Microfluidic CE separations of two blood samples are shown in Figure 4.11. The bottom trace shows a separation of whole blood lysate from a patient with normal levels of HbA1c, and the top trace shows a separation of the same sample spiked with about 10% more pure HbA1c. The separation is performed in under two minutes, and three peaks are detected in each sample, corresponding to the two major subunits of hemoglobin, α and β, and the glycated β subunit. The

same separations were performed on a commercial mass spectrometer to confirm the identities of the peaks. In the previous study with a commercial mass spectrometer, the glycated α subunit was also detected, but that variant was not detected with HPMS. Nonetheless, when the sample is spiked with HbA1c, there is a clear increase in the intensity of peak 3 in Figure 4.11. This peak corresponds the glycated β subunit and agrees with previous results, indicating that monitoring relative sizes of the hemoglobin subunit peaks could be used to track HbA1c. It is worth noting that there are a number of additional proteins present in blood that were not detected here. This method was optimized for hemoglobin analysis, so additional undetected species were either below the current detection limit or out of the set mass range for these experiments.

HPMS mass spectra of the major subunits of hemoglobin are shown in Figure 4.12. Each subunit has a set of well-resolved charge states in the range from 600 to 1000 *m/z*. The center of the α subunit distribution is at slightly lower *m/z* than the β subunit distribution, which could be used to distinguish the subunits in addition to the migration time information given by the separation. In addition, the charge state peaks for the two subunits would have significant overlap but do have different locations. When a deconvolution is performed on each of the spectra, the center of the deconvoluted spectrum for the α subunit was around 15.1 kDa, and the center of the deconvoluted β subunit spectrum was about 15.8 kDa. While the same degree of precision is not obtained as a commercial mass spectrometer, the deconvoluted masses from the HPMS spectra agree with the expected masses for the α and β subunits based on their amino acid sequences: 15126.4 Da and 15867.2 Da, respectively.[26,32] The mass spectral information plus the electrophoretic migration times provide multiple criteria for the identification of different chemical species.

The CE-HPMS platform was assessed as a tool for measuring HbA1c levels by analyzing a set of fifteen clinical samples with HbA1c levels from 5.0 to 13.0%. Each of the samples were analyzed by the same method used for the separation in Figure 4.11. Sample electropherograms of three of the samples with HbA1c values of 5.0, 7.2, and 13.0% are shown in Figure 4.13. The separation of the hemoglobin subunits (two tallest peaks) and the glycated β subunit (labeled with arrows) is completed in under two minutes. As the quantity of HbA1c increases, the height of the glycated β peak increases as well. Some other small peaks are present in electropherograms with similar migration times to the hemoglobin subunits of interest. These peaks likely correspond to other variants of hemoglobin. In addition, a small peak around 2.1 minutes is observed in the 7.2 and 13.0% separations. This peak is probably due to another protein in the blood.

Glycation levels in each of the blood samples were calculated using the relative peak areas of the glycated β subunit and the non-glycated β subunit, according to Equation 4.2:

$$Ratio_{gly-HPMS} = \frac{A_{gly-Hb-\beta}}{A_{gly-Hb-\beta} + A_{Hb-\beta}} \qquad 4.2$$

Each of the peaks from the BPI electropherograms were fit to a Gaussian profile in Igor Pro 6.3 in order to calculate the areas. The ratio calculated from Equation 4.2 is plotted against the clinical HbA1c values in Figure 4.14. A linear regression was performed on the data, and a line of best-fit is shown in the Figure. The slope of the line is 1.2 with an intercept of 2.1. The R^2 value for the fit was 0.75, indicating a slight trend. The points at lower HbA1c values appear to have less variance and a more predictable trend than the points at higher HbA1c values, with the exception of the point at about 5.5% HbA1c. Given that there is a weak correlation between the

experimental values and the clinical values, this platform could possibly be used as an initial screening tool for diabetes diagnostics, perhaps distinguishing between a "high" and "low" HbA1c state. Previous work using this assay with a commercial mass spectrometer achieved an R^2 of 0.99,[26] indicating that this is a viable strategy for determining HbA1c levels. Further development and a stronger correlation would be needed for CE-HPMS to be used as an absolute quantitative method for HbA1c detection. The main difficulty with this measurement is the limited dynamic range of the HPMS system. The concentrations of the hemoglobin subunits and their structural variants vary over several orders of magnitude, and the HPMS system could currently be optimized for only one end of the range. Improvements using SLIT traps to increase the ion storage capacity or implementing some gain control might aid in increasing the dynamic range of the instrument. As shown in Figure 4.8, the HPMS system can operated over several orders of magnitude in concentration, but the ion injection time was adjusted at each step. During each separation, the ion injection time remained constant. While improvements to the system can be made, the correlation indicates that CE-HPMS could be used as a useful clinical tool for diabetes diagnostics.

4.4   Conclusions

The viability of HPMS to measure proteins has been shown. SIMION simulations were used to guide the development of a small PCB ion funnel that was successfully used to improve the transmission of proteins over simple DC optics. Small proteins (~15 kDa) were infused and analyzed at 1.5 Torr with ambient air as the buffer gas. Large proteins, including a mAb (~150 kDa), were also infused and detected at pressures up to 6 Torr, showing the possibility of HPMS for the analysis of biotherapeutic agents. Finally, variants of hemoglobin were separated

and detected using CE-HPMS. Clinical blood samples were analyzed and HbA1c values were

correlated with clinical measurements. With further development, a CE-HPMS platform could

provide a low cost, targeted alternative to conventional mass spectrometry analysis of proteins.
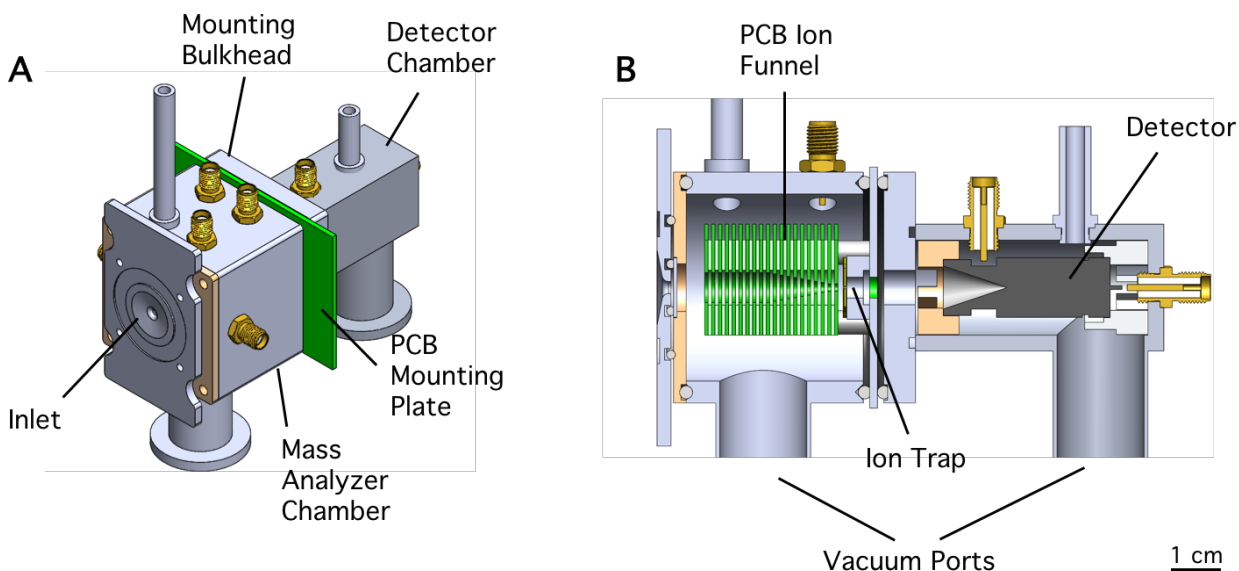
4.5 Figures and Tables

Figure 4.1: Instrument diagram (CAD) in A) isometric and B) cross-sectional view. The instrument consists of two chambers. The first chamber is operated at high pressure (>1 Torr) and contains the PCB ion funnel and the ion trap, and the second chamber is operated at lower pressure (<50 mTorr) and contains an electron multiplier detector.
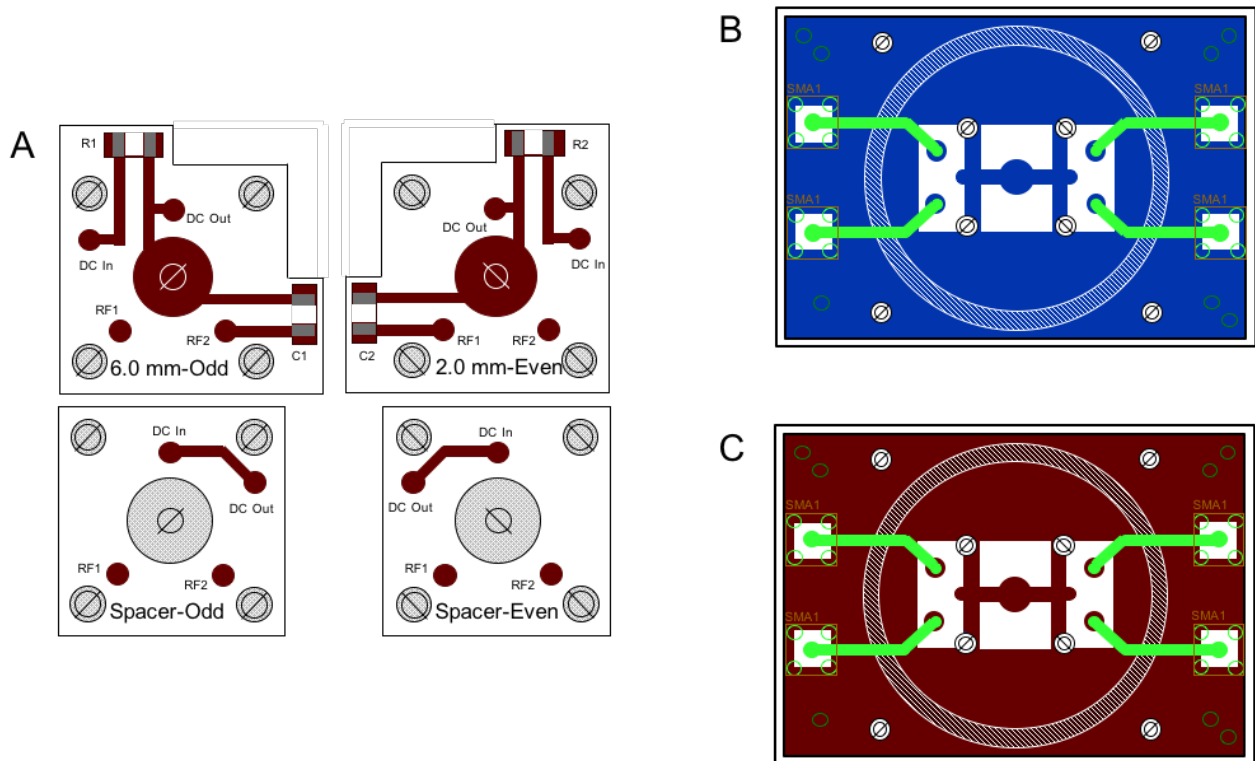
Figure 4.2: PCB schematics of A) the first and last plates of the ion funnel and two spacers, B) the bottom and inner layer of the PCB mounting plate, and C) the top and inner layers of the PCB mounting plate. The first ion funnel electrode is 6 mm in diameter, and the last is 2 mm in diameter. The spacers are used to make electrical connection between the boards. The blue and red sections in B) and C) are ground planes, and the green traces act as feedthroughs to carry electrical signals from atmosphere into the vacuum chamber. The trap is mounted in the center and vacuum sealed around the large circle (white, striped) with an o-ring.

Table 4.1: Parameters Used for SIMION Simulations.

Parameter	Value
RF Frequency	1.07 MHz
RF Amplitude	35 $V_{0\text{-}p}$
DC High	175 V
DC Low	50 V
DC Extract	30 V
DC Collect	0 V
Pressure	1.5 Torr
Temperature	298 K
Ion Initial Kinetic Energy	265 eV
Number of Ions	1000
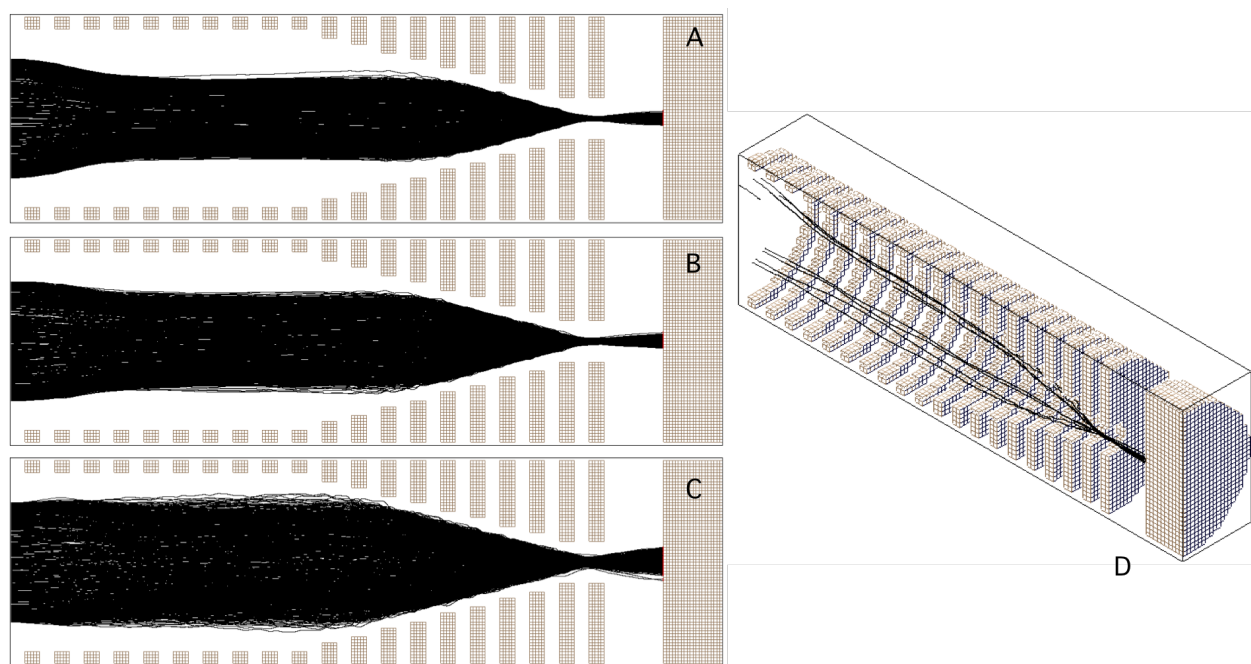
Figure 4.3: SIMION simulations of ion funnel in cross-section view with ion trajectories for A) mass 17000 Da and +10 charge, B) mass 8500 Da and +5 charge, and C) mass 1700 Da with +1 charge (all 1700 *m/z*) D) Isometric and cross-section view of ion funnel and trajectories with ions of 17000 Da and +10 charge.
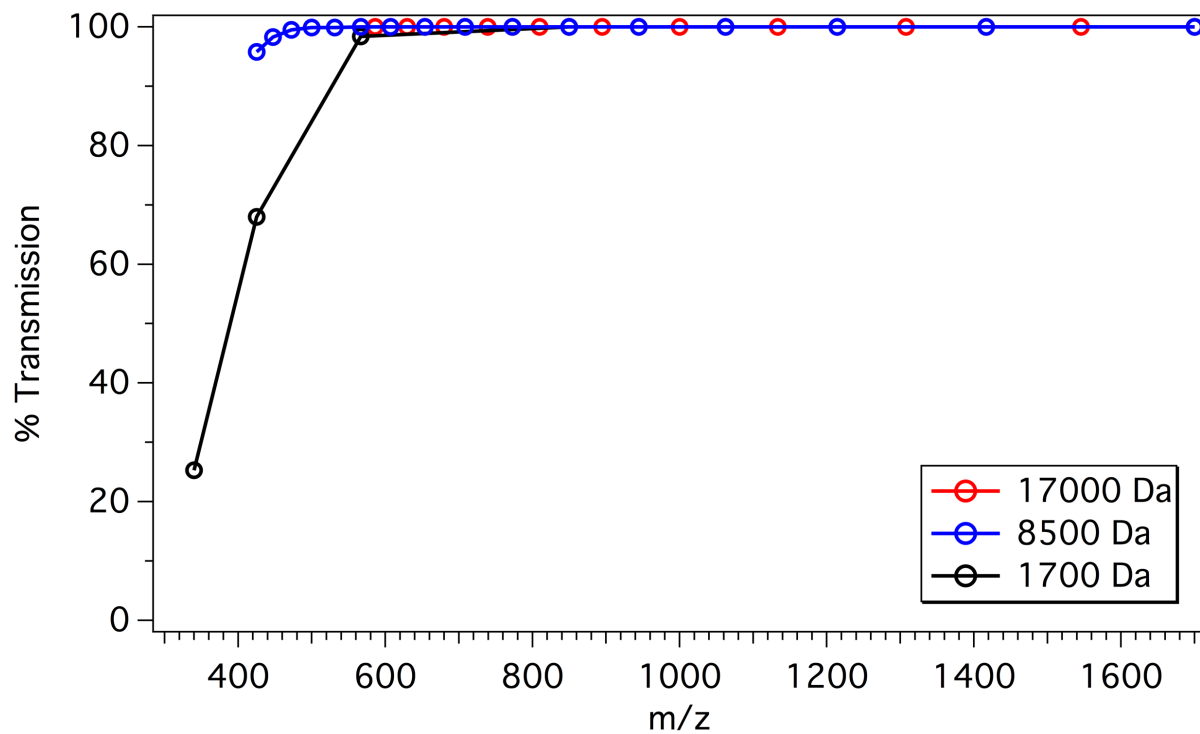
Figure 4.4: Ion % transmission as a function of *m/z* from SIMION simulations with ions of three different masses.
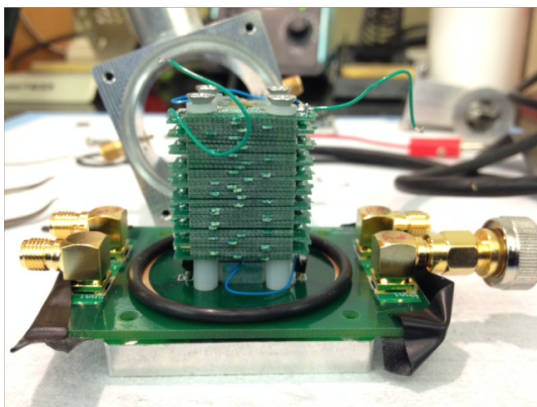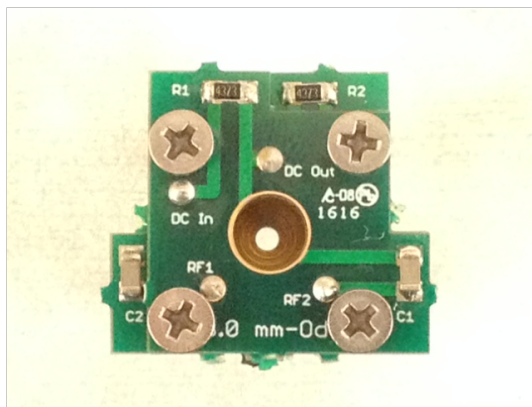
Figure 4.5: Pictures of PCB ion funnel A) mounted to bulkhead with trap and PCB mounting plate and B) in axial view. The largest electrode is 6 mm in diameter, and the smallest is 2 mm in diameter. Surface mount resistors and capacitors are mounted to tabs on the PCBs.
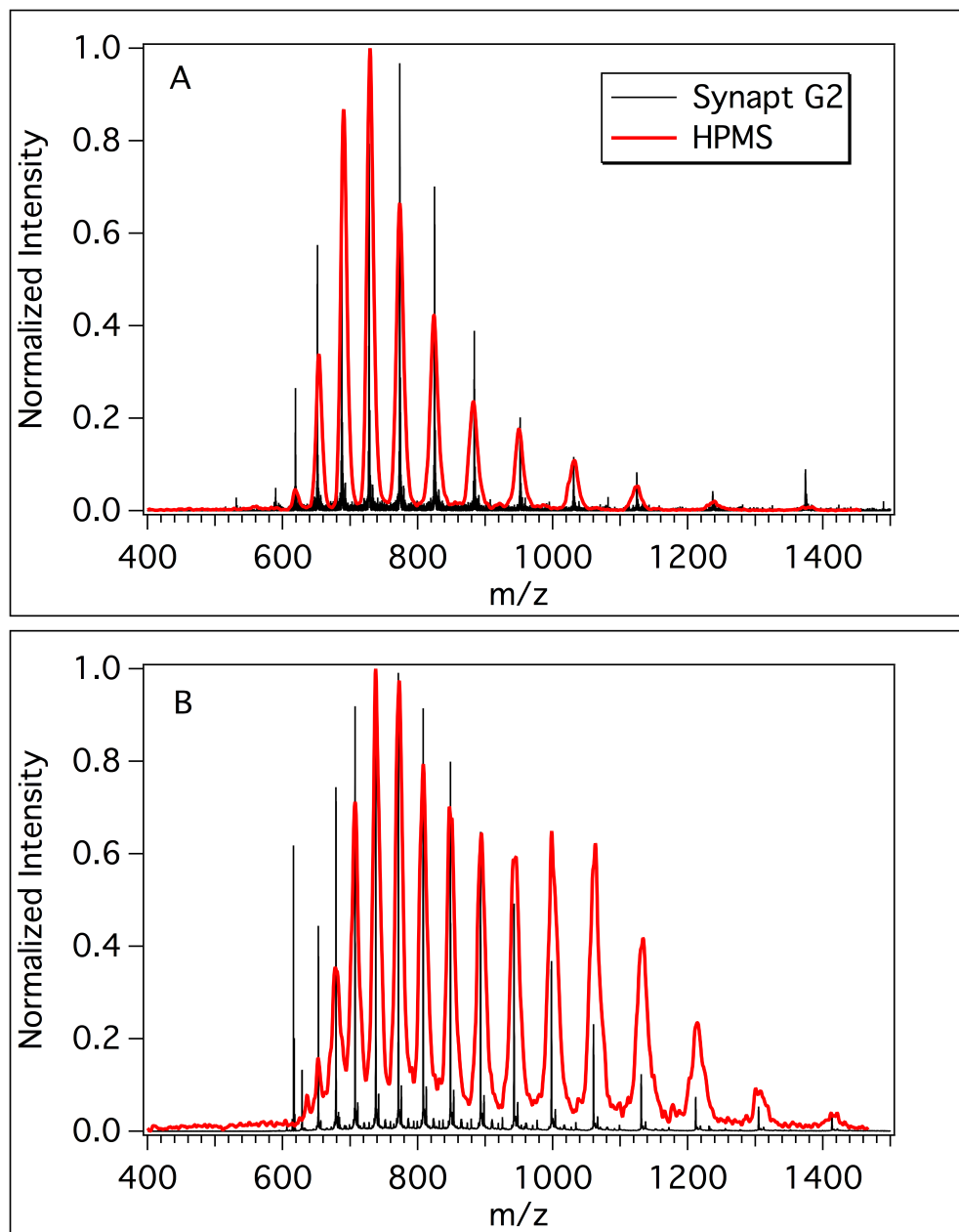
Figure 4.6: ESI infusions of A) cytochrome c and B) myoglobin with HPMS and a commercial mass spectrometer (Synapt G2).
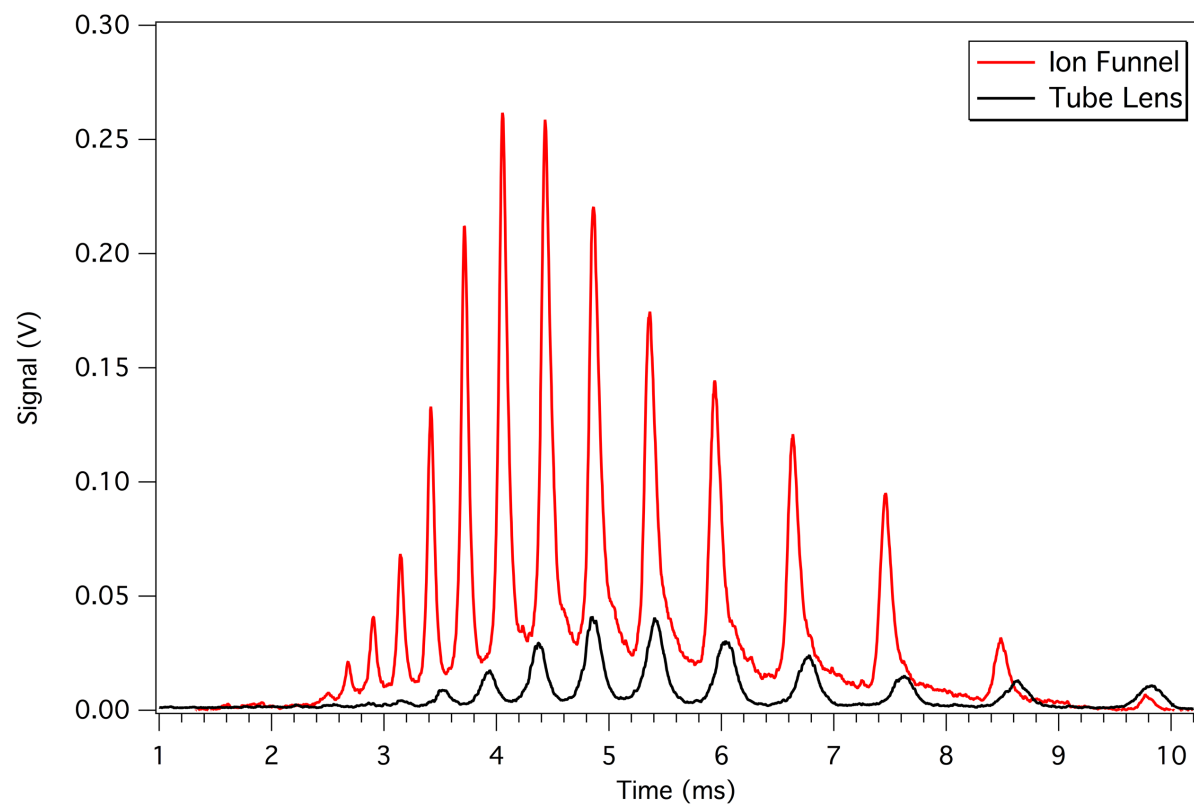
Figure 4.7: Ion focusing optics comparison for an infusion of myoglobin using the PCB ion funnel and DC optics (Tube Lens).

Table 4.2: Ion injection times used for different concentrations of myoglobin.

Concentration (nM)	Ion injection time (ms)
2500	0.05
1250	0.05
625	0.05
313	0.2
156	0.2
78	0.5
39	1
20	2
10	5
5	10
1	20
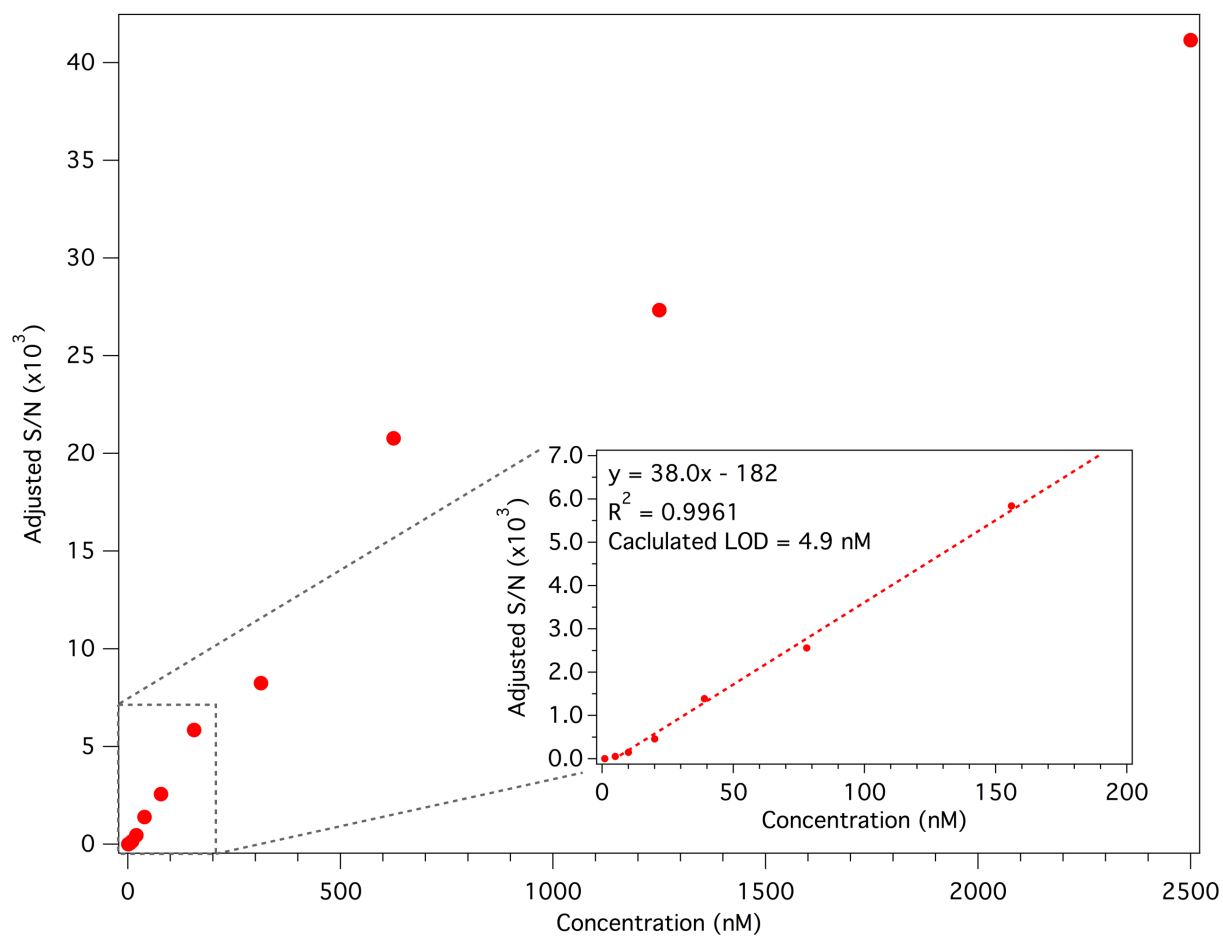
Figure 4.8: Adjusted S/N plotted for different concentrations of myoglobin. The inset shows the lowest seven concentrations with a linear fit to determine the limit of the detection.
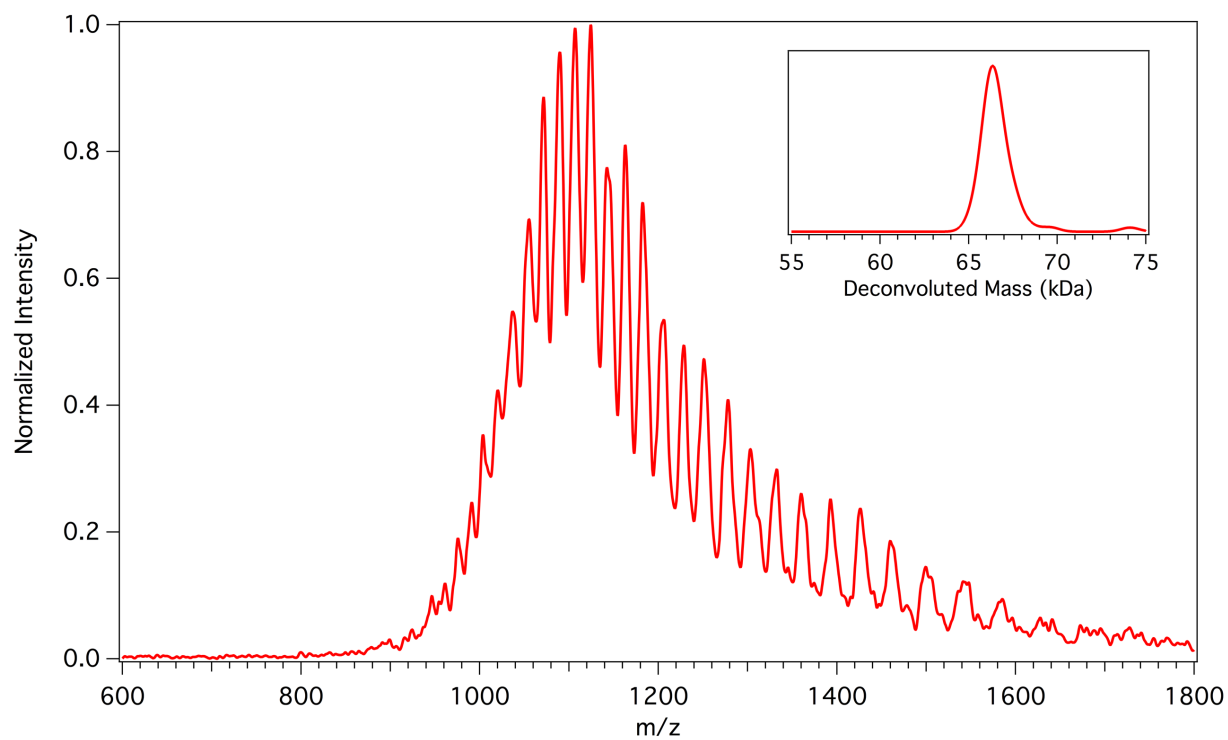
Figure 4.9: ESI-HPMS infusion spectrum of bovine serum albumin (BSA). A deconvoluted spectrum of BSA is shown in the inset.
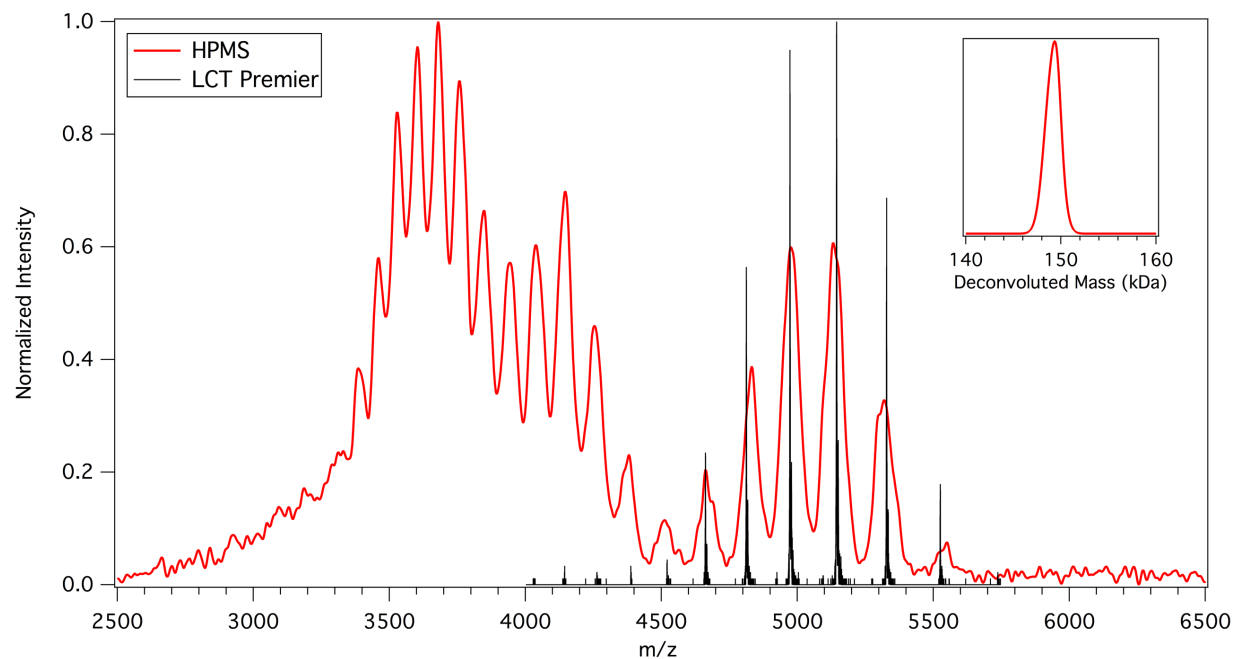
Figure 4.10: ESI infusion spectra of an IgG2 with both HPMS and a commerical mass spectrometer (LCT Premier). A deconvolution of the lowest charge states (highest *m/z*) is shown in the inset.
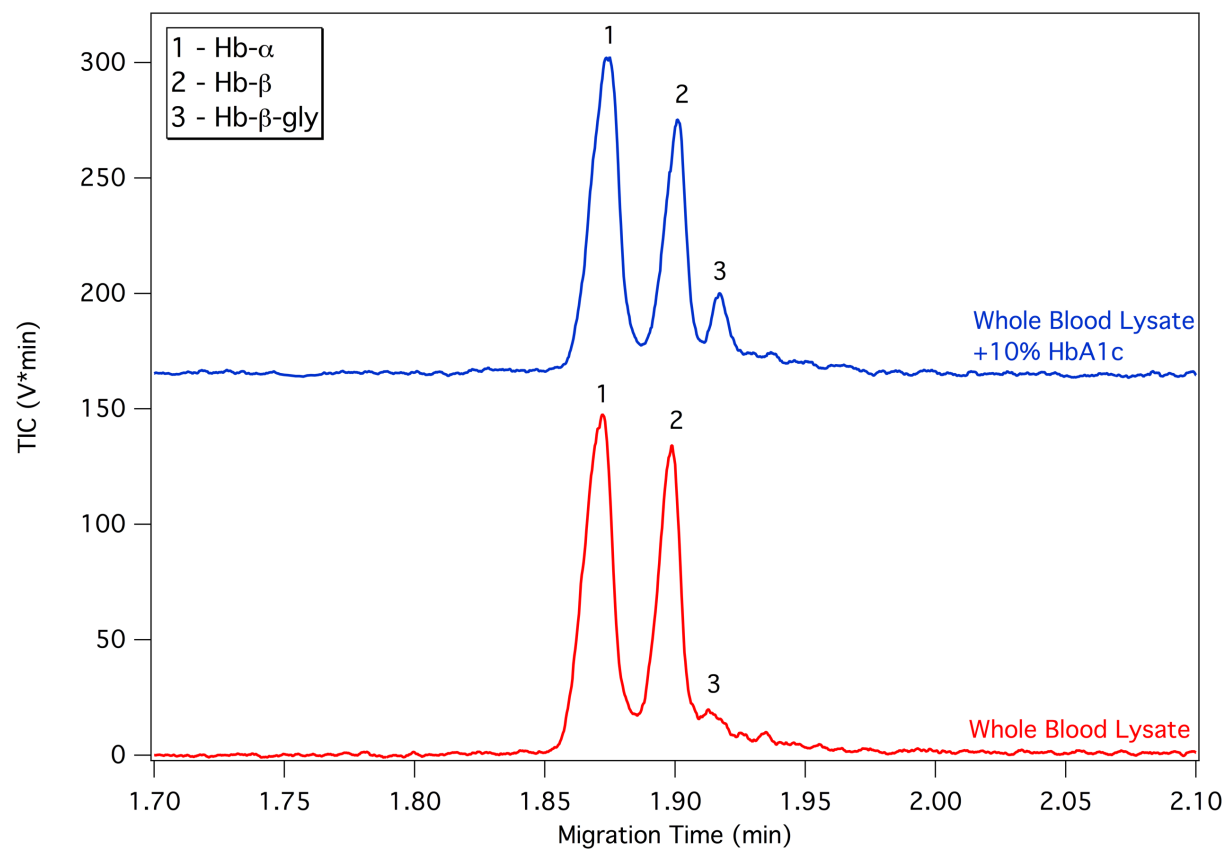
Figure 4.11: Electropherograms from CE-HPMS runs of whole blood lysate with normal levels of HbA1c (bottom) and spiked with 10% HbA1c (top).
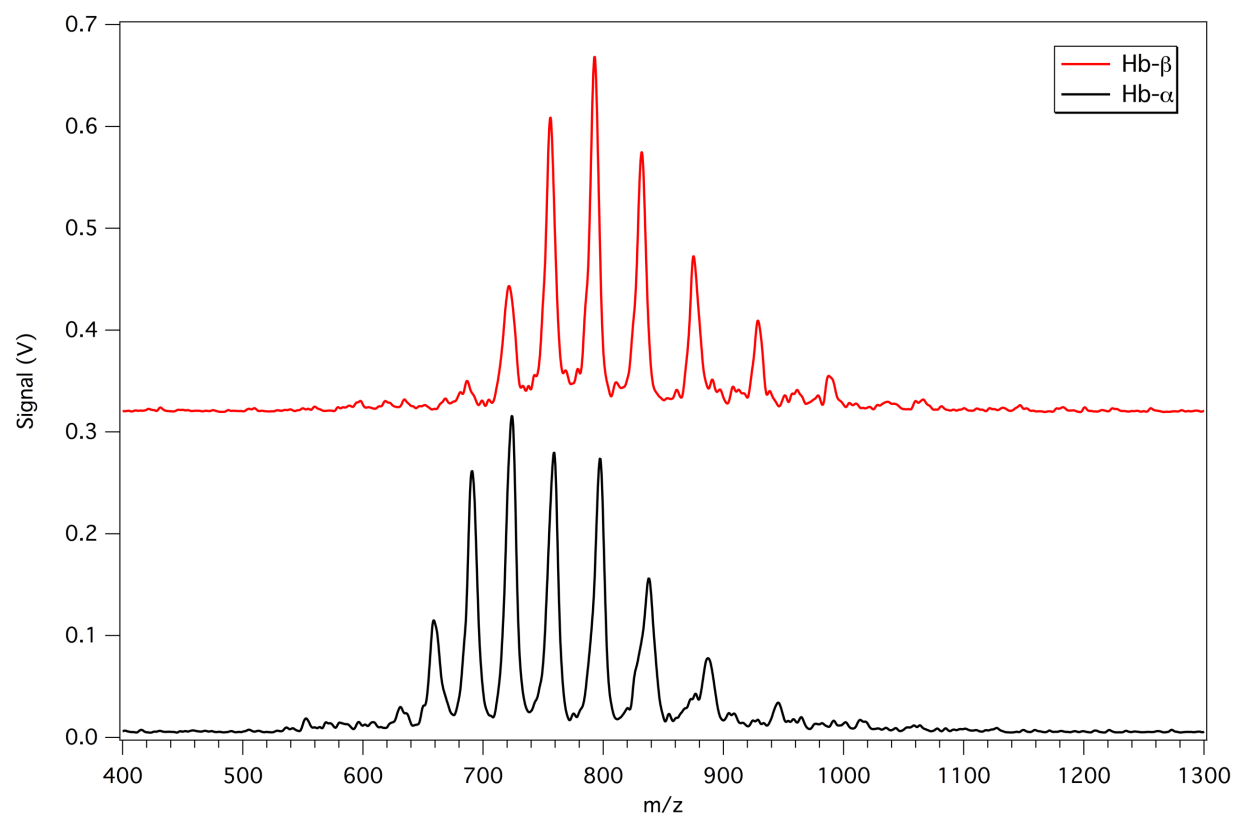
Figure 4.12: Sample HPMS spectra of the subunits of hemoglobin from a microchip CE separation.
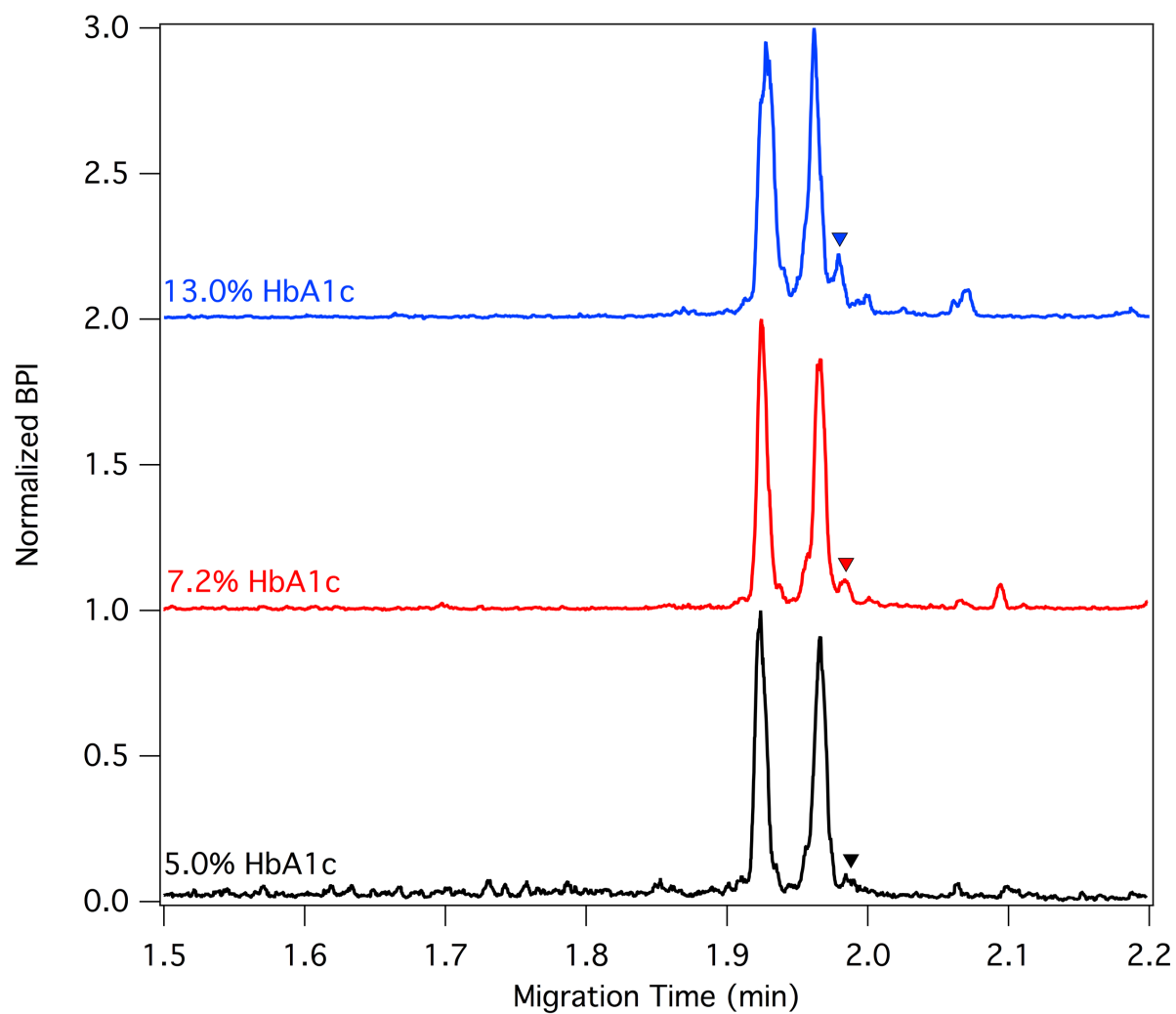
Figure 4.13: Sample CE-HPMS electropherograms of clinical blood samples with varying concentrations of HbA1c. The peak corresponding to the glycated β subunit is shown with an arrow.
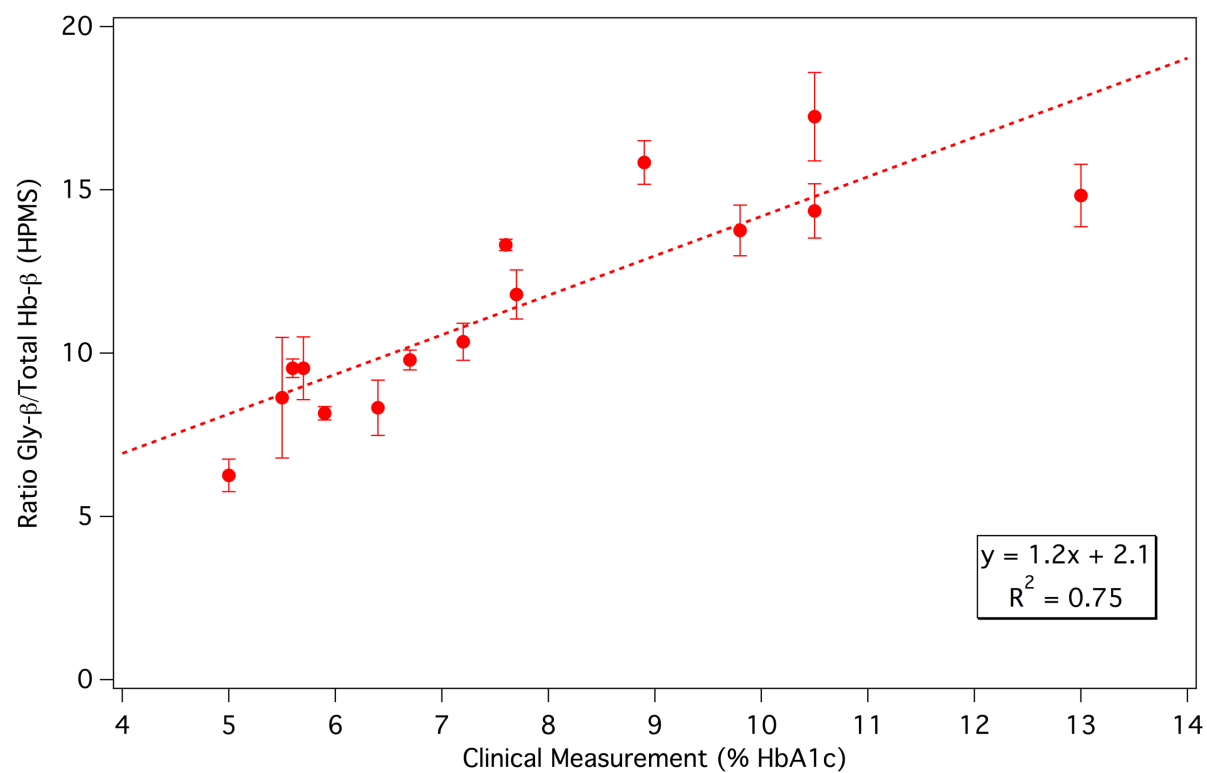
Figure 4.14: Correlation of glycated β subunit to unmodified β subunit from CE-HPMS with clinically measured HbA1c.

4.6   REFERENCES

(1)   Aebersold, R.; Mann, M. *Nature* **2016**, *537* (7620), 347–355.

(2)   Qu, M.; An, B.; Shen, S.; Zhang, M.; Shen, X.; Duan, X.; Balthasar, J. P.; Qu, J. *Mass Spectrom. Rev.* **2016**.

(3)   Fenn, J.; Mann, M.; Meng, C.; Wong, S.; Whitehouse, C. *Science.* **1989**, *246* (4926).

(4)   Whitehouse, C. M.; Dreyer, R. N.; Yamashita, M.; Fenn, J. B. *Anal. Chem.* **1985**, *57* (3), 675–679.

(5)   Tanaka, K.; Waki, H.; Ido, Y.; Akita, S.; Yoshida, Y.; Yoshida, T.; Matsuo, T. *Rapid Commun. Mass Spectrom.* **1988**, *2* (8), 151–153.

(6)   Karas, M.; Hillenkamp, F. *Anal. Chem.* **1988**, *60* (20), 2299–2301.

(7)   Blakeman, K. H.; Wolfe, D. W.; Cavanaugh, C. A.; Ramsey, J. M. *Anal. Chem.* **2016**, *88* (10), 5378–5384.

(8)   Blakeman, K. H.; Cavanaugh, C. A.; Gilliland, W. M.; Ramsey, J. M. *Rapid Commun. Mass Spectrom.* **2016**, *31* (1), 27–32.

(9)   R. E. March and J. F. J. Todd. *Practical Aspects of Ion Trap Mass Spectrometry, Volume 1*; CRC Press, 1995.

(10)   Schaffer, S. A.; Tang, K.; Anderson, G. A.; Prior, D. C.; Udseth, H. R.; Smith, R. D. *Rapid Commun. Mass Spectrom.* **1997**, *11* (16), 1813–1817.

(11)   Kim, T.; Tolmachev, A. V.; Harkewicz, R.; Prior, D. C.; Anderson, G.; Udseth, H. R.; Smith, R. D.; Bailey, T. H.; Rakov, S.; Futrell, J. H. *Anal. Chem.* **2000**, *72* (10), 2247–2255.

(12)   Chen, T. C.; Webb, I. K.; Prost, S. A.; Harrer, M. B.; Norheim, R. V.; Tang, K.; Ibrahim, Y. M.; Smith, R. D. *Anal. Chem.* **2015**, *87* (1), 716–722.

(13)   Ibrahim, Y. M.; Baker, E. S.; Danielson, W. F.; Norheim, R. V.; Prior, D. C.; Anderson, G. A.; Belov, M. E.; Smith, R. D. *Int. J. Mass Spectrom.* **2015**, *377*, 655–662.

(14)   Larrick, J. W. *Immunotherapy* **2012**, *4* (3), 257–261.

(15)   Zhang, H.; Cui, W.; Gross, M. L. *FEBS Lett.* **2014**, *588* (2), 308–317.

(16)   Liu, H.; Gaza-Bulseco, G.; Faldu, D.; Chumsae, C.; Sun, J. *J. Pharm. Sci.* **2008**, *97* (7), 2426–2447.

(17)   Redman, E. A.; Batz, N. G.; Mellors, J. S.; Ramsey, J. M. *Anal. Chem.* **2015**, *87* (4), 2264–2272.

(18)   Redman, E. A.; Mellors, J. S.; Starkey, J. A.; Ramsey, J. M. *Anal. Chem.* **2016**, *88* (4), 2220–2226.

(19)   Diabetes: facts and figures | International Diabetes Federation http://www.idf.org/about-diabetes/facts-figures (accessed Jan 20, 2017).

(20)   Little, R. R.; Sacks, D. B. *Curr. Opin. Endocrinol. Diabetes Obes.* **2009**, *16* (2), 113–118.

(21)   Sacks, D. B. *Diabetes Care* **2011**, *34* (2), 518–523.

(22)   Goldstein, D. E.; Little, R. R.; Lorenz, R. A.; Malone, J. I.; Nathan, D.; Peterson, C. M.; Sacks, D. B. Tests of glycemia in diabetes. *Diabetes Care*, 2004, *27*, 1761–1773.

(23)   Rai, D. K.; Landin, B.; Alvelius, G.; Griffiths, W. J. *Anal. Chem.* **2002**, *74* (9), 2097–2102.

(24)   Zhang, X.; Medzihradszky, K. F.; Cunningham, J.; Lee, P. D. .; Rognerud, C. L.; Ou, C.-N.; Harmatz, P.; Witkowska, H. E. *J. Chromatogr. B Biomed. Sci. Appl.* **2001**, *759* (1), 1–15.

(25)   Roberts, N. B.; Green, B. N.; Morris, M. *Clin. Chem.* **1997**, *43* (5), 771–778.

(26)   Redman, E. A.; Ramos-Payan, M.; Mellors, J. S.; Ramsey, J. M. *Anal. Chem.* **2016**, *88* (10), 5324–5330.

(27)   Redman, E. A. Development of a Microfluidic Capillary Electrophoresis-Mass Spectrometry Platform for the Characterization of Biotherapeutic Proteins, University of North Carolina at Chapel Hill, 2016.

(28)   Gerlich, D. *Inhomogeneous RF Fields: A Versatile Tool for the Study of Processes with Slow Ions*; John Wiley & Sons, Inc., 1992.

(29)   Iavarone, A. T.; Williams, E. R. *J. Am. Chem. Soc.* **2003**, *125* (8), 2319–2327.

(30)   Zhang, Z.; Marshall, A. G. *J. Am. Soc. Mass Spectrom.* **1998**, *9* (3), 225–233.

(31)   Hirayama, K.; Akashi, S.; Furuya, M.; Fukuhara, K. *Biochem. Biophys. Res. Commun.* **1990**, *173* (2), 639–646.

(32)   Nakanishi, T.; Miyazaki, A.; Kishikawa, M.; Yasuda, M.; Tokuchi, Y.; Kanada, Y.; Shimizu, A. *J. Mass Spectrom.* **1997**, *32* (7), 773–778.

Chapter 5: Conclusions and Future Directions

5.1   Conclusions

The overall goal of this work was to couple microchip electrospray ionization (ESI) sources with high pressure mass spectrometry (HPMS), specifically microfluidic devices that perform capillary electrophoresis (CE) with integrated ESI emitters. Prior to this work, HPMS development focused primarily on small, volatile and gas-phase analytes for applications in chemical threat detection.[1,2] HPMS research with these targets has produced a hand-portable mass spectrometer from 908 Devices, Inc. that has been used successfully in the field, weighing 2 kg and having a battery life of about 4 hours.[3,4] While HPMS is now a commercially available technology, the available suite of possible analytes is limited to those already in the gas phase and ionizable by glow discharge ionization. Using HPMS with ESI greatly expands its capabilities and applications to include nonvolatile and liquid analytes, especially those of biological relevance. Adding a small separations platform (microchip CE) to the front end of HPMS analysis greatly increases the selectivity of the instrument and is an opportunity to develop an inexpensive alternative to conventional liquid chromatography-MS analyses. The development of CE-ESI-HPMS described here progressed in three stages. First, the initial proof-of-concept for ESI-HPMS was shown followed by improvements for the analysis of small molecules. Finally, the system was adapted to investigate intact proteins.

A capillary interface was implemented to first demonstrate the possibility of ESI-HPMS. A small "gate lens" was used to focus ions into the miniature ion trap and prevent ions from

154

entering the trap during mass analysis. Using this interface, infusions of the 20 common amino acids were detected at 1 Torr with ambient air as the buffer gas. Peptides were infused and detected with much better sensitivity than the amino acids, most likely due to the fact that peptides have larger mass than single amino acids and are less likely to be scattered by collisions with buffer gas. The first demonstration of CE-ESI-HPMS was performed with a set of peptide standards that were detected with comparable efficiency to a commercial mass spectrometer. MS/MS was demonstrated with proton-bound dimers of tryptophan, MS^4 was shown with clusters of acetaminophen. MS/MS was also performed on a peptide, leucine enkephalin, but with limited conversion efficiency and sensitivity.

After the initial ESI-HPMS experiments, HPMS performance was optimized for the analysis of small molecules. SIMION simulations were used to guide the implementation of a tube lens to increase ion transmission. The RF drive frequency was increased to 30 MHz to improve resolution. With these improvements, the S/N for amino acid samples increased 28-fold on average, and the peak width as measured by FWHM decreased 2.6-fold on average. CE separations of amino acid standards were performed, and 18 of the 20 common amino acids were detected with HPMS. Two potential applications to validate the CE-HPMS platform were explored. The first application was as a rapid method for process control monitoring in the area of biopharmaceuticals. This work focused on tracking the amino acid content in LB growth medium over time with the growth of bacterial cells. It was determined that several amino acids (i.e. serine, tryptophan, proline) were consumed at different rates over the course of cell growth. The rapid separations and detection indicate that this platform may be a viable method for monitoring cell growth in bioreactors for biopharmaceutical or other applications. The second application was in forensic analysis for the detection of opiates in urine where a small system

155

could eliminate the need for "two-tiered" testing. Opiate standards were first tested and compared with a commercial mass spectrometer. Similar detection was observed, with only 2 of 13 standards going undetected by HPMS. Codeine was spiked into urine at various concentrations, and, after sample preparation by solid phase extraction, codeine was detected as low as 10 ng/mL, well below the standard LOQ of 25 ng/mL necessary for forensic applications.[5]

One of the primary advantages of ESI is the ability to ionize large, liquid-borne biomolecules and get them into the gas phase for MS analysis.[6] HPMS was adapted for the analysis of proteins by optimizing the parameters of ion trap operation and improving ion optics. Small ion traps ($r_0 = 100$ μm) and low frequencies compared to previous analysis (as low as 5 MHz) were implemented to scale the mass range for protein charge state detection. SIMION simulations guided the development of a PCB ion funnel, which improved signal intensity approximately 8-fold over the DC tube lens for an infusion of myoglobin. Infusions of small proteins (cytochrome c and myoglobin) were demonstrated and compared with a commercial mass spectrometer with good agreement between charge states detected on the two instruments. The practical LOD for myoglobin was determined to be ~5 nM. The frequency was adjusted to extend the mass range even further, and the proteins BSA (~66 kDa) and an IgG2 mAb (~150 kDa) were detected with HPMS. To investigate the possibility of using CE-HPMS in a clinical setting, whole blood lysate was analyzed to monitor hemoglobin A1c (HbA1c) ratios for diabetes diagnostics. Whole blood spiked with HbA1c showed an increase in intensity for the peak corresponding to the glycated β subunit of hemoglobin. Clinical blood samples with known HbA1c values were then analyzed by CE-HPMS. Using the ratio of the glycated β subunit to the total β concentration, the results from the HPMS platform showed some correlation ($R^2 = 0.75$)

with the known values from the clinical samples. The current assay could possibly be used as a screening tool, but improvements still need to be made for definitive clinical diagnosis.

CE-HPMS has been shown to be a viable tool for the analysis of a wide range of analytes, from amino acids to intact proteins. Future improvements and development should make it a valuable tool for many targeted analyses and a rapid and inexpensive alternative to large LC-MS platforms.

5.2   Future Directions

The initial development of a microchip CE-ESI-HPMS platform has been demonstrated, but there are improvements that could be made to optimize the system's performance. Increases in ion transmission would increase the sensitivity of the instrument. The dynamic range, mass accuracy, and resolution of the mass analyzer could all be improved. Finally, a pressure tolerant detector like a Faraday cup could be used in place of an electron multiplier, eliminating the need for a turbo pump and significantly reducing the size and cost of the instrument.

Relatively simple ion optics were used for this work, and modifications could be implemented to improve ion transmission. For example, the PCB ion funnel worked well for species of higher mass (i.e. proteins), but did not perform well for the transmission of amino acids. Changes in the funnel geometry including ring size, spacing, and number of electrodes could be optimized for transmission of small species or alternately to improve transmission of larger species. Another possibility to improve ion transmission would be to perform ESI inside the vacuum chamber. The Smith group at PNNL has shown significant gains in ion transmission using sub-ambient pressure ESI in combination with an ion funnel.[7,8] Moving the ESI into the vacuum chamber eliminates losses of ions incurred at the atmospheric interface. If this strategy is

implemented, there will likely need to be optimization of the microchip source to operate at these pressures, along with significant changes in instrument design.

One parameter of the mass analyzer that could be improved is the dynamic range, especially for protein analysis, which are large and highly charged. CITs were used for most of the work here, but different geometries, like SLITs, have increased ion storage and would increase the dynamic range. Furthermore, arrays of SLITs could be used for even greater ion storage, but uniformity of the trapping elements will be critical for maintaining mass resolution. SLITs were only used for some of the work here because the fabrication of the electrodes at small scales ($r_0 \approx 100$ μm) resulted in nonuniform geometries and resulted in poor mass spectral resolution. Other fabrication techniques and electrode materials, such as deep reactive ion etching (DRIE) of silicon, could be used to produce uniform electrode surfaces at these small scales and ion storage could be increased without loss in (and possibly improve) mass spectral performance.[9]

The mass accuracy of the mass analyzer could also be improved. While some loss of resolution is incurred operating at high pressure, mass accuracy is critical for proper identification of chemical species. While not rigorously characterized here, the mass accuracy was about 1 ppth at 1000 *m/z* for the HPMS platform. With proper calibration and standards, the mass accuracy could likely be improved. Another possibility for increasing mass accuracy is improved RF electronics. Small variations in voltage could cause significant variation in determination of *m/z*. Even with proper calibration, a reproducible and linear drive RF voltage are important for maintaining mass accuracy.

Greater resolution of the mass spectrometer for ESI applications would greatly increase the selectivity of the instrument. Previous work has shown unit mass resolution for *p*-xylene at

1 Torr pressures with the RF drive frequency operated at around 60 MHz.[9] Higher RF frequencies could be implemented in ESI-HPMS to improve resolution, but smaller traps will be needed to maintain a reasonable mass range for electrosprayed species. As mentioned above, small trapping features are difficult to fabricate with our current strategies, so other fabrication strategies (DRIE) and electrode materials (silicon) will be necessary to produce traps at sub-100 μm scales. Reducing the size of the trap for higher frequencies and improved resolution will result in lower charge capacity, so SLITs and arrays of traps will likely be necessary to maintain charge capacity and dynamic range of the mass spectrometer.

Though not the goal of this work, a sensitive detection method is crucial for mass spectrometer performance. A pressure tolerant Faraday cup detector would eliminate the need for a turbo pump. A differential chamber setup with electron multiplier detection was used for this work because electron multipliers have high gain and bandwidth, making them excellent detectors for ESI-HPMS development. Current Faraday cup technology does not have the sensitivity of electron multipliers, so the implementation of a Faraday cup detector will depend on the ability of the mass spectrometer to accumulate more charges (i.e. SLITs, arrays) or improved Faraday cup technology.

5.3   REFERENCES

(1)   Blakeman, K. H.; Wolfe, D. W.; Cavanaugh, C. A.; Ramsey, J. M. *Anal. Chem.* **2016**, *88* (10), 5378–5384.

(2)   Blakeman, K. H.; Cavanaugh, C. A.; Gilliland, W. M.; Ramsey, J. M. *Rapid Commun. Mass Spectrom.* **2016**, *31* (1), 27–32.

(3)   M908 - 908 Devices http://908devices.com/products/m908/ (accessed Feb 16, 2017).

(4)   CASE STUDY The Evolving Threat Landscape First Responders Encounter http://908devices.com/wp-content/uploads/2016/07/908D_ThreatLandscape_CaseStudy.pdf (accessed Feb 16, 2017).

(5)   Drugs of Abuse: Opiates - Mayo Medical Laboratories http://www.mayomedicallaboratories.com/test-info/drug-book/opiates.html (accessed Feb 2, 2017).

(6)   Fenn, J.; Mann, M.; Meng, C.; Wong, S.; Whitehouse, C. *Science (80-.).* **1989**, *246* (4926).

(7)   Page, J. S.; Tang, K.; Kelly, R. T.; Smith, R. D. *Anal. Chem.* **2008**, *80* (5), 1800–1805.

(8)   Tang, K.; Page, J. S.; Marginean, I.; Kelly, R. T.; Smith, R. D. *J. Am. Soc. Mass Spectrom.* **2011**, *22* (8), 1318–1325.

(9)   Blakeman, K. Development of High Pressure Mass Spectrometry for Handheld Instruments, University of North Carolina at Chapel Hill, 2015.

Appendix I: ESI Device Fabrication and Coating

A1.1 Microfabrication Procedure

Microchip devices were fabricated using photolithography and wet etching techniques. The substrates were 0.5 mm thick 5" x 5" B270 glass from Perkin Elmer (Waltham, MA) pre-made with a layer of chrome and AZ1518 photoresist. The devices were patterned using a mask made in-house from soda lime glass and exposed to UV light (365 nm) for 60 s. The resist was then developed in AZ 400K developer (Integrated Micro Materials, Argyle, TX) for 90 s. The chrome was removed from the patterned areas using Chrome Etchant 1020 (Transene Company, Inc. Danvers, MA), stirred for 3 min. Channels were then etched into the glass using diluted 10:1 buffered oxide etchant (BOE). Channels were etched to a depth of approximately 10 μm and a width of 70 μm, measured using a KLA Tencor P15 surface profiler (KLA Tencor Corp., San Jose, CA). Both sides of the device were then coated with AZ1518 photoresist before powder blasting vias through the substrate to provide fluidic connection to the channels. The photoresist was then removed using acetone. The remaining chrome was etched away using the same chrome etchant used above. The etched substrate was dry bonded to a blank 5" x 5" substrate of the same material before fusion bonding overnight at 550 °C. Devices were then diced using a precision dicer (Disco Technologies, Santa Clara, CA). Dicing cuts were made at 90° and served both to separate the devices on the substrate and to form the ESI emitter at one corner of each device. The emitter corner was then polished on a lapping wheel using 3 μm cerium oxide abrasive lapping paper (Ultra Tec, Santa Ana, CA). Finally, 8 mm x 8 mm cloning cylinders

were used as reservoirs and fixed to the devices using chemically resistant Loctite E-120HP

epoxy (Henkel Corporation, Germany).

A1.2 Device Coating Procedure

Coating of the devices is a two-stage process. First, an aminopropyl silane (APS) reagent is

chemically bonded to the surface of the devices in a gas-phase reaction. Second, a polyethylene

glycol (PEG) reagent in the liquid phase is chemically bonded to the APS coating.

A1.2.1 Chemical Vapor Deposition of APS Coating

All devices (CE and infusion) were coated with (3-Aminopropyl)di-

isopropylethoxysilane (APDIPES) via chemical vapor deposition (CVD), resulting in uniform

coatings across the surface of the devices. A commercial LabKote CVD system (Yield

Engineering Systems, Livermore, CA) was used to coat the devices. The chamber was under

vacuum and held at 160 °C throughout the coating. A 0.1 mL aliquot of APDIPES was injected

into the chamber and reacted with the glass surfaces for approximately 15 min before purging the

chamber with nitrogen. For a full coating procedure, 3 injections of APDIPES were performed.

A1.2.2 PEGylation of APS Coating

Two microchip configurations of PEG coatings were used. In one configuration, only the

pumping channel was coated with PEG, while in the other, all channels were coated with PEG.

The reagent used was NHS-PEG$_{450}$ from NanoCS (Boston, MA). The PEG reagent was

dissolved in 10 mM phosphate buffer (pH 7.5) at a concentration of 10 mg/mL. To flow

solutions through the device, the PEG reagent was loaded into the reservoirs and vacuum was

applied at the corner with the ESI emitter. Before coating with PEG solution, devices were

treated with a solution of 0.1% formic acid, then rinsed with phosphate buffer (without PEG).

Devices were then treated with the PEG reagent solution for 30 to 45 minutes, depending on the length of the separation channel. After coating with PEG, devices were rinsed with DI water for at least 10 minutes. An alternate "residue coating" method has also been implemented, in which the devices are baked in the CVD oven for one cycle (without reagent injection) immediately after PEG coating and before rinsing. The devices were then rinsed with DI water for at least 10 minutes after baking in the oven.

Appendix II: Microchip Device Operation

A2.1 Instrument Hardware

Voltages were applied via platinum wire electrodes soldered to high voltage wire. The power was supplied to the electrodes with a custom-built power supply using high voltage modules from UltraVolt (Ronkonkoma, NY). Pressure to the devices was applied via rubber tubing and controlled using 3-way valves from Clippard (Cincinnati, OH). Air or nitrogen was used to apply pressure and regulated at 2 psi for all analyses. Timing for the application of voltages and pressures was controlled using a custom LabVIEW program.

A2.2 CE-ESI Device Injection and Operation

A sample schematic of a CE-ESI device is shown in Figure A2.1a, reprinted here from Chapter 2. Two types of injections were performed: electrokinetic and hydrodynamic.

A2.2.1 Electrokinetic Injections

For electrokinetic injections, voltages are applied to all four reservoirs: sample (S), background electrolyte (BG), sample waste (SW), and pumping channel (EO). Sample is loaded into reservoir S with background electrolyte in each of the other reservoirs. To perform an injection, voltages are switched from a "run" configuration to an "inject" configuration, and then back to the "run" configuration. Sample voltages from Chapter 2 are shown in Table A2.1. During the "run" configuration, the electric field drives sample from S to SW without entering the separation channel while BGE from B enters the separation channel and effectively gates the

sample to SW. When switched to "inject," the voltages applied to reservoirs SW and BG are balanced, and sample enters the separation channel. The voltages are switched back to "run" thereby defining the sample plug length in the separation channel and zone electrophoresis occurs.

For operation of these devices, a differential surface coating provided the flow necessary for ESI. The separation channel had an APDIPES coating (positive surface charge at low pH), which produces a strong anodic electroosmotic flow (EOF). The EO channel had PEG covalently bound to the APDIPES coating, suppressing the EOF. The difference in EOF at the junction of these two channels results in pressure driven flow towards the corner of the device, which, in combination with the voltage applied to the EO channel, results in electrospray. It is important to note that electrokinetic injections could be performed with other coating configurations, but all electrokinetic injections in this work were performed with this surface coating configuration.

A2.2.2 Hydrodynamic Injections

For hydrodynamic injections, pressure is applied to reservoirs S, BG, and EO at different intensities between injection and the separation "run". Voltage in this case is only applied between S and EO to perform the electrophoretic separation in the "run" phase. The sample is loaded into reservoir BG with the other reservoirs containing BGE. During the "run" phase, voltages are applied to reservoirs S and EO, and pressure is applied to EO to provide the flow necessary for ESI. To perform an injection, the voltages are turned off to S and EO and pressure is applied to reservoirs BG (containing sample) and S. This drives the sample into the separation channel and to SW. The injection profile is shown in Table A2.2. After injection, a short "clear" step is performed where pressure is applied to S to load the sample plug completely into the

separation channel and prevent excess sample from being injected. The voltages and pressures are then switched back to "run" and zone electrophoresis occurs.

For hydrodynamic injections, all channels in the devices are coated with PEG, suppressing the EOF. Because there is no differential EOF between the separation and EO channel, pressure is applied to the EO reservoir to provide the flow necessary for sustaining ESI.

A2.3 Infusion Device Operation

A sample schematic of an infusion device is shown in Figure A2.1b. For normal operation, sample is loaded in each reservoir with +5 kV applied to the EO reservoir and 0 kV (GND) applied to the S reservoir. If the channels are differentially coated with APIDES in the infusion channel and APDIPES+PEG in the EO channel, the difference in EOF at the junction of the channels provides the flow necessary for ESI. For some applications, head pressure (2 psi, air or N_2) was applied to the EO reservoir to produce a more stable electrospray over time.
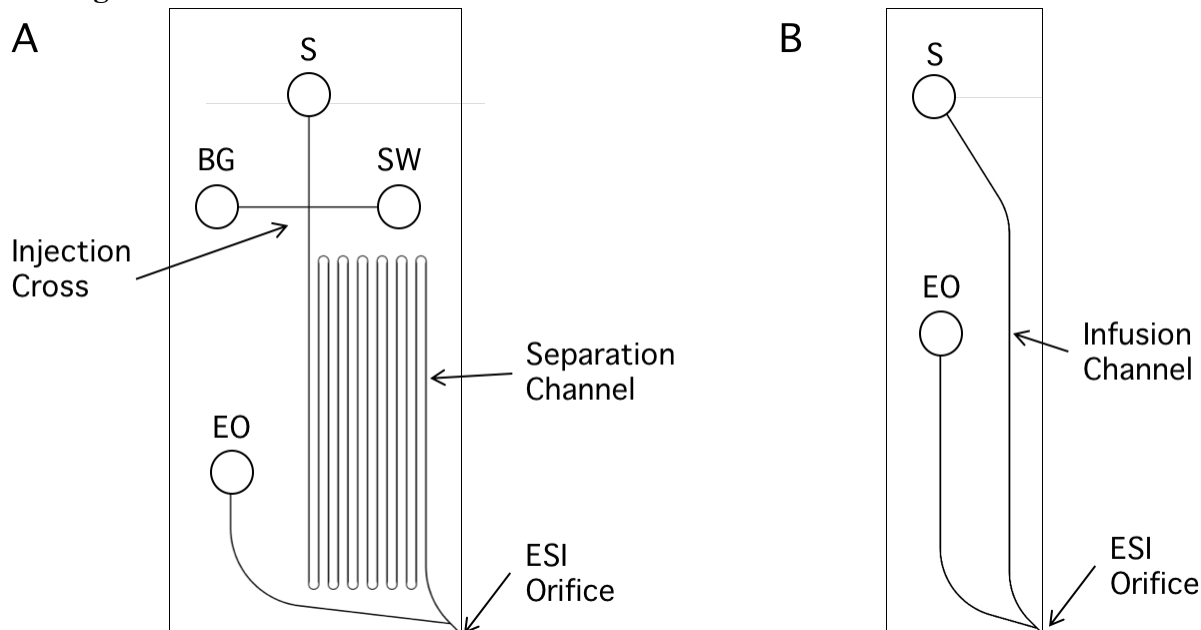
A2.4 Figures and Tables

Figure A2.1: Schematics for capillary electrophoresis (A) and infusion (B) glass microfluidic devices. All channels were etched to a depth of 10 µm. Reservoirs are designated with circles and indicate sample (S), background electrolyte (BG), sample waste (SW), and electroosmotic pump (EO). The microchip in A consists of an injection cross, a 46-cm serpentine separation channel, and an electroosmotic pumping channel. The infusion device (B) consists of a 5.5-cm channel and an electroosmotic pumping channel, and both reservoirs are filled with the sample.

Table A2.1: Sample operational voltages for electrokinetic injections.

	V_{run} (kV)	V_{inj} (kV)
S	-14	-14
BG	-14	-13
SW	-12	-13
EO	+6	+6

Table A2.2 Voltages and pressures used in hydrodynamic injection sequence. A "V" subscript indicates a voltage applied to the reservoir, and a "P" subscript indicates a pressure.

	Run	*Inject*	*Clear*
S_V	+20	0	0
EO_V	+1.5	0	0
EO_P	On	Off	Off
S_P	Off	On	On
BG_P	Off	On	Off